Structural and biophysical study of the KlebC import mechanism

Qiaoyu Tian 田乔宇

Merton College

MSc by Res in Biochemistry (2022-2023)

Supervisor: Professor Colin Kleanthous

Abstract

The cell envelope of Gram-negative bacteria hosts many different protein machineries. These protein machineries are used by bacteria to perform different functions, such as cell division and nutrient acquisition. TolC is a trimeric protein that anchors at the OM and extends into the periplasm. TolC is used as a channel for exporting protein toxins and xenobiotics out of the cell but is also hijacked by bacteriocins as an import channel. This unique double-sided function of TolC has drawn interest to understand its roles in different biological processes and apply them to combat increasingly serious global antimicrobial crisis. The exploitation of TolC by a group B bacteriocin, KlebC, was studied using biochemical, biophysical and structural methods. It was previously discovered that the Ton system, known for its role in nutrient acquisition, is required to uptake KlebC into cells. Although the interactions between different group B bacteriocins and their outer membrane receptors have been elucidated, there has been no published studies on the interaction between group B bacteriocins and periplasmic TonB. This study has successfully demonstrated binding between KlebC and TonB, by analytical size exclusion chromatography and isothermal titration calorimetry. A binding affinity of 66 µM was measured between KlebC and TonB. The structure of the complex was predicted by Alphafold 2.0 and validated by mutational approaches. To fully understand the uptake mechanism of KlebC, the ternary KlebC translocon (KlebC-TolC-TonB) was assembled in nanodiscs. Grids, containing the KlebC translocon, were optimised for single-particle cryogenic electron microscopy data collection and analysis for future structure determination of the complex.

Acknowledgements

I would like to first thank Professor Colin Kleanthous for his supervision and providing me this valuable opportunity to research in his lab. 我也十分感激我的父母及家人对我一直以来的教育和支持，是他们的一路陪伴才有了我如今的成就。(I also would like to thank my grandma 李素梅, my mom 刘一嬴, my dad 田野, and my sister 田鑫禹 for all their education and support during my life.)

I would not finish this project without the help from Dr. Melissa Webby and Dr. Nicholas Housden. Thanks for all their teaching and suggestions. I also want to take the opportunity to thank Dr. David Staunton for his help on SEC-MALS experiments. And also thank everyone else in the lab for creating a happy and relaxed environment.

It has been a year that l moved again out of my comfort zone to study all new knowledge and skills in a new city. Merton College, especially the 2022-2023 MCR community, has made this challenge much easier and more joyful. I would like to thank my friends from college for their kindness and wisdom. Appreciate all those fun moments together!

Table of Contents

ABSTRACT 2

ACKNOWLEDGEMENTS 3

CHAPTER 1. INTRODUCTION 7

1.1 Global antimicrobial crisis 7

1.2 Outer membrane organization of Gram-negative bacteria 8

1.3 TolC tripartite protein machinery 11

1.3.1 Functional insights 11

1.3.2 Structural insights 14

1.4 Cytotoxic and uptake mechanisms of bacteriocins 18

1.4.1 Cytotoxic mechanisms of bacteriocins 19

1.4.2 Group A bacteriocin uptake mechanism 21

1.4.3 Group B bacteriocin uptake mechanism 24

1.5 Therapeutic uses of bacteriocins 29

AIMS OF THIS WORK 31

CHAPTER 2. MATERIALS AND METHODS 32

2.1 Microbiology and molecular biology 32

2.2 Expression and purification of soluble proteins 34

2.3 Expression and purification of TolC 35

2.4 Lyophilization of Kq $TonB_{156-248}$ 36

2.5 SDS-polyacrylamide gel electrophoresis (SDS-PAGE) 37

2.6 Protein concentration quantification 37

2.7 Size exclusion chromatography – multi-angle light scattering (SEC-MALS) 38

2.8 KlebC activity assay 38

2.9 Isothermal titration calorimetry (ITC) 38

2.10 Analytical SEC 39

2.11 Preparation of KlebC-TolC-TonB ternary complexes in nanodisc 39

2.12 Grid preparation 41

2.13 Alphafold 2.0 prediction and structural analysis 42

CHAPTER 3. THE IMPORT OF KLEBC THROUGH THE TON SYSTEM 43

3.1 Purification of KlebC constructs 43

3.2 Cytotoxic activities of KlebC constructs 46

3.3 *tonb* cloning and TonB purification 48

3.3.1 *K. quasipneumoniae tonb* cloning 48

3.3.2 Kq $TonB_{156-248}$ purification 49

3.3.3 Ec $TonB_{33-240}$ purification 52

3.4 *In vitro* complex formation investigation between $KlebC_{1-254}$ and TonB 54

3.5 Thermodynamic characterisation between KlebC and TonB through ITC 58

3.6 Predicted binding site between $KlebC_{1-254}$ and *K. quasipneumoniae* TonB 61

3.7 Discussion 67

CHAPTER 4. ASSEMBLY OF THE KLEBC TRANSLOCON 69

4.1 Purification optimisation of TolC 69

4.2 The validation of KlebC-TolC complex formation 73

4.3 TolC-nanodisc formation optimisation 75

4.4 Ternary complex formation in nanodisc 79

4.5 Visualisation of ternary complex on grids 86

4.6 Discussion 90

CHAPTER 5. CONCLUSION 92

REFERENCES 93

Chapter 1. Introduction

1.1 Global antimicrobial resistance crisis

Since the discovery of penicillin by Alexander Fleming in 1929, antibiotics have become indispensable for fighting diseases caused by bacterial pathogens (Fleming, 1929). Since 1929, many new antibiotics have been developed and the administration of antibiotics has increased exponentially. However, these antibiotics become less and less effective, as more and more pathogens develop resistance to them. The antimicrobial resistance has become a global healthcare threat. It has been predicted that antimicrobial resistance (AMR) could kill 10 million people per year by 2050 (O'Neill, 2016). In 2019, the number of deaths associated with bacterial AMR reached an estimated 4.95 million globally (Murray, 2022). The World health organisation (WHO) has grouped bacteria based on their potential threats into three groups: critical, high and medium. Three critical pathogens, namely carbapenem-resistant *Acinetobacter baumannii*, carbapenem-resistant *Pseudomonas aeruginosa* and carbapenem-resistant, extended spectrum beta-lactamase (ESBL)-producing Enterobacteriaceae, are all Gram-negative bacteria. The Enterobacteriaceae contains several genera, one of which is *Klebsiella*. Species in the *Klebsiella* genus, such as *Klebsiella pneumoniae* and *Klebsiella quasipneumoniae*, cause severe nosocomial infections, with high mortality rates globally (Mathers et al., 2019; Wyres and Holt, 2018).

Novel antibiotics targeting these drug-resistant Gram-negative bacteria are urgently required. With the slow development of new antibiotics, only 12 antibiotics have

been approved since 2017. There is an urgent need for research and drug development to combat the rising AMR threat.

1.2 Outer membrane organization of Gram-negative bacteria

One of the features of Gram-negative bacteria that makes them so resistant to antibiotics is their special cell envelope structure. The cell envelope is composed of three layers; the outer membrane (OM), peptidoglycan (PG), and inner membrane (IM) (figure 1.1). These layers host different protein machineries, which allow bacteria to perform complex biological processes, such as toxin secretion and cell division. Different kinds of proteins are embedded in both the OM and the IM. Proteins that are embedded in the OM are usually β-barrel proteins and are called outer membrane proteins (OMPs). Those embedded in the IM are usually α-helical and are called inner membrane proteins (IMPs). OMPs are essential for OM stability, nutrient and small molecule import and bacterial survival.

The OM is an asymmetric lipid bilayer. The inner leaflet is composed of phospholipids (PL) whilst the outer leaflet is composed of lipopolysaccharides (LPS) (figure 1.1) (Henderson et al., 2016). This bilayer architecture of OM is different from other biological membranes, such as mitochondrial, and mammalian cell membranes, which are all bilayers of PL. Three types of PLs are produced by *Escherichia coli*, namely phosphatidylethanolamine (PE), phosphatidylglycerol (PG) and cardiolipin (CL) (Dowhan, 1997). While the amounts of PE and PG remain relatively constant during cell growth, the level of CL increases during stationary phase (Hiraoka, Matsuzaki and Shibuya, 1993). LPS is composed of three components: lipid A, a core

oligosaccharide, and an O-antigen, which are covalently linked to each other (Raetz and Whitfield, 2002). The lipid A moiety of LPS gives it a negative charge which contributes to the membrane selectivity, restricting the entry of some anionic detergents, hydrophobic antibiotics, and dyes, making LPS an effective permeability barrier (Nikaido and Vaara, 1985). By comparison, a phospholipid-bilayer allows the direct diffusion of small hydrophobic molecules through the membrane (Van den Berg, 2010). The deletion of LPS in *Pseudomonas aeruginosa* significantly increases bacterial susceptibility to hydrophobic antibiotics, such as chloramphenicol and erythromycin (Plésiat and Nikaido, 1992; Plésiat et al., 1997). Divalent cations (Ca^{2+} and Mg^{2+}) are chelated within the LPS network (Nikaido, 2003), further stabilizing the OM. It was also shown that divalent cations are also important for interactions between LPS and OMPs. When the OmpE36 structure was studied, a calcium ion was detected between OmpE36 and LPS (Arunmanee et al., 2016).

The OM is a highly crowded and rigid structure filled with numerous lipids and proteins (Jarosławski et al., 2009; Kleanthous, Rassam and Baumann, 2015). Monitoring of OMP diffusion in the OM by fluorescence recovery after photobleaching (FRAP) and single particle tracking showed that OMPs within the membrane have highly restricted diffusion (Verhoeven, Dogterom and den Blaauwen, 2013; Meddens, de Keijzer and Cambi, 2014; Kleanthous, Rassam and Baumann, 2015). Despite limited diffusion, OMPs have been shown to cluster into supramolecular assemblies referred to as islands within which OM biogenesis machineries, Bam and LptD are co-localised (Rassam et al., 2015). In the *E. coli* OM,

LPS also forms distinct patches, where OMPs are excluded (Benn et al., 2021). LPS is also important for stabilising associations between OMPs (Webby et al, 2022).

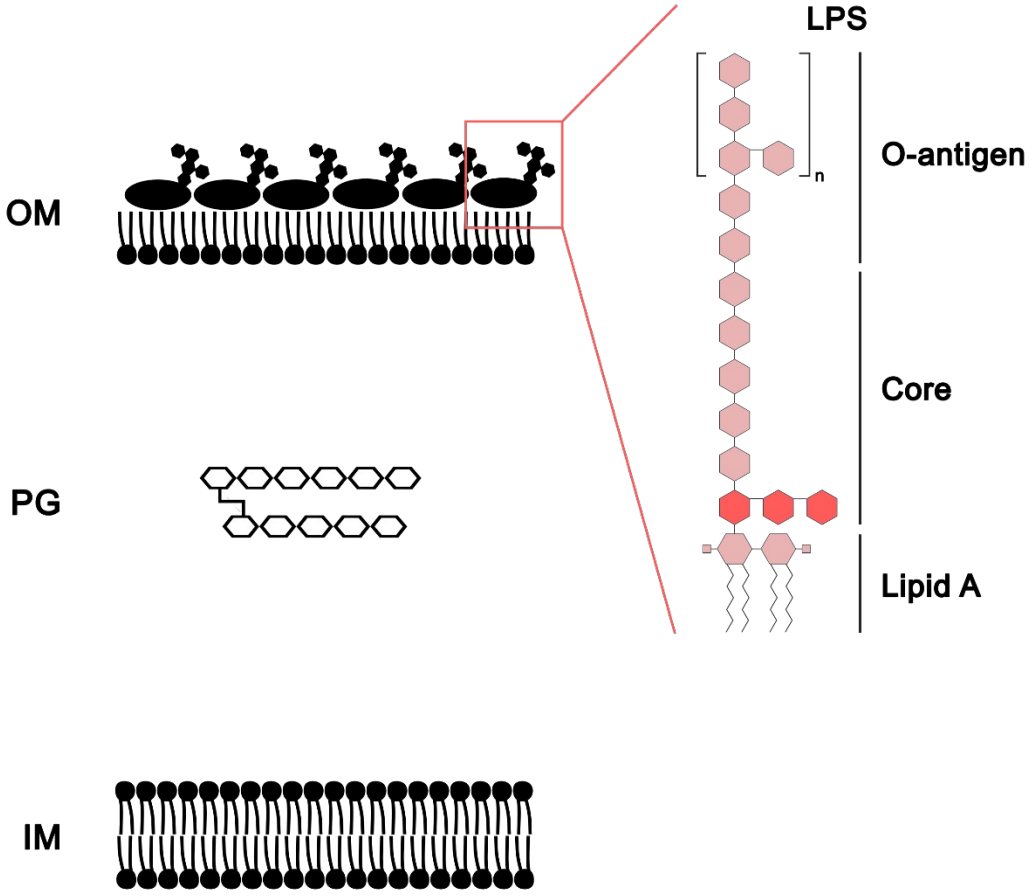


Figure 1.1 Schematic diagram of Gram-negative bacterial cell envelope
The cell envelope of gram-negative bacteria is composed of outer membrane (OM), peptidoglycan (PG) and inner membrane (IM). The outermost layer protects bacteria by the special structure of lipopolysaccharide (LPS).

Chapter 1.3 TolC tripartite protein machinery

There are different OMPs in Gram-negative bacteria. Some have very specific functions, such as vitamin B_{12} transporter BtuB, while others have more generic functions, such as porins and drug efflux pumps. One of the essential tools for Gram-negative bacteria to combat antibiotics is drug efflux. Drug efflux pumps are usually composed of OM, periplasmic and IM components. These components interact with each other and span the entire cell envelope. One of the examples of the OM component is TolC, which can export small molecules, but is also implicated in the import of bacterial protein toxins known as bacteriocins.

1.3.1 Functional insights

TolC was initially discovered and named because the mutation of this gene is associated with the tolerance to colicin E1 (ColE1), but not to colicin K, A, E2, E3 or bacteriophage (BF23 and T6) (de Zwaig and Luria, 1967; Taylor and Trotter, 1967). Despite the identification of the gene locus of *tolC*, scientists were puzzled by its resistance to colicin E1. To understand the resistance mechanism, the transport of [^{14}C] proline through the membrane of a TolC mutant strain was measured, which confirmed the location of TolC at the OM (Morona, Manning and Reeves, 1983). This revealed that TolC was located in the OM making it accessible to ColE1 (Bhattacharyya et al., 1970). Additionally, it was later shown that the oligomeric form of TolC is required for function, likely through the formation of an import channel that allowed for insertion into the OM and transport of peptides (Benz, Maier and Gentschev, 1993). TolC can both import and export substrates. For example, TolC plays a role in the secretion of hemolysin (HlyA) (Wandersman and Delepelaire,

1990). Hemolysin is a well-studied toxin, secreted by uropathogenic and enterohemorrhagic *E. coli* and is the culprit in lysing erythrocytes (Welch et al., 1981; Thomas, Holland and Schmitt, 2014).

The role of TolC in multidrug efflux has drawn massive attention for scientists to understand it and apply it in combating AMR. Facilitating the efflux of diverse substrates, TolC can function together with four families of inner membrane transporters, namely the ATP-binding cassette (ABC) family, the major facilitator family (MFS), the small multidrug resistance (SMR) family, and the resistance-nodulation-cell division (RND) family (Saier et al., 1998; Koronakis, Eswaran and Hughes, 2004). Among these families, AcrA-AcrB, members of the RND family in *E. coli*, have been widely studied. A tripartite protein machinery is formed by TolC, periplasmic adaptor protein AcrA, and inner membrane antiporter AcrB (figure 1.2) (Rajapaksha et al., 2021; Kobylka et al., 2019). This TolC-AcrAB complex spans the entire bacterial envelope, transporting drugs from the outer leaflet of the inner membrane to the cell exterior (Aires and Nikaido, 2005; Bohnert, Karamian and Nikaido, 2010). It can pump a large variety of substrates, such as bile salts, detergents and diverse range of antibiotics, out of bacteria. Deletion of *tolC* in *E. coli* W3110 strain increased its susceptibility to a diverse range of antibiotics (Sulavik et al., 2001). Notably, at least a 4-fold increase in susceptibility was observed for several antibiotics, such as chloramphenicol, florfenicol and tetracycline.

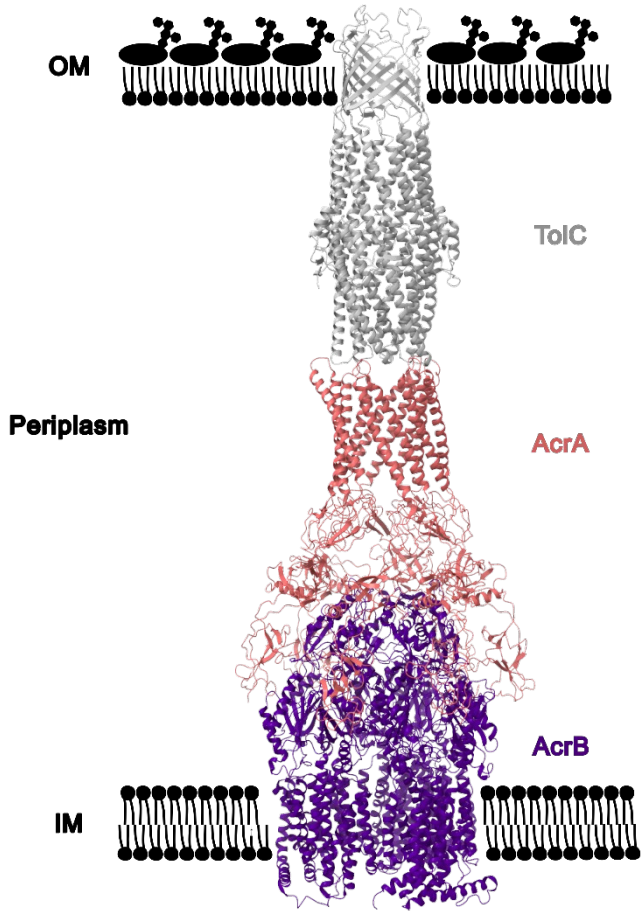


Figure 1.2 Organization of TolC-AcrA-AcrB multidrug efflux pump
TolC, AcrA and AcrB form a tunnel that spans the entire cell envelope. This protein complex can pump different substrates, including several antibiotics, out of bacteria. PDB: 5V5S

1.3.2 Structural insights

The structure of membrane reconstituted TolC was first solved to 12 Å using crystallography (Koronakis et al., 1997), and solved to a higher resolution (2.1 Å) three years later (figure 1.3) (Koronakis et al., 2000). TolC is trimeric and composed of a 12-stranded β-barrel and a periplasmic α-helical tunnel (length: 100 Å). Each monomer of TolC contributes four strands to form a 12-stranded β-barrel structure that inserts into the OM. The rest of the monomer forms a long periplasmic tunnel which is a unique feature of TolC and may contribute to important roles of TolC. The structure of the β-barrel domain of TolC also varies between species. Comparing protein sequences and structures of TolC from *E. coli* and *K. quasipneumoniae*, the sequence of the extracellular loop region in *E. coli* is longer than that in *K. quasipneumoniae*. As a result, the extracellular loops of the *E. coli* β-barrel form a smaller opening at the extracellular side (figure 1.4). The apo-state of wild type *E.coli*

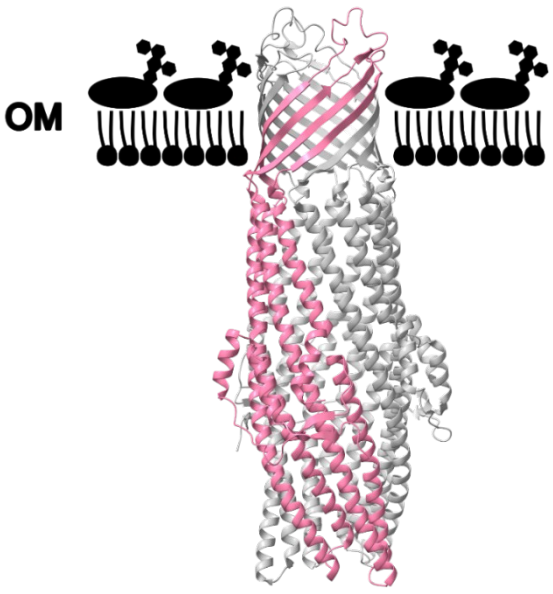


Figure 1.3 The structure of *E. coli* TolC
TolC is a trimeric OMP. Each monomer (one monomer is labelled pink) contributes four β-strands to the final 12 β-stranded barrel. The α-helices make up a periplasmic open tunnel. The relative position of the OM is shown. PDB: 1EK9

TolC adopts a closed conformation at the periplasmic end (figure 1.5) (Koronakis et al., 2000). It has been proposed that the periplasmic end of this tunnel needs to dilate to form an open-state for the transport of substrates. Mutagenesis studies (TolC Y362F, R367S), disrupting interactions between tunnel helices, led to an opened configuration of TolC (Andersen et al., 2002). Comparing closed (WT) and opened states (TolC Y362F, R367S), the periplasmic pore of TolC can increase from 11.3 $Å^2$ to 50.2 $Å^2$, expansion of the pore diameter would allow passages of different substrates through TolC (figure 1.5) (Pei et al., 2011).

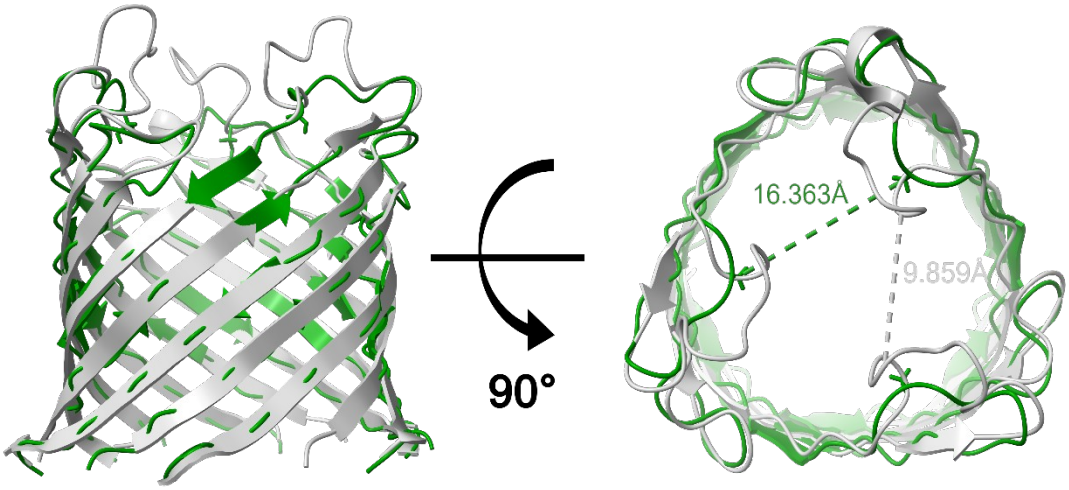


Figure 1.4 Comparison of the β-barrel domain between *E. coli* TolC and *K. quasipneumoniae* TolC
Structures of *E. coli* TolC (grey, PDB: 1EK9) and *K. quasipneumoniae* TolC (green, PDB: 7NG9) differ in their extracellular loops. β-barrel domains of TolC from two species were aligned (left). *E. coli* TolC extends its extracellular loops more away from the β-barrel domain and has a smaller opening at the extracellular side than *K. quasipneumoniae* TolC (right). The shortest distance between these loops from

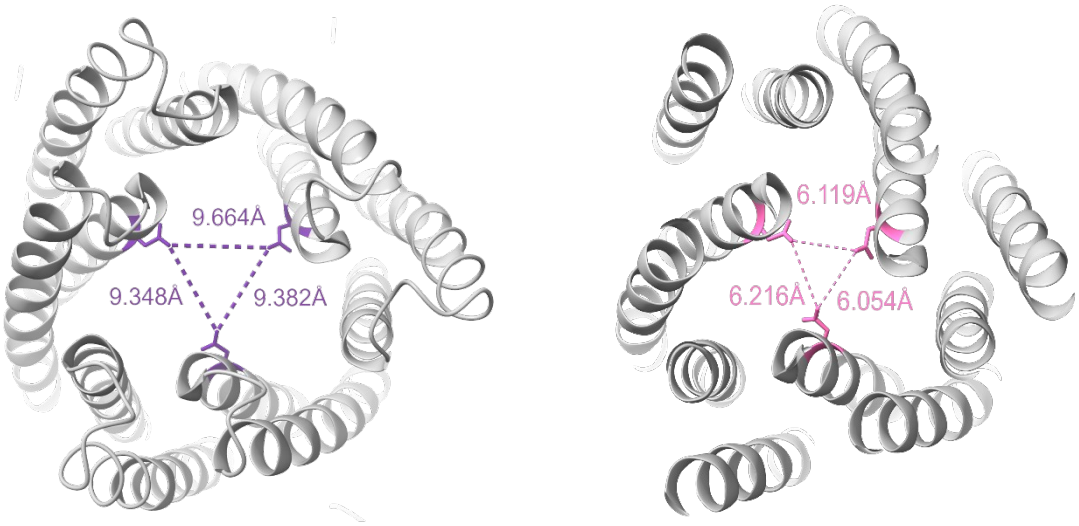


Figure 1.5 Comparison between open-state and close-state *E. coli* TolC
TolC can dilate its periplasmic end to allow passage of substrates. The interior tunnel structures of TolC, at open-state (Y362F, R367S, left, PDB: 2XMN) and close-state (WT, right, PDB: 1EK9), are shown. Distances between Asp374 residues of three monomers increase from 6.1 Å to 9.6 Å when the interactions between helices are disrupted.

Before solving the structure of the TolC-AcrAB complex, it was hypothesised that AcrB directly interacts with TolC via its TolC docking domain. However, this hypothesis proved to be inaccurate when the entire complex structure of TolC-AcrA-AcrB was solved by cryo-electron microscopy to 16 Å (Du et al., 2014) and later improved to 3.6 Å (Wang et al., 2017). No direct interaction between TolC and AcrB was observed. Instead AcrA acts as a bridge between the two proteins. Structures of other tripartite protein machineries, similar structures to TolC-AcrAB, such as the MacA-MacB-TolC complex, show a structurally conserved assembly (Fitzpatrick et al., 2017).

The TolC-AcrAB complex is largely involved in drug and small molecule efflux. Recent insights into TolC's function as a bacterial toxin importer were gained from the

structures of *E. coli* TolC in complex with ColE1 (Budiardjo et al., 2022) and *K. quasipneumoniae* TolC in complex with klebicin C (KlebC) (figure 1.6) (Housden et al., 2021). These structures of TolC-ColE1 and TolC-KlebC were solved both to 3.1 Å but in nanodisc and amphipol, respectively.

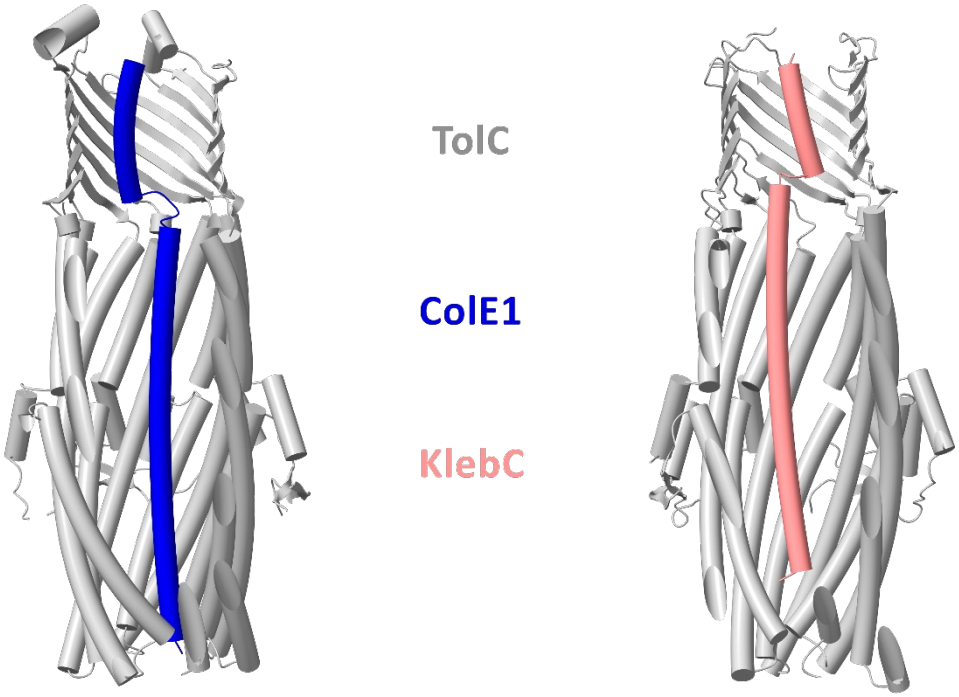


Figure 1.6 Structures of the TolC-ColE1 and TolC-KlebC complexes.
ColE1$_{46\text{-}131}$ and KlebC$_{77\text{-}151}$ have been successfully trapped in *E. coli* and *K. quasipneumoniae* TolC, respectively. ColE1 and KlebC both spread themselves throughout the tunnel of TolC unsymmetrically and only interacts with one monomer of TolC. Cutaway side view of the TolC is shown here. PDB: 6WXH and 7NG8

1.4 Cytotoxic and uptake mechanisms of bacteriocins

Within microbial communities, bacteria secrete toxins to kill competitors that compete for the same niche or nutrient source. Secreted protein toxins are called bacteriocins and are released into the environment, diffusing and binding to nearby target cells. Bacteriocins target related species by parasitizing specific OMPs. Both Gram-positive and Gram-negative bacteria can secrete bacteriocins. Gram-negative bacteriocins are named after the species from which they are secreted. For example, colicins (Col) are bacteriocins secreted by and target *E. coli*, pyocins (Pyo) target *Pseudomonas*, and klebicins (Kleb) target *Klebsiella*. Colicins were first discovered in 1925 by Gratia, and since then many different bacteriocins have been isolated and their killing mechanisms have been investigated (Gratia, 1925). Although they vary in sizes, most protein bacteriocins adopt a conserved domain organization, composed of a disordered N-terminus, receptor-binding domain, translocation domain and cytotoxic domain. The N-terminal domain is mostly disordered and is required for the transport through the OM. This is because the epitope pattern at the N-terminus decides the IM energization complex that they couple to. Bacteriocins can use two different IM systems to enter target cells and are thus classified into two groups, group A and B bacteriocins. Group A bacteriocins use the Tol system, while the group B ones use the Ton system. At the C-terminus, the cytotoxic domain causes cell death via either pore-forming or enzymatic reactions. To prevent targeting themselves, bacteria also synthesize immunity proteins (Im). Common bacteriocins are summarized in table 1.4.1.

Table 1.1 Summary of bacteriocins, adapted from (Kleanthous, 2010; White et al., 2017; Atanasković et al., 2020; Housden et al., 2021)

Bacteriocins	Outer membrane receptor	Translocator	Cytotoxic mechanism	Producing species
Group A				
ColA	BtuB	OmpF, TolQRAB	Pore-forming	*Escherichia coli*
ColE2, ColE7, ColE8 and ColE9	BtuB	OmpF, TolQRAB	DNase	*Escherichia coli*
ColE3, ColE4 and ColE6	BtuB	OmpF, TolQRAB	16S rRNase	*Escherichia coli*
ColE1	BtuB	TolC, TolQRA	Pore-forming	*Escherichia coli*
ColE5	BtuB	OmpF, TolQRAB	tRNase	*Escherichia coli*
ColN	OmpF	OmpF, TolQRA	Pore-forming	*Escherichia coli*
ColK	Tsx	OmpF, TolQRAB	Pore-forming	*Escherichia coli*
ColS4	OmpW	OmpF, TolQRAB	Pore-forming	*Escherichia coli*
GroupB				
Col5–Col10	Tsx	TolC, TonB, ExbBD	Pore-forming	*Escherichia coli*
ColIa and ColIb	Cir	Cir, TonB, ExbBD	Pore-forming	*Escherichia coli*
ColB	FepA	TonB, ExbBD	Pore-forming	*Escherichia coli*
ColD	FepA	TonB, ExbBD	tRNase	*Escherichia coli*
ColM	FhuA	TonB, ExbBD	Inhibiting peptidoglycan synthesis	*Escherichia coli*
KlebC	TolC	TonB, ExbBD	16S rRNase	*Klebsiella pneumoniae*
PyoS2	FpvAI	TonB, ExbBD	DNase	*Peudomonas aeruginosa*
PyoG	Hur	TonB, ExbBD	DNase	*Peudomonas aeruginosa*

1.4.1 Cytotoxic mechanisms of bacteriocins

Cytotoxic domains of bacteriocins kill target cells through two main mechanisms, enzymatic activity or mechanical pore-forming (table 1.4.1). Major targets for enzymatic bacteriocins are 16S rRNA, tRNA, DNA, and peptidoglycan precursors. For nuclease bacteriocins, their cytotoxic domains need to interact with nucleic acids in the cytoplasm, thus they need to translocate across the IM as well as the OM. Nuclease bacteriocins, such as ColE3 and ColD, are cleaved by FtsH, an IM AAA^{+} ATPase and protease (Chauleau et al., 2011). After cleavage, the cytotoxic domain can enter the cytoplasm. FtsH is essential for all nuclease colicins toxicity as tested in *ΔftsH E. coli* strains (Walker et al., 2007).

16S rRNase bacteriocins, such as colicin E3, cleave the 16S ribosomal RNA. A detailed mechanism has been elaborated from the crystal structure of ColE3-bound 70S

ribosome, at a post-cleavage state (Chyan Leong Ng et al., 2010). The binding of the cytotoxic domain of ColE3 does not change the overall structure of the 70S ribosome but blocks the access of A-site tRNA, release factors and elongation factors. Its cytotoxic domain cleaves the phosphodiester bond between A1493 and G1494 in 16S ribosome. This modification prevents further protein translation.

tRNases ColE5 and ColD hydrolyse different tRNAs to inhibit protein translation. ColE5 specifically targets tRNAs carrying Tyr, His, Asn and Asp, because they have a guanine at the wobble position (Ogawa et al., 1999). ColD cleaves all four Arg tRNA isoacceptors (Tomita et al., 2000). Histidine plays important roles in the catalysis of most RNases. The C-terminal His residue in ColD is essential for the specific cleavage but ColE5 does not have a histidine at its active site (Graille et al., 2004). DNase bacteriocins, such as ColE9 contains a metal-dependent endonuclease, which can cleave both single-stranded and double-stranded DNA (Maté and Kleanthous, 2004).

Among all colicins known, ColM is the only colicin that targets the peptidoglycan synthesis. It hydrolyzes peptidoglycan precursors, lipid I and lipid II, into lipid and pyrophosphoryl groups (El Ghachi et al., 2006).

Nuclease bacteriocins are synthesized and released together with their immunity proteins. Immunity proteins function by directly (tRNases) or indirectly (DNases and rRNases) occluding the active site of bacteriocins (Papadakos, Wojdyla and Kleanthous, 2012). Immunity protein, Im9, binds to the active site of the cytotoxic domain of ColE9, with high affinity ($K_D = 9.3\times10^{-17}$ M) (Wallis et al., 1995). In

comparison, the immunity protein of ColE3, Im3, fits into a cleft formed between the cytotoxic and translocation domains of ColE3 (Soelaiman et al., 2001).

For pore-forming bacteriocins, their cytotoxic domains kill target cells by forming voltage-dependent ion channels in the IM. Before interacting with the IM, the cytotoxic domain forms an α-helical three-layered bundle, composed of two hydrophobic helices surrounded by eight helices (Parker et al., 1989). An opened channel is formed by the insertion of helices into the membrane which leads to membrane depolarization and cell death (Parker et al., 1989).

1.4.2 Group A bacteriocin uptake mechanism

Despite bacteriocins differing in their cytotoxic mechanisms, they all need to cross the OM. Most group A bacteriocins need two OMPs, one outer membrane receptor and one translocation protein to facilitate their entry to periplasm (table 1.4.1). The representative example is ColE9 whose import has been studied in detail (Housden et al., 2013; Francis et al., 2021). ColE9 is a 60-kDa group A bacteriocin composed of four domains (figure 1.4.1.1). The disordered N-terminus of ColE9 forms an intrinsically unstructured translocation domain (IUTD), containing one TolB-binding epitope (TolB box) sandwiched between two OmpF-binding sites (OBS1 and OBS2). This IUTD is followed by the structured translocation (T-) domain and the receptor-binding (R-) domain (Francis et al., 2021). The cytotoxic domain is at the C-terminus. The immunity protein (Im9) binds to the cytotoxic domain and protects the producing cell from suicide. When ColE9 targets cells, its R-domain binds to BtuB, the outer membrane receptor, which forms an acute angle with the outer membrane to

assist the binding of the translocation domain to the translocator OmpF, a trimeric porin (Figure 1.4.1.2). Subsequently, ColE9 threads its intrinsically-disordered N-terminus through one pore of OmpF. The two OBS epitopes bind into two separate pores of OmpF. This places the TolB box on the periplasmic side such that it can be accessed by periplasmic TolB. Through TolB, ColE9 harnesses the energy from the PMF from other Tol-Pal system components, TolA-TolQ-TolR. The Tol system is essential for bacterial survival and mainly involved in cell division (Szczepaniak, Press and Kleanthous, 2020). Some bacteriocins, such as ColE1, can directly interact with TolA, bypassing the need for TolB. TolA is an inner membrane protein whose helical domain spans the periplasm. TolA, coupled to the proton motive force (PMF) from the inner membrane complex TolQ-TolR, facilitates the uptake of group A bacteriocins across the OM.

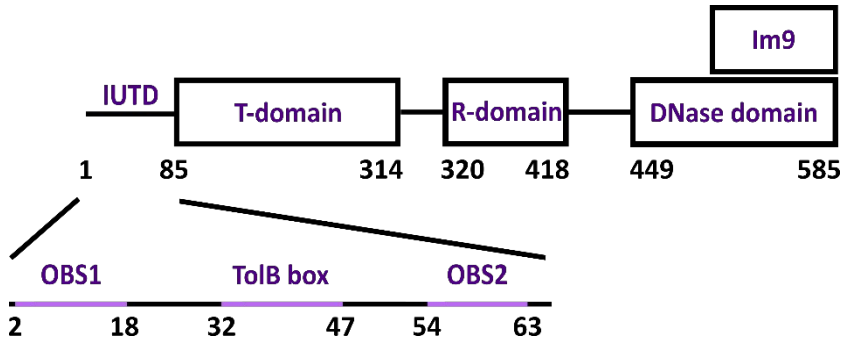


Figure 1.7 Domain organisation of ColE9
ColE9, similar to other group A bacteriocins, is composed of a disordered N-terminus and three structural domains. At its N-terminus, the intrinsically unstructured translocation domain (IUTD) contains three epitopes, two OmpF-binding sites (OBS1, OBS2) and a TolB box. This N-terminus is followed by translocation (T-), receptor-binding (R-) and cytotoxic (C-) domains.

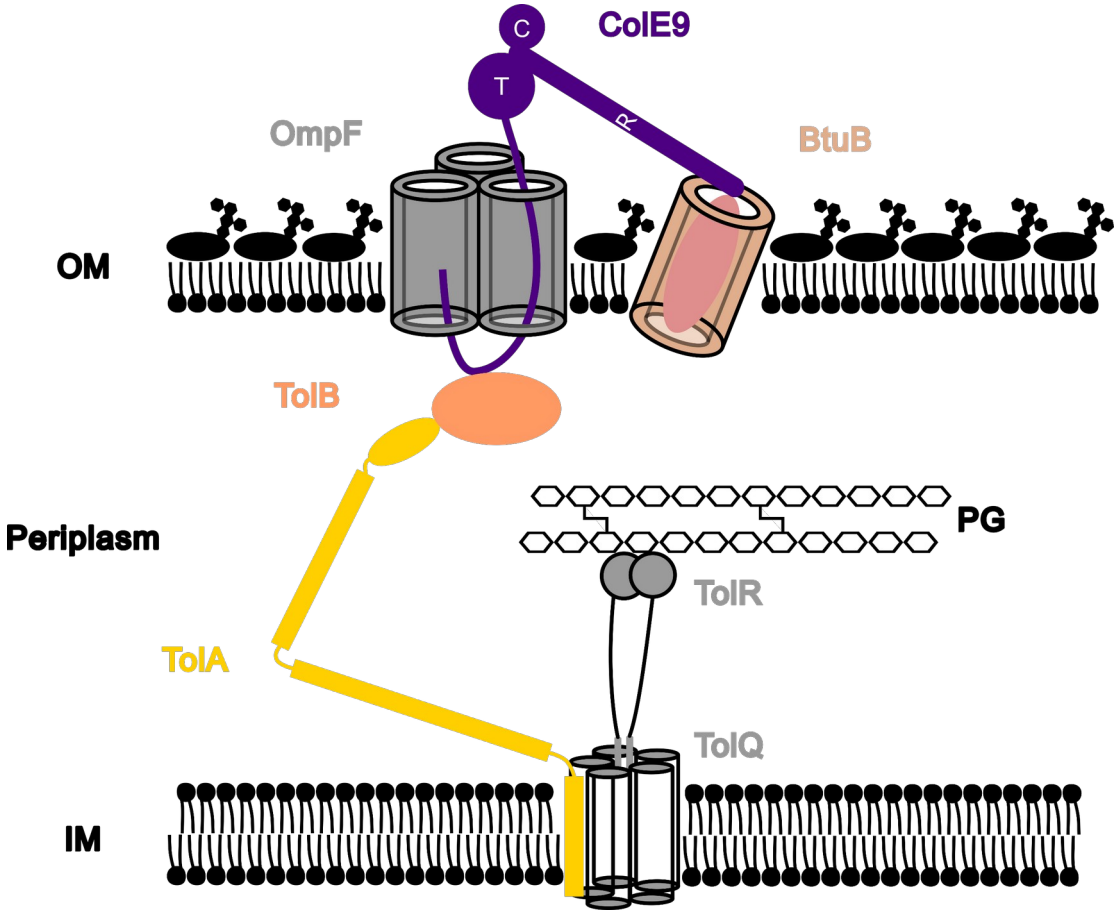


Figure 1.8 Schematic illustration of the uptake mechanism of ColE9
The structure of the ColE9 translocon (ColE9, BtuB, OmpF and TolB) was solved by cryoEM by Francis et al. (2021). A schematic cartoon of the structure is shown here. TolA is shown in its energized state to facilitate entry of ColE9 through a single subunit of the porin OmpF. The TolQ-TolR complex in the IM provides energy for the entire import of ColE9, through interacting with the IM helical domain of TolA, which extends across the periplasm to contact TolB bound to ColE9.

1.4.3 Group B bacteriocin uptake mechanism

Bacteria require a vast number of metabolites from the environment. The Ton system is a PMF-driven system required for nutrient uptake in bacterial cells. The system consists of the inner membrane ExbB-ExbD, which forms the stator complex that is coupled to PMF, and TonB, which spans the periplasm (Noinaj et al., 2010). Acquisition of scarce nutrients from the environment requires specific OMPs, TonB-dependent transporters (TBDTs). They couple to the Ton system and use energy from the PMF to import these scarce ligands, namely iron-siderophores, cobalamin, carbohydrates and divalent cations (Ratliff, Buchanan and Celia, 2022; Schauer, Rodionov and de Reuse, 2008). This process is hijacked by bacteriocins to enter into cells (figure 1.4.2.3). Compared to the narrow but open tunnels within porins, TBDTs, such as BtuB, FepA and FhuA, have globular plug domains, which occludes the 22-stranded β-barrel, preventing passive diffusion of substrates (figure 1.4.2.1 and 1.4.2.2) (Noinaj et al., 2010).

Structures of many TBDTs have been solved, either in an apo-state or a substrate-bound state. The binding of some substrates leads to a conformational change in the TonB box motif, at the N-terminus of plug domain, which transits the TonB box from a folded orientation within the β-barrel to an unfolded state exposing to periplasm (Merianos et al., 2000; Cadieux et al., 2003). The exposed TonB box binds the C-terminal globular domain of TonB (Ratliff, Buchanan and Celia, 2022). Interactions between TonB and TBDTs have been studied via biochemical, structural and biophysical methods. Crystal structures of FhuA-TonB and BtuB-TonB from *E. coli* were both solved in 2006 (figure 1.4.2.1 and 1.4.2.2) (Shultis et al., 2006; Pawelek et

al., 2006). Both structures showed that β-strands of TonB interact with the TonB box to form a parallel strand-swapped structure. A K_D within a nanomolar range was measured between BtuB, FhuA and TonB (Freed et al., 2013; Khursigara et al., 2003). Atomic force microscopy (AFM) has been used to pull plug domain out of the β-barrel of BtuB through TonB (Hickman et al., 2017). This led to the discovery of a force-labile subdomain of the plug domain, which unfolds and opens a tunnel for ligand transport. The mechanical stability of the TonB-TonB box complex is high enough to support this partial unfolding. These experimental results support the previous molecular simulation data, which postulated a pulling model for TonB-dependent plug domain removal (Gumbart, Wiener and Tajkhorshid, 2007; Ratliff, Buchanan and Celia, 2022). However, the OM of the Gram-negative bacteria is an ATP- and PMF-free environment, the energy for the entry needs to come from IM. Through association with the ExbBD complex in the IM, TonB transduces force from the PMF to energize plug removal. ExbB forms a pentameric pore in the IM within which the ExbD dimer resides (Celia et al., 2019). This 5:2 stoichiometry is also the same as MotAB and TolQR complexes, the homologues of ExbBD complex (Deme et al., 2020).

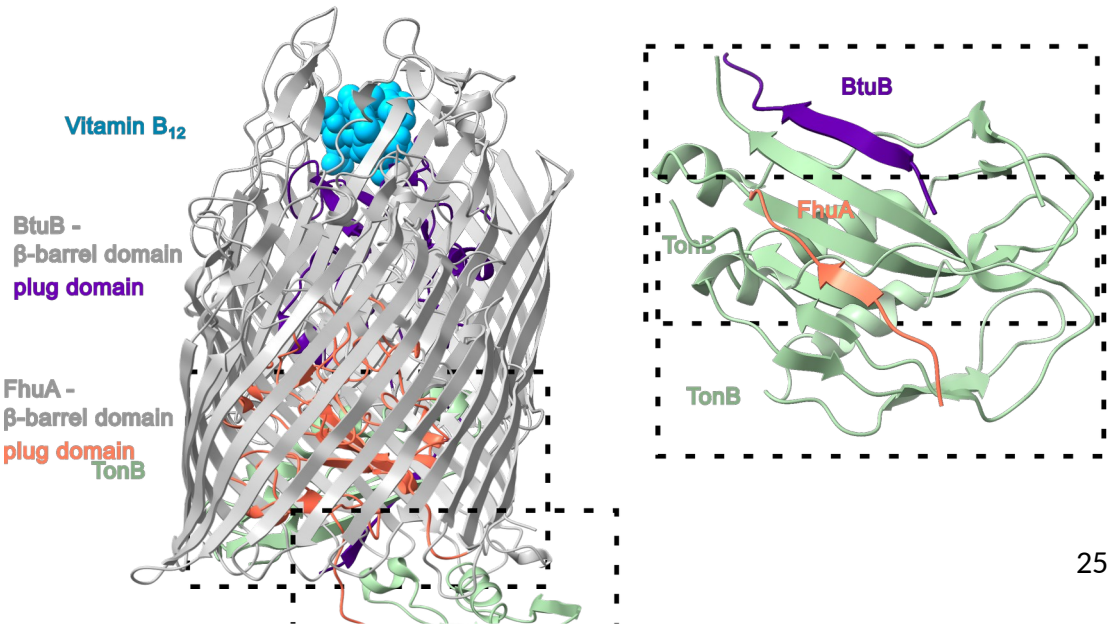


Figure 1.9 Structure of substrate bound BtuB-TonB
The crystal structure of vitamin B_{12}-bound BtuB and TonB is shown (left). The N-

Group B bacteriocins hijack the Ton system to enter target cells (figure 1.4.2.3). One well studied group B bacteriocin is pyocin S2 (PyoS2), an endonuclease secreted by *P. aeruginosa*, that binds to FpvAI, a TBDT (White et al., 2017). PyoS2 can outcompete the natural substrate of FpvAI, ferripyoverdine (Fe-Pvd) for receptor binding through a mimicry mechanism. TonB first interacts with the TonB box on the plug domain of FpvAI and opens the passage for PyoS2. The disordered N-terminus of PyoS2 threads through FpvAI and interacts with TonB. Association of TonB with the ExbBD complex

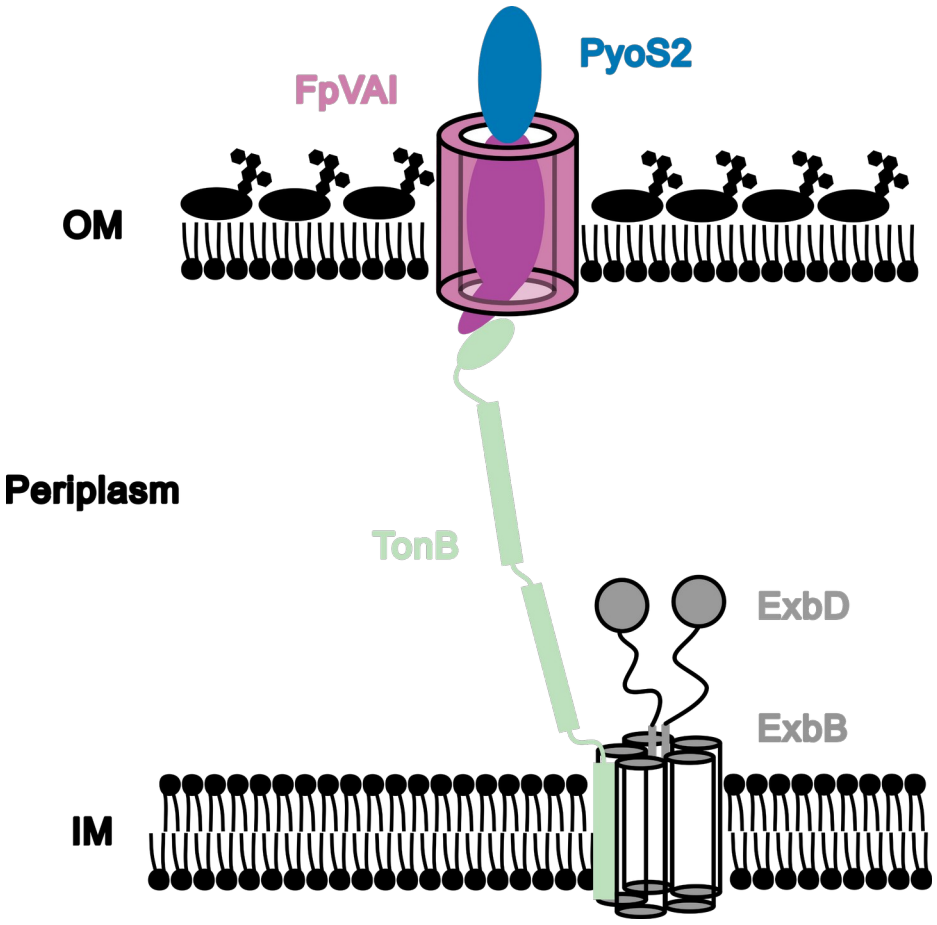
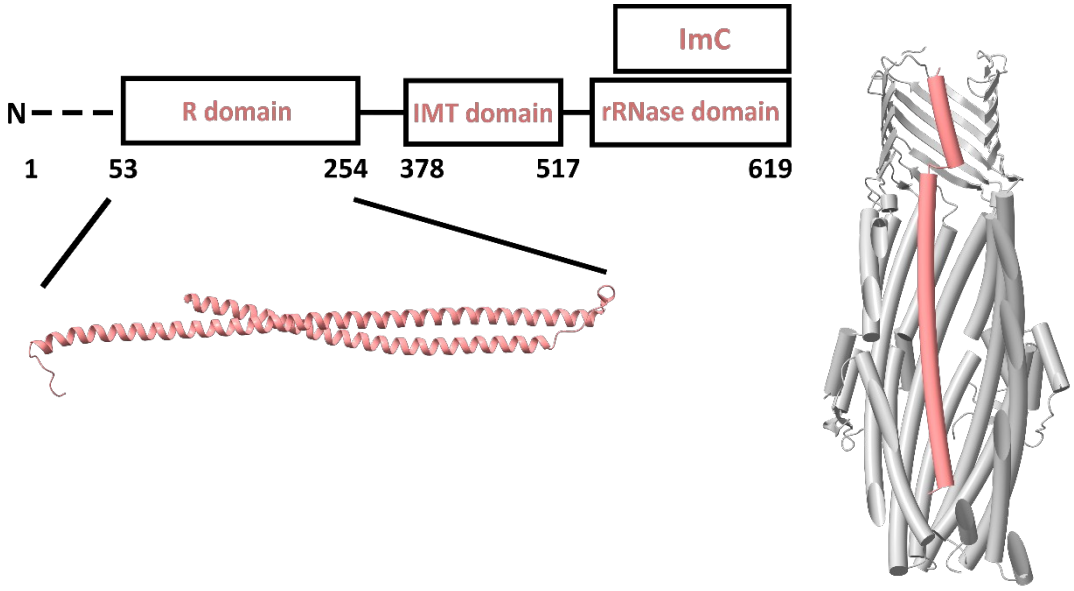


Figure 1.11 Schematic illustration of the uptake of group B bacteriocin
The crystal structure of PyoS2-bound FpvAI was shown here as a schematic cartoon (White et al., 2017). This hijack of PyoS2 mimics the binding of the natural substrate of FpVAI, which recruits TonB. The N-terminus of TonB interacts with the ExbBD complex at the IM, which provides energy for the complete entry of PyoS2.

urgently required to tackle the emergence of its drug-resistance. The import of KlebC requires OMP TolC (figure 1.4.2.4) (Housden et al., 2021). As described previously (section 1.3), TolC is an OMP, composed of a β-barrel domain and a periplasmic open tunnel. KlebC unfurls its hairpin-structured R domain to enter the channel of TolC and then expose its N-terminus to TonB in the periplasm. The structure of *K. quasipneumoniae* $KlebC_{77\text{-}151}$-TolC has been solved in amphipol (figure 1.4.2.4).



Truncation of the C-terminus of KlebC ($KlebC_{1\text{-}254}$) does not affect binding to TolC, with a K_D ~ 35 nM measured by ITC. However, the deletion of the N-terminus (residues 1-50) abolishes killing activity. Mutagenesis study, targeting Met16, Val17 and Leu19 residues at the N-terminus also abolishes the killing activity, which leads to the identification of these residues as the likely TonB box. The detailed molecular

mechanism of how KlebC, TolC and TonB coordinate to drive import into cells is however unknown.

1.5 Therapeutic uses of bacteriocins

Since bacteriocins are natural toxins secreted for intraspecies competition, their potential uses as new antibiotics have huge potential. Bacteriocins, produced by Gram-positive bacteria, have been used in the food industry and agriculture. Nisin, a bacteriocin naturally produced by certain Group N *Streptococcus*, is widely used as a food preservative (Field et al., 2023). The diversity of bacteriocins make them applicable to a wide range of uses. For example, colicin-like bacteriocins are able to target plant pathogens (Grinter, Milner and Walker, 2012). The application of them in agriculture has the potential to increase crop yield and help reduce the global food shortage crisis.

Considering the narrow spectrum of Gram-negative bacteriocins, they are powerful and selective tools for targeting infectious human pathogens. Moreover, Gram-negative bacteriocins have unique cytotoxic mechanisms and have evolved within bacterial community, which decreases the possibilities for developing resistance against them. To date, no Gram-negative bacteriocins have been approved for clinical uses. Different companies are looking at developing colicin-like bacteriocins to treat infectious diseases. For example, GangaGen is developing klebicin to target diseases, caused by multidrug-resistant *K. pneumoniae* and NOMAD bioscience has discovered nine klebicins that show promising killing activities against *Klebsiella* species from

clinical isolates (Denkovskienė et al., 2019; Denkovskiene, Misiunas and Ražanskienė, 2020). A new company, GLOX Therapeutics (founded by Professors Colin Kleanthous and Daniel Walker), is also focusing on the translational application of bacteriocins. However, in order to administer Gram-negative bacteriocins safely and efficiently as antibiotics, their uptake mechanisms still require further elucidation.

Aims of this work

The OM of Gram-negative bacteria is the first barrier in bacterial warfare. Gram-negative bacteria can prevent antibiotic damage using drug efflux pumps, but can also be targeted by bacteriocins. Biochemical, biophysical, structural and computational methods have been used to characterise functions and structures of

TolC. The TolC-AcrAB multidrug efflux pump can pump small molecules out of cells. TolC can also be hijacked by both group A bacteriocin (ColE1) and group B bacteriocin (KlebC). The entry of KlebC through TolC has been previously studied (Housden et al., 2021). However, the molecular mechanism of how KlebC uses the Ton system to gain entry into cells remains to be determined.

This work will continue investigating the uptake mechanism of KlebC, involving TolC and the Ton system. Biophysical and biochemical methods will be used to characterise the KlebC-TolC interaction *in vitro*. To directly observe the complex and rationalise biochemical data, single particle cryogenic electron microscopy (Cryo-EM) will be used to determine the ternary KlebC translocon.

Chapter 2. Materials and Methods

2.1 Microbiology and molecular biology

All plasmids used in this study are summarised in table 2.1. To clone full length KlebC-E9/Im9 with a M29S mutation, whole plasmid PCR was performed. 1 ng/µl of the full length KlebC-E9/Im9 plasmid (Housden et al., 2021) was transformed into 20 µl DH5α cells (NEB), and DNA was extracted from a single colony using a Monarch

Plasmid DNA Minipret kit (NEB). Primers were designed (F1 and R1 in table 2.2), with ATG to AGC codon mutation. PCR reaction was carried out in the thermal cycler (Bio-Rad), using following parameters: 98°C for 2 min; 16 cycles of 98°C for 15 s, 45°C for 30 s, 72°C for 5 min; 72°C for 5 min. The PCR product was digested with DpnI (NEB) for 2 h at 37°C and was transformed into chemically competent commercial NEB5α (DE3) cells (NEB). Colonies were selected, and plasmid DNA was extracted from 5 mL overnight culture (LB) using Monarch Plasmid DNA Minipret kit (NEB). The sequence of each clone was confirmed via sanger sequencing using T7 promoter primer (table 2.2). To generate the KlebC-E9/Im9, E26A/E27A/M29S mutant, the KlebC-E9/Im9 M29S DNA was mutated by whole plasmid PCR following the same protocol as described above, using primer F2 and R2, with GAGGAA to GCGGCG codon mutation, instead (table 2.2).

Table 2.1 Summary of all plasmids used in this study

Plasmid	Insert	Parent vector	Antibiotic resistance	Source
pNGH322	Full length KlebC-E9/Im9	pET21a	Ampicillin	(Housden et al., 2021)
pNGH323	$KlebC_{1-254}$	pET21a	Kanamycin	(Housden et al., 2021)
pNGH337	$KlebC_{51-254}$	pET24a	Kanamycin	(Housden et al., 2021)
pNGH184	*E. coli* $TonB_{33-240}$-Im9	pQE2-Im9	Ampicillin	Lab stock[a]
pNGH365	Met16Ser, Val17Gly, Leu19Gly full-length KlebC-E9/Im9	pET21a	Ampicillin	(Housden et al., 2021)
pNGH317	*K. quasipneumoniae* TolC	pET24a	Kanamycin	(Housden et al., 2021)
pQT1	*K. quasipneumoniae* $TonB_{156-248}$	pET21a	Ampicillin	This study
pQT2	Glu26Ala, Glu27Ala, Met29Ser full-length KlebC-E9/Im9	pET21a	Ampicillin	This study
pMSP1D1G1	MSP1D1G1	pET28a	Kanamycin	Addgene[b]

a: This was a gift from Dr. Nicholas Housden in the lab

b: pMSP1D1G1 was a gift from Michael Marty (Addgene plasmid # 97325; http://n2t.net/addgene:97325 ; RRID:Addgene_97325)

To clone the *Klebsiella quasipneumoniae* $TonB_{156-248}$ construct, *K. quasipneumoniae* QMP M1-977 genomic DNA was extracted from a 5 mL overnight culture (LB) using a Monarch Plasmid DNA Minipret kit (NEB). Genomic DNA was used as the template to amplify target gene by PCR, using F3 and R3 (table 2.2). PCR products were visualised on a 1% (w/v) agarose gel (running for 30 min and 100 V) stained with SYBR safe dye. Following successful identification of target fragment, products were purified using PCR clean-up kit (NEB). Prior to assemble fragments, the pET21a vector was digested at 37°C for 1 h with NdeI (20 units per µg of DNA, NEB) and XhoI (20 units per µg of DNA, NEB) and visualised on a 1% (w/v) agarose gel (run for 30 min and 200 V). Linearized vector band was gel extracted and purified using Monarch DNA gel extraction kit (NEB). DNA concentrations were determined by absorbance at 260 nm. Fragments were assembled into pET21a vector using Gibson assembly. A ratio of 2:1 (insert : vector) was mixed with BuilderHiFi DNA assembly master mix (NEB). The mixture was incubated at 50°C for 15 min and 1 µl of the mixture was transformed into 25 µl of chemically competent commercial NEB5α (DE3) cells (NEB). Colonies were selected, and plasmid DNA was extracted from 5 ml overnight culture (LB) using Monarch Plasmid DNA Minipret kit (NEB). The sequence of each clone was confirmed via sanger sequencing using T7 promoter primer (table 2).

Table 2.2 Summary of primer information used in this study

Name	Sequence (5'-3')	Annealing temperature
F1	GATTACCGTGCTCGCCGCCTCTCCGTTCTC	45
R1	GAGAACGGAGAGGCGGCGAGCACGGTAATC	
F2	GATTACCGTGCTCGCCGCCTCTCCGTTCTC	45

R2	GAGAACGGAGAGGCGGCGAGCACGGTAATC	
F3	GAAGGAGATATACATATGATGACCGTCACTGCCCCG	55
R3	GGTGGTGGTGGTGCTCGAGGCCCTGAAAATAAAGATTCTCGTTAATCTCGAC	
T7	TAATACGACTCACTATAGGG	na

2.2 Expression and purification of soluble proteins

Soluble proteins with C-terminal hexahistidine tags including; KlebC, MSP1D1G1, *E. coli* $TonB_{33-240}$-Im9 (Ec $TonB_{33-240}$) and *K. quasipneumoniae* $TonB_{156-248}$ (Kq $TonB_{156-248}$) were purified using affinity chromatography followed by size exclusion chromatography (SEC). Plasmids were transformed into chemically competent BL21 cells (NEB). Cells were grown in LB, supplemented with either 50 µg ml^{-1} kanamycin or 100 µg ml^{-1} ampicillin (according to table 1.1) to an OD_{600} of ~0.7. A final concentration of 1 mM isopropyl ß-D-1-thiogalactopyranoside (IPTG) was added to induce protein expression. KlebC constructs were induced for 4 h at 28°C. MSP1D1G1 was induced for 3 h at 37°C. Ec $TonB_{33-240}$ was induced at 20°C overnight. Kq $TonB_{156-248}$ was induced at 20°C overnight. Cell pellets were harvested by centrifugation at 4200 × rpm (JLA-8.1000 rotor) for 12 min at 4°C, before re-suspending in 50 mM Tris-HCl, pH 8.0, 500 mM NaCl, 8 mM imidazole and 1 mM PMSF. Cells (35 mL) were lysed by sonication (MiSonix S-4000) (amplitude: 50, process time: 90 s, pulse-on time: 3 s, pulse-off time: 7 s). Supernatant containing soluble protein was collected after centrifugation (16000 × g for 30 min at 4°C) and filtered (0.45 µm) before loading on to a 5 ml HisTrap FF column (Cytiva), using an ÄKTA prime (Cytiva). Bound proteins were eluted with an imidazole gradient from 8 to 500 mM over 12 column volumes (CV). Fractions corresponding with an increased absorbance at 280 nm were analysed on SDS-PAGE gels and those containing

proteins of interest were collected and dialysed overnight at 4°C into 25 mM Tris-HCl, pH 7.5, 150 mM NaCl, using a 3.5 kDa MWCO membrane (SpectrumLabs). Proteins were syringe filtered (0.45 µm). KlebC$_{1-254}$, KlebC$_{51-254}$, *E. coli* TonB$_{33-240}$, *K. quasipneumoniae* TonB$_{156-248}$ and MSP1D1G1 were loaded onto a HiLoad 26/600 Superdex 75 pg column (Cytiva), equilibrated in SEC buffer (25 mM Tris-HCl, pH 7.5, 150 mM NaCl). Full-length KlebC-E9/Im9 was loaded onto a HiLoad 26/600 Superdex 200 pg column (Cytiva), equilibrated in SEC buffer. Fractions containing proteins of interest were determined by SDS-PAGE gels. Purified proteins were stored at -20°C.

2.3 Expression and purification of TolC

A plasmid encoding TolC-His$_6$ was transformed into T7 Express *lysY/Iq* competent *E. coli* cells (NEB). Cells were grown in LB supplemented with 50 µg ml^{-1} kanamycin, to an OD$_{600}$ of 1. IPTG was added to a final concentration of 1 mM to induce TolC expression. Cells were maintained at 18°C, with shaking (140 rpm) overnight. Cells were harvested by centrifugation (4200 rpm (JLA-8.1000) for 12 min at 4°C) and pellets were re-suspended in 10 mM Tris-HCl, pH 8.0, 0.25% (w/v) LIS, 1 mM PMSF. Cells were lysed via sonication (MiSonix S-4000) amplitude: 50, process time: 90 s, pulse-on time: 3 s, pulse-off time: 7 s (2x). Cell debris was removed by centrifugation (5,000 × g, 15 min at 4°C) and the supernatant was collected and centrifuged again at higher speed (200,000 × g for 1 hr at 4°C) to pellet the total membrane fraction. Membrane pellet was homogenised in 10 mM Tris-HCl, pH 8, 5 mM EDTA, 2% (w/v) β-OG and soluble proteins were isolated in supernatant following centrifugation (200,000 x g for 1 h at 4°C. Soluble membrane fraction was syringe filtered (0.45 µm) and loaded onto a 5 ml HisTrap Excel column (Cytiva) equilibrated in binding buffer

(25 mM Tris-HCl, pH 7.5, 150 mM NaCl, 1% (w/v) β-OG) using an ÄKTA prime (Cytiva). Bound materials were eluted using an imidazole gradient (0-100%) from binding to elution buffer (50 mM Tris-HCl, pH 8.0, 500 mM NaCl, 500 mM imidazole, 1% (w/v) β-OG) over 12 CVs. Fractions corresponding to an increase in absorbance at 280 nm were collected and analysed by SDS-PAGE. Fractions containing TolC were concentrated to 5 ml and syringe filtered (0.45 µm) and loaded on a HiLoad 16/600 Superdex 200 pg column (Cytiva), equilibrated in 25 mM Tris-HCl, pH 7.5, 150 mM NaCl, 1% (w/v) β-OG. Fractions associated with an increased absorbance at 280 nm were analysed by SDS-PAGE to assess protein purify. Purified protein was stored at -20°C.

2.4 Lyophilization of Kq TonB$_{156-248}$

Kq TonB$_{156-248}$ (4 ml, 86 µM) was dialysed overnight at 4°C in milliQ H_2O, using a 6 – 8 kDa MWCO membrane (SpectrumLabs). Dialysed protein was frozen in liquid nitrogen and stored at -80°C. Lyophilization was performed in a benchtop lyophilizer (Virtis), over four days.

2.5 SDS-polyacrylamide gel electrophoresis (SDS-PAGE)

Protein samples were separated using SDS-PAGE. Samples were mixed with 4x SDS-PAGE loading dye (200 mM Tris-HCl, pH 6.8, 8% (w/v) SDS, 0.4% (w/v) bromophenol blue, 40% (w/v) glycerol, 0.56 M β-mercaptothanol) and were boiled at 98°C for 10 min. Boiled samples and unstained protein MW marker (Pierce, 26610) were run on

12% or 15% (w/v) gels, composed of 5% (w/v) bis-acrylamide stacking gel and 12% (w/v) or 15% (w/v) bis-acrylamide resolving gel. Gel was run in Tris-glycine running buffer (0.25 M Tris, 1% (w/v) SDS, 1.92 M glycine) at 35 mA for 25 min. Gels were stained with 0.2% (w/v) Coomassie Brilliant blue R250 (Pierce) in 10% (v/v) acetic acid and 10% (v/v) ethanol for 30 min at RT with shaking. Destaining was performed in 10% (v/v) acetic acid and 10% (v/v) ethanol overnight at RT with shaking. Silver staining was performed on destained gels using the ProteoSilver silver stain kit (Sigma), following manufacturer's instructions.

2.6 Protein concentration quantification

Protein concentrations in this study were all calculated using the Beer-Lambert law:

$$A = \varepsilon c l$$

Where A is the absorbance of the sample at 280 nm, ε is the molar extinction coefficient (M^{-1} cm^{-1}), c is the concentration of proteins (M^{-1}), and l is the optical path length (cm). The absorbance was measured using BioSpectrometer (Eppendorf), with a path length of 1 cm. The molar extinction coefficients were calculated using the ProtParam tool (Expasy).

2.7 Size exclusion chromatography – multi-angle light scattering (SEC-MALS)

Fractions from both peaks during the purification of Ec $TonB_{33-240}$ were pooled separately. A two-fold dilution series (from 1 mg/ml to 0.25 mg/ml) of both samples were prepared. SEC-MALS experiment was performed on Wyatt Dawn HELEOS-II 8-angle light scattering detector and Wyatt Optilab rEX reflective index monitor linked

to a Shimadzu HPLC system, comprising LC-20AD pump, SIL-20A autosampler and SPD20A UV/Vis detector, by Dr. David Stauton. The samples were loaded onto a Superdex 200 HR10/30 column, equilibrated in 25 mM Tris-HCl, pH 7.5, 150 mM NaCl. Data were analysed using ASTRA (6.1.1.17).

2.8 KlebC activity assay

Killing assays to determine the cytotoxicity of KlebC constructs were performed against either *K. quasipneumoniae* QMP M1-977 or *E. coli* MG1655. Cells were grown at 37°C in 5 ml of LB until an OD_{600} of 0.6 was reached. 0.2 ml of cells were added to 5 ml of molten LB agar 0.75% (w/v) and poured over LB agar plate (1.5%) in a 90-mm petri dish. 5 µl of KlebC was spotted onto plates in a dilution series (4-fold) starting from 16 µM. Plates were incubated at 37°C overnight. KlebC cytotoxicity was qualitatively assessed by analysis of clearance zones on the plates.

2.9 Isothermal titration calorimetry (ITC)

Titrations were performed on an iTC200 isothermal titration calorimeter (Malvern instruments), with proteins dialysed overnight at 4°C into 25 mM Tris-HCl, pH 6.0 or 7.5, 150 mM NaCl using a dialysis membrane (MWCO = 6-8 kDa, SpectrumLabs). $KlebC_{1-254}$ was used in the syringe at various concentrations (140 µM – 800 µM), and Kq $TonB_{156-248}$ or Ec $TonB_{33-240}$ in the cell were used at various concentrations (14 µM – 140 µM). Injection was lasted for 5s, with 180s spacing between each injection. Data were fitted to a single set of identical sites binding model (Origin 7).

2.10 Analytical SEC

Samples (500 µL) were incubated at 4°C overnight and centrifuged at 21,000 × g for 5 min in a table top centrifuge (Eppendorf, 5425) before loading onto SEC columns (0.5 ml/min, absorbance measured at 230 nm, 280 nm or 647 nm, fraction size of 0.2 ml) for analysis.

KlebC and TonB were mixed in an eqimolar ratio (28 µM) and analysed using a superdex 75 increase 10/300 column equilibrated in buffer containing 25 mM Tris-HCl, pH 7.5, 150 mM NaCl. KlebC and TolC were mixed in an eqimolar ratio (5 µM) and analysed using a Superdex 200 increase 10/300 column equilibrated in buffer containing 25 mM Tris-HCl, pH 7.5, 150 mM NaCl, 1% (w/v) β-OG. Where required proteins were exchanged into 25 mM Tris-HCl, pH 7.5, 150 mM NaCl, 1% (w/v) β-OG prior to experiment, using a HiTrap desalting column (Cytiva) on ÄKTA pure (Cytiva). The presence of protein aggregates was determined by the absorbance of the sample at 320 nm, using the BioSpectrometer (Eppendorf).

2.11 Preparation of KlebC-TolC-TonB ternary complexes in nanodisc

1-palmitoyl-2-oleoyl-glycero-3-phosphocholine (POPC, Avanti Polar Lipids) was dissolved in 25 mM Tris-HCl. pH 7.5, 150 mM NaCl, 0.5 mM EDTA, 100 mM sodium cholate, to a final concentration of 50 mM. POPC (50 mM) was mixed with MSP1D1G1 (387 µM) at five molar ratios (10:1, 20:1, 30:1, 50:1 and 100:1) for optimisation. For the assembly of TolC-nanodiscs, a ratio of 50:1:0.2 (POPC:MSP1D1G1:TolC) was used. Sample volumes were made to 500 µL using buffer containing 25 mM Tris-HCl, pH 7.5, 150 mM NaCl, 1% (w/v) β-OG. Bio-Beads SM-2 (BioRad), at a concentration of 10 mg beads per mg of β-OG, was incubated

with samples for 2 h at room temperature, before leaving at 4°C overnight. Beads were pelleted by centrifugation (21,000 x g for 2 min) and supernatant was extracted. To ensure removal of detergent, samples were buffer exchanged into 25 mM NaCl, pH 7.5, 150 mM NaCl, using a HiTrap column (Cytiva) attached to an ÄKTA pure (Cytiva). Fractions associated with absorbance at 280 nm were pooled, centrifuged to pellet precipitate (21,000 xg 5 minutes), and loaded (500 µL) onto a Superose 6 Increase 10/300 GL column (Cytiva), equilibrated in 25 mM Tris-HCl, pH 7.5, 150 mM NaCl. A flow rate of 0.5 ml/min was used and absorbance was monitored at 230 nm to track protein elution. Corresponding protein containing fractions (200 µL) analysed by SDS-PAGE to identify species present. Fractions containing TolC were pooled and protein concentration was calculated as described in chapter 2.4.

$KlebC_{1\text{-}254}$ (270 µM) was added to TolC-nanodisc (6.3 µM) at a molar ratio of 2:1 (KlebC:TolC) and incubated at room temperature for 2 h. Ec $TonB_{33\text{-}240}$ (564 µM) was added to the mixture at a molar ratio of 10:1 (TonB:KlebC), and incubated at room temperature for 2 h, and then 4°C overnight. The mixtures were centrifuged (21,000 × g for 2 min), and loaded onto Superose 6 Increase 10/300 GL column (Cytiva), equilibrated in 25 mM Tris-HCl pH 7.5, 150 mM NaCl. Fractions from each peak were analysed by SDS-PAGE to identify species present. Gels were stained using both Coomassie blue and silver staining. Fractions with correct components were collected and concentrated using spin concentrator (50 kDa MWCO, 4,200 xg, 18°C, 10 min). Protein concentration was calculated as described in chapter 2.4.

For the crosslinked KlebC$_{1-254}$-TolC-Kq TonB$_{156-248}$ complex, all components were exchanged to 25 mM HEPES, pH 7.5, 150 mM NaCl prior to mixing. KlebC$_{1-254}$-TolC-nanodisc was prepared as previously described. Kq TonB$_{156-248}$ (800 µM) was incubated with the complex for 10 min. Formaldehyde was added to a final concentration of 1% (v/v) and crosslinking was allowed to proceed on ice for 30 min. 1M Tris-HCl, pH 7.5, was added to give a final concentration of 100 mM to quench the crosslinking. Sample was subsequently processed as above, however SEC column was equilibrated in 25 mM HEPES, pH 7.5, 150 mM NaCl.

2.12 Grid preparation for single-particle cryogenic electron microscopy

KlebC$_{1-254}$-TolC-Ec TonB$_{33-240}$ (0.8 and 1.9 mg/ml) and crosslinked KlebC$_{1-254}$-TolC-Kq TonB$_{156-248}$ (0.7 mg/ml) ternary complexes (3 µL) were applied to Quantifoil R1.2/1.3 Cu 300 mesh grids using a Mark VI vitrobot (Thermo Fisher). Grids were glow-discharged for 70 s with current of 15 mA (Leica EM ACE200). A blot time of 2s and a blot force of 10 were used with the chamber at 8°C and 100% humidity. Grids were imaged on Talos Arctica microscope (Thermo Fisher). EPU software was used for Atlases and snapshot collection at different defocus levels (-1 to -2).

2.13 Alphafold 2 prediction and structural analysis

Sequences of KlebC$_{1-254}$ and *K. quasipneumoniae* TonB were entered into the Alphafold 2_mmseqs2 Google Colab platform (Jumper et al., 2021; Mirdita et al., 2022). Structures were predicted with default settings.

Chapter 3. The import of KlebC through the Ton system

Bacteriocins are effective antimicrobials used in bacterial warfare. The molecular details of bacteriocin uptake, particularly for group B bacteriocins utilizing the Ton system for import, still require further investigation. One important step for group B bacteriocin import is the association with TonB in the periplasm, allowing the system

to become energised by the PMF. The interaction is thought to mimic that between TBDTs and TonB for which structural and biochemical data exists.

To investigate Ton-dependent bacteriocin import, we characterised the import of KlebC, a group B bacteriocin from *Klebsiella* (Housden et al., 2021). KlebC enters cells by threading through TolC, an essential drug efflux pump in the outer membrane of most Gram-negative bacteria. Exposure of the disordered N-terminal domain into the periplasmic space is required for killing in a Ton-dependent manner (Housden et al., 2021). The cytotoxic domain of KlebC is similar to that of ColE3, which is a 16S rRNase. It was considered that KlebC also kills target cells using a similar mechanism (chapter 1.4.1).

3.1 Purification of KlebC constructs

In order to assess the toxicity of KlebC against different bacterial strains, the protein was first expressed and purified. KlebC residues 1-517 C-terminally fused to a ColE9 (E9) DNase, co-purified with immunity protein (Im9) (full-length KlebC), $KlebC_{1-254}$ and $KlebC_{51-254}$ constructs were purified as described by Housden et al. (2021). In short, proteins were expressed in *E. coli* BL21 cells and affinity purified via C-terminal hexahistidine tags, followed by size exclusion chromatography (figure 3.1). Protein purity was assessed following SEC by SDS-PAGE (figure 3.1). The SEC elution profile for full-length KlebC showed two peaks, one at 171 ml and a second at 252 ml. SDS-PAGE analysis confirmed that full-length KlebC eluted in the first peak with none detected in the second peak, which is just excess Im9 (figure 3.1 A). Some Im9 remains associated with the E9 domain fused to KlebC and runs as a second band on

the SDS-PAGE due to dissociation upon SDS treatment (figure 3.1 A). KlebC$_{1-254}$, eluted as a single peak from the SEC column (figure 3.1 B). SDS-PAGE confirmed that the protein was pure (Figure 3.1 B). For KlebC$_{51-254}$, a major peak and a minor peak were detected (figure 3.1 C). Purified KlebC$_{51-254}$ was detected in the major peak. Purified proteins were used in subsequent experiments.

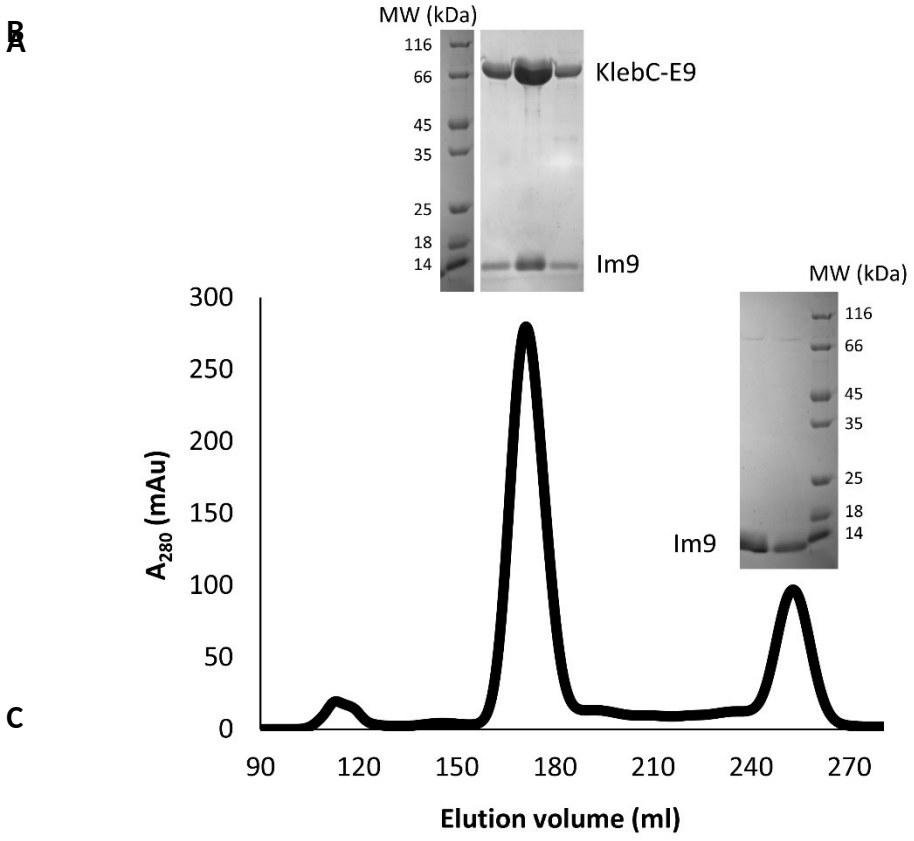


Figure 3.1 KlebC with a C-terminal His$_6$ tag was purified following affinity and size exclusion chromatography

Proteins after nickel affinity chromatography and dialysis were further purified through SEC (A – full-length KlebC, B – KlebC$_{1-254}$, C – KlebC$_{51-254}$). HiLoad 26/600 Superdex 200 pg column was used to purify full-length KlebC. HiLoad 26/600 Superdex 75 pg column was used to purify KlebC$_{1-254}$ and KlebC$_{51-254}$. The same buffer (25 mM Tris-HCl, pH=7.5, 150 mM NaCl) was used to equilibrate columns. Boiled fractions from peaks were run on 12% SDS-PAGE gels, stained with Coomassie blue (insets shown above absorbance peaks), to check their molecular weights (full-length KlebC-E9: 70.37 kDa; Im9: 10.65 kDa; KlebC$_{1-254}$: 28.29 kDa; KlebC$_{51-254}$: 23.56 kDa).

3.2 Cytotoxic activities of KlebC constructs

To confirm cytotoxic activities of purified KlebC constructs, plate killing assays were performed. For these assays, bacterial strains are plated in soft-LB agar and bacteriocin is spotted on it at decreasing concentrations. Following overnight incubation at 37°C, areas of clearance are indicative of toxin induced killing. Full-length KlebC was effective against both *K. quasipneumoniae* QMP M1-977 (figure 3.2 A) and *E. coli* MG1655 (figure 3.2 D), killing down to 0.98 nM and 1 µM, respectively. The cytotoxic activity of full-length KlebC against *K. quasipneumoniae* QMP M1-977 was three orders of magnitude higher than that against *E. coli* MG1655. This has been observed previously (Housden et al., 2021) and is proposed to result from different structures of TolC in each of the strains (figure 1.3.1.3). The more closed conformation of the β-barrel structure in *E. coli* due to longer extracellular loop sequences, likely impairs binding and thus import of KlebC. As expected, truncated forms of KlebC ($KlebC_{1-254}$ and $KlebC_{51-254}$), which lack the cytotoxic domain, showed no killing activity on either species (figure 3.2 B, C, E, F). These data confirm that purified proteins have similar activities to those previously described (Housden et al., 2021).

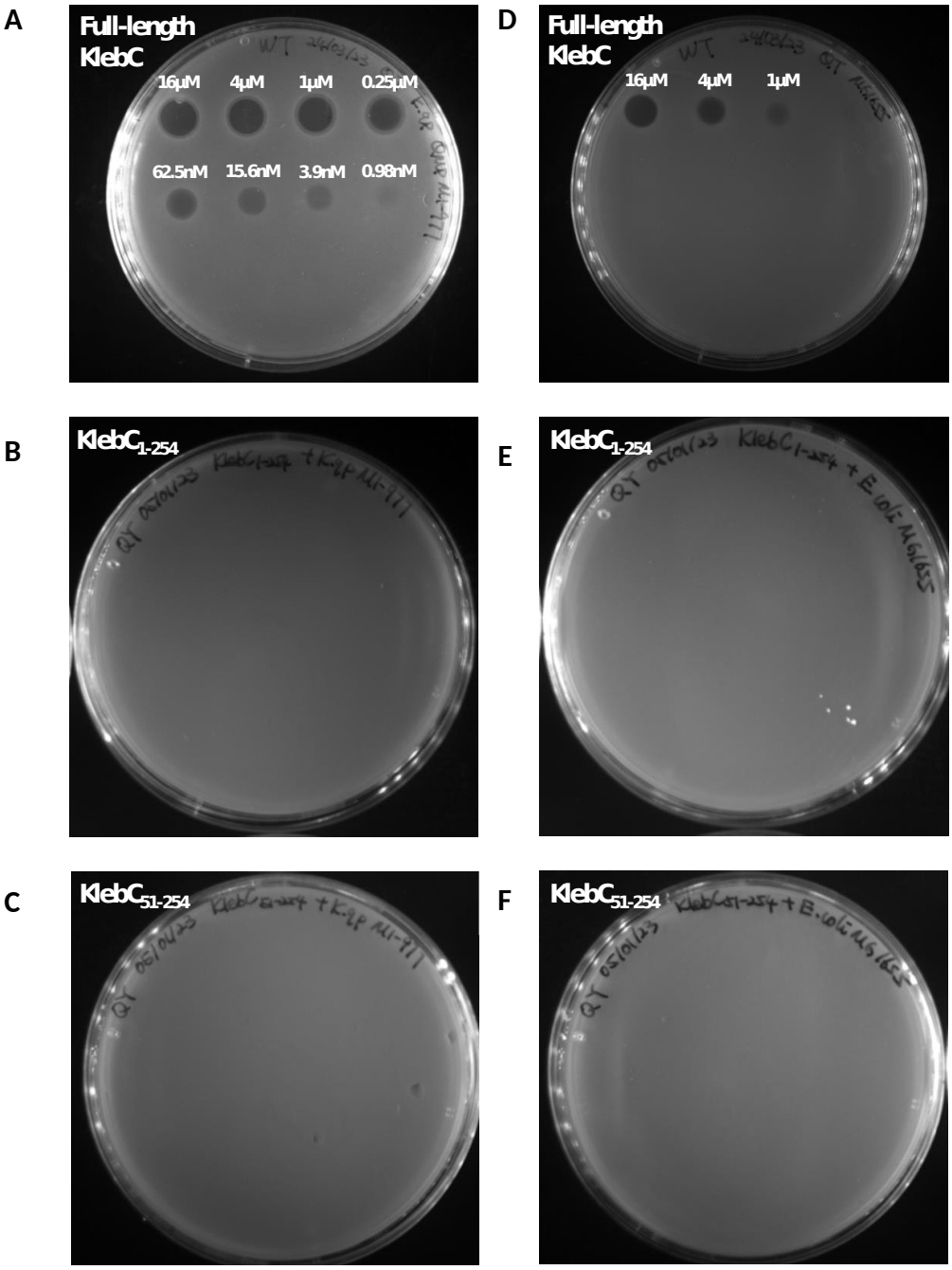


Figure 3.2 Full-length KlebC is active against both *K. quasipneumoniae* and *E. coli*

A dilution series (4-fold) from 16 μM to 3.81 pM of purified KlebC proteins; full-length KlebC (A, D), $KlebC_{1-254}$ (B, E), and $KlebC_{51-254}$ (C, F)) were spotted (5 μL) on agar plates, containing *K. quasipneumoniae* QMP M1-977 (A-C) or *E. coli* MG1655 (D-E). After overnight incubation at 37°C, zones of clearance were assessed to evaluate killing activities. Full-length KlebC showed killing activities against both *K. quasipneumoniae* and *E. coli*. $KlebC_{1-254}$ and $KlebC_{51-254}$ were inactive against both strains. n = 2

3.3 *tonB* cloning and TonB purification

Housden et al. (2021) showed that KlebC killing is dependent on TonB. Taken together with the killing assay data in section 3.2. It suggests that KlebC can associate with TonB from both *E. coli* and *K. quasipneumoniae* to enter into cells. To further rationalise these data, we aimed to determine the molecular details of how KlebC binds TonB. For biochemical analysis, *K. quasipneumoniae* TonB was cloned into a pET21a expression vector for purification. *E. coli* $TonB_{33-240}$-Im9 (Ec $TonB_{33-240}$) construct was already available in the lab.

3.3.1 *K. quasipneumoniae tonB* cloning

The genome of *K. quasipneumoniae* QMP M1-977 was downloaded from European Nucleotide Archive (Sample Accession: SAMEA882192, SRA accession: ERS011989). One TonB sequence (contig000119, ID=5235_2#4_02687) was annotated in the genome. To check the accuracy of this annotation, the sequence of *K. pneumoniae* TonB (Entry: P45610) was downloaded from Uniprot. Two protein sequences were aligned, which showed the same sequence. This TonB sequence from *K. quasipneumoniae* QMP M1-977 was applied to design primers which amplify the sequence and add His_6-tag at its C-terminus. The forward primer was deigned to incorporate NdeI restriction site prior to the 5' of the *tonB* sequence. The reverse primer was designed to incorporate XhoI, TEV site and His_6-tag after the 3' of the *tonB* sequence. Attempts to insert the gene fragment into pET21a using Gibson assembly failed. Independent controls confirmed that the protocol was successful for incorporation of another PCR fragment into the vector, thus suggesting that PCR amplification of the Kq *tonB* was a problem. Amplifying a gene from genomic DNA

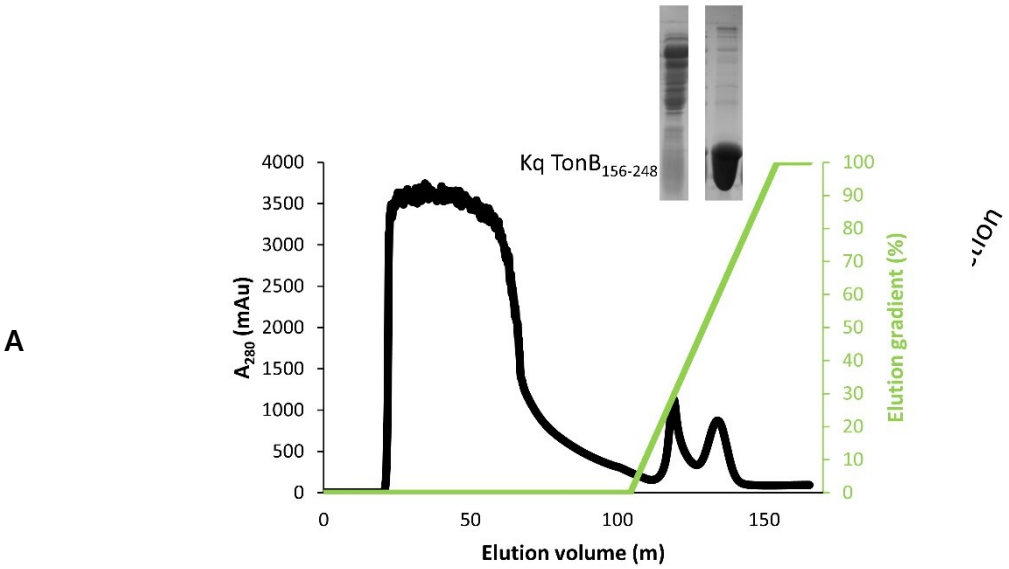
resulted in many non-specific products. This is likely due to the repeating sequence within domain II. To overcome this, primers were designed to amplify only domain III (residue 156-248) of Kq TonB. PCR amplification and Gibson assembly were successfully used to generate an expression construct of Kq $TonB_{156-248}$ with a C-terminal His-tag.

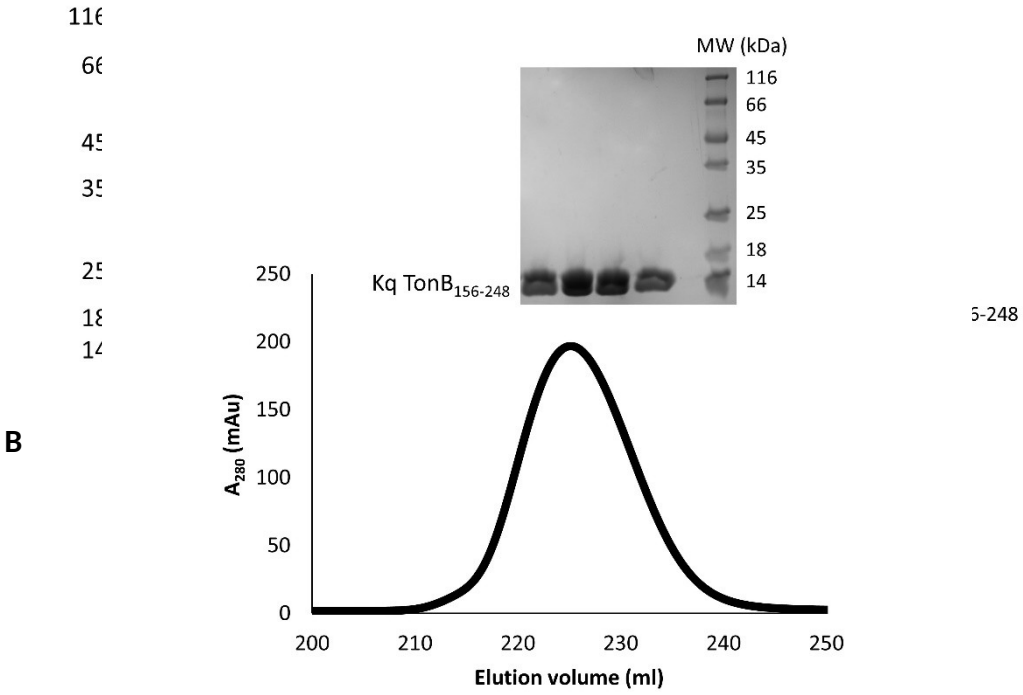
3.3.2 Kq $TonB_{156-248}$ purification

The previously developed purification method for Ec $TonB_{33-240}$ was applied to isolate Kq $TonB_{156-248}$ expressed in *E. coli* (Shultis et al., 2006). Following the transformation of expression plasmid into BL21 cells, induction conditions were trialled to assess protein expression. Comparison of two expression conditions; 33 ℃ for 5h and 33 ℃ overnight, using SDS-PAGE revealed that the majority of Kq $TonB_{156-248}$ remained in the cell pellet after lysis when protein was expressed at 33 ℃. This suggested that proteins were aggregated in inclusion bodies (figure 3.3 A). Reduction of the expression temperature to 20 ℃, resulted in an increased yield of TonB in the soluble fraction (figure 3.3 B). Nickel affinity chromatography, followed by SEC, was successfully used to isolate pure protein (figure 3.4 A, B). Gradient (imidazole) elution of Kq $TonB_{156-248}$ from the nickel resin resulted in two absorbance (280 nm) peaks. SDS-PAGE analysis confirmed that Kq $TonB_{156-248}$ was present in the second

Figure 3.3 Optimisation of of Kq $TonB_{156-248}$ expression in BL21 (DE3) *E. coli* Cells
(A) Different induction times were tested to determine optimal conditions for maximising soluble Kq $TonB_{156-248}$. Cells were grown in LB to an OD_{600} of 0.7. A sample was taken (1 mL) prior to induce TonB expression with 1 mM IPTG. Cells were harvested and lysed by sonication. The insoluble (pellet) fraction was separated from soluble protein (lysate) by centrifugation (16000 x g, 15 min, 4 ℃). (B) The induction temperature was decreased to 20 ℃ and the appearance of inclusion bodies was tested again on the gel.

peak, with weakly bound contaminant proteins eluting in the first peak (figure 3.4 A). Application of Kq TonB$_{156-248}$ to Superdex 75 pg column gave a single symmetrical peak (figure 3.4 B). Two closely positioned gel bands were observed, which results from running small proteins on 15% SDS-PAGE gels (figure 3.4 B). At the bottom of the same gel, the molecular weight marker also run as two bands instead of one.



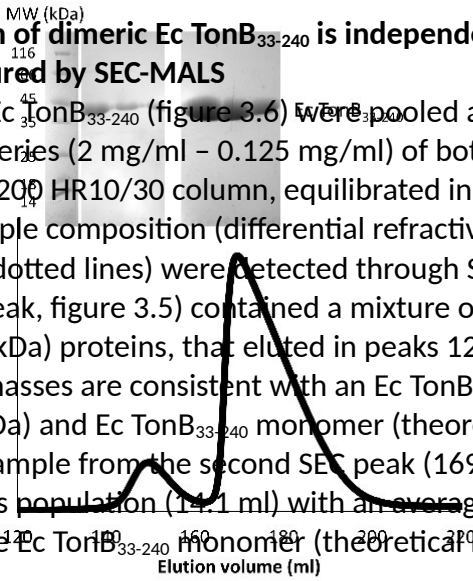


3.3.3 Ec TonB$_{33-240}$ purification

For comparative binding studies, the purification of Ec TonB$_{33-240}$ was performed as

It has been reported in the literature that the C-terminal domain of Ec TonB can form dimers *in vitro* (Jiri Koedding et al., 2004). Analysis of samples from both peaks by SEC-MALS (figure 3.6) confirmed that Ec TonB$_{33-240}$ eluting at 149.5 ml in peak 1 is in fact a dimeric form (theoretical MW = 66.06 kDa, experimental MW = 78.5 kDa) of the protein (figure 3.6 A). However, it cannot exclude the possibility that the dimeric Ec TonB is because of overexpression and does not exist *in vivo*. The molecular weight of the sample did not change across the dilution series indicating that dimer formation was independent of concentration. For the species within the second peak, the major species in solution was monomeric Ec TonB$_{33-240}$ (theoretical MW = 33.03 kDa, experimental MW = 32.2 kDa) as confirmed by SEC-MALS (figure 3.6 B). Monomeric Ec TonB$_{33-240}$ was used for future studies.

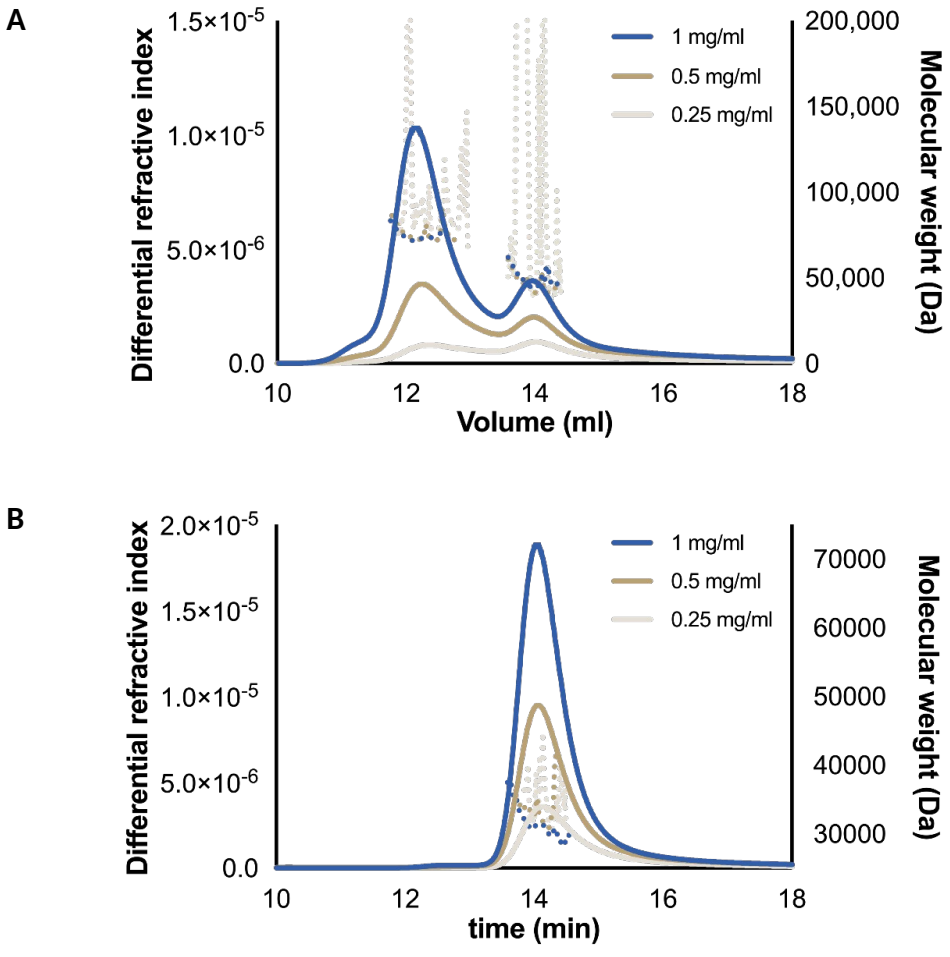
Figure 3.6 The formation of dimeric Ec TonB$_{33-240}$ is independent of concentration, as measured by SEC-MALS



Two separate peaks for Ec TonB$_{33-240}$ (figure 3.6) were pooled and analysed by SEC-MALS. A 2-fold dilution series (2 mg/ml – 0.125 mg/ml) of both samples were loaded onto a Superdex 200 HR10/30 column, equilibrated in 25 mM Tris-HCl, pH 7.50, 150 mM NaCl. Sample composition (differential refractive index – solid lines) and molecular weights (dotted lines) were detected through SEC-MALS. Samples from peak 1 (149.5 ml peak, figure 3.5) contained a mixture of high MW (78.5 kDa) and low MW (48.3 kDa) proteins, that eluted in peaks 12.2 ml and 14.1 ml, respectively (A). These masses are consistent with an Ec TonB$_{33-240}$ dimer (theoretical MW: 66.1 kDa) and Ec TonB$_{33-240}$ monomer (theoretical MW: 33.0 kDa), respectively. The sample from the second SEC peak (169.6 ml, figure 3.5) contained a homogenous population (14.1 ml) with an average of MW: 32.2 kDa, which corresponds to the Ec TonB$_{33-240}$ monomer (theoretical MW: 33.0 kDa).

Figure 3.5 Purification of Ec TonB$_{33-240}$

After nickel affinity chromatography and dialysis, Ec TonB$_{33-240}$ was further purified by SEC using a HiLoad 26/600 S75 pg column, equilibrated in 25 mM Tris-HCl, pH 7.50, 150 mM NaCl. Two elution peaks were detected and fractions from two peaks were evaluated on a 12% SDS-PAGE gel confirmed that Ec TonB$_{33-240}$ was present in both peaks.



3.4 *In vitro* complex formation between KlebC$_{1-254}$ and TonB

To investigate the interaction between KlebC and TonB *in vitro*, proteins were mixed and complex formation was tested using analytical SEC. Analytical SEC allows for comparison of protein sizes, thus can be used to detect complex formation relative to single protein controls. The formation of a KlebC-TonB complex results in an increased molecular weight, which can be observed by analytical SEC as a peak shift towards a lower elution volume. Both crystal structures of BtuB-TonB and FhuA-TonB show a stoichiometry of 1:1 (figure 1.4.2.1, 1.4.2.2). Therefore it was assumed that interactions between KlebC and TonB would adopt a similar mechanism. KlebC$_{1-254}$ lacking its C-terminal domain that is not required for interacting with TonB (Housden et al., 2021), was mixed with Kq TonB$_{156-248}$ and Ec TonB$_{33-240}$ separately in a 1:1 ratio. Individual proteins were also prepared at the same concentration and total sample volume. Control samples eluted as single peaks at an elution volume of 9.64, 10.36 and 9.08 ml for KlebC$_{1-254}$, KlebC$_{51-254}$, and Ec TonB$_{33-240}$, respectively. Mixing KlebC$_{1-254}$ and Ec TonB$_{33-240}$ resulted in a peak shift to 8.89 ml indicating that a larger species has been formed in this sample relative to controls (figure 3.7 A). SDS-PAGE analysis of fractions from the mixture peak confirmed that both KlebC and TonB were present, indicative of complex formation. As predicted, the mixture of KlebC$_{51-254}$ and Ec TonB$_{33-240}$ resulted in elution profiles aligned with single protein controls (figure 3.7 B). This was also confirmed by SDS-PAGE where only a single protein was detected in each peak from the mixture trace. These confirm that the N-terminal 50 residues of KlebC are essential for the interaction with Ec TonB$_{33-240}$.

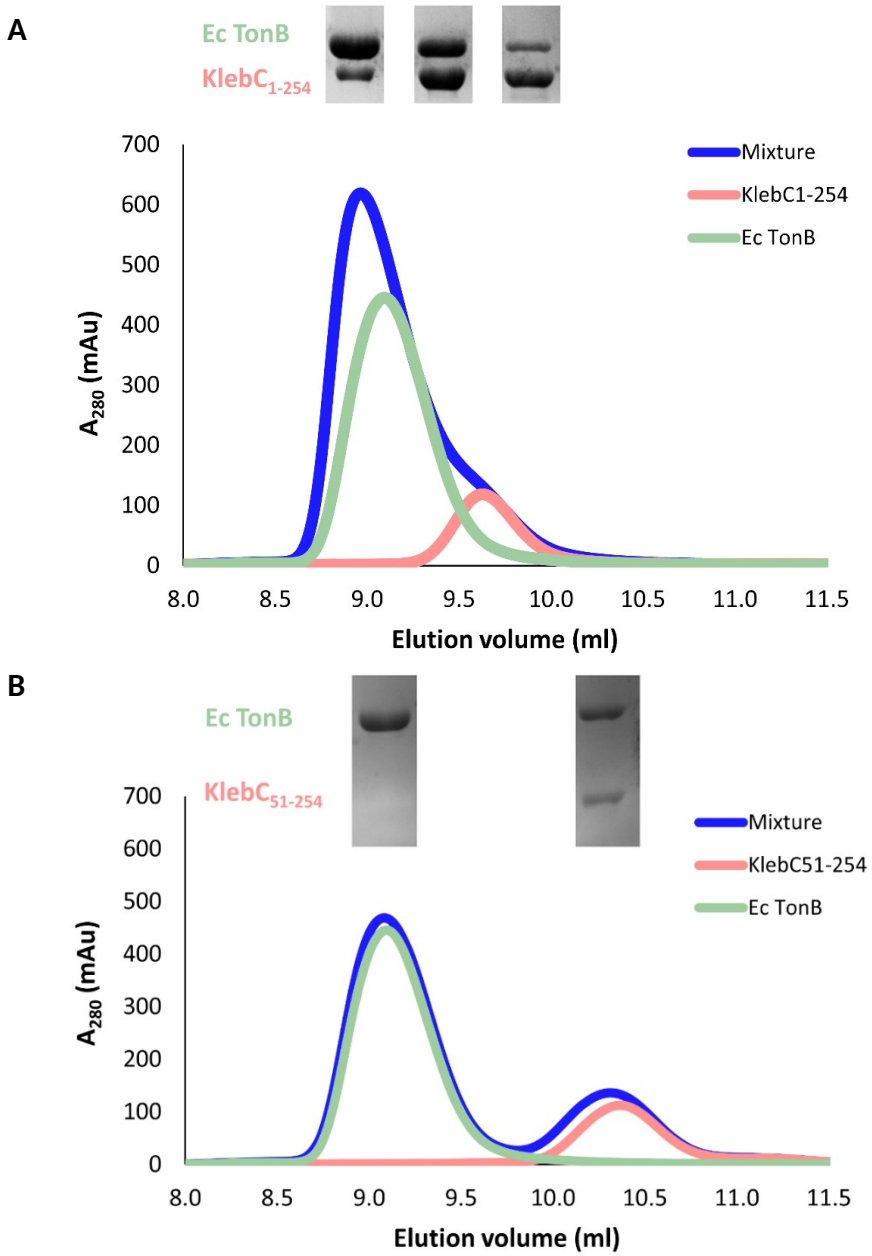


Figure 3.7 Analytical SEC confirms that Ec TonB$_{33-240}$ forms a complex with KlebC$_{1-254}$ but truncation of the N-terminus impairs complex formation

Ec TonB$_{33-240}$ (28 µM) was incubated overnight at 4°C with either KlebC$_{1-254}$ (28µm, A) or KlebC$_{51-254}$ (28 µM, B). The mixture (0.5 ml) was run (0.5 ml/min) on a Superdex 75 Increase 10/300 GL column, equilibrated in 25 mM Tris-HCl, pH 7.50, 150 mM NaCl (blue trace). Individual protein controls (Ec TonB$_{33-240}$ – green trace, KlebC – pink trace) were run separately. Traces from different runs were overlaid. Fractions from different sections of the mixture trace were run on 12% SDS-PAGE gels, stained with Coomassie blue. (A) The mixture trace eluted at 8.89 ml, earlier than individual protein controls. Combining with two protein bands at the start of the mixture trace measured by SDS-PAGE, this peak shift indicated the formation of the binary complex. (B) There is no peak shift of the mixture trace and fractions only contained one protein, shown as one protein band detected by SDS-PAGE. No complex formed in the negative control.

To test if Kq TonB$_{156-248}$ forms a complex with KlebC$_{1-254}$, samples were mixed and analysed as described above (chapter 2.10). Unlike the KlebC$_{1-254}$ – Ec TonB$_{33-240}$ mixture no peak shift was observed (figure 3.8). Proteins eluted as two separate peaks containing either KlebC$_{1-254}$ or Kq TonB$_{156-248}$ suggesting that no complex could be detected under these conditinons.

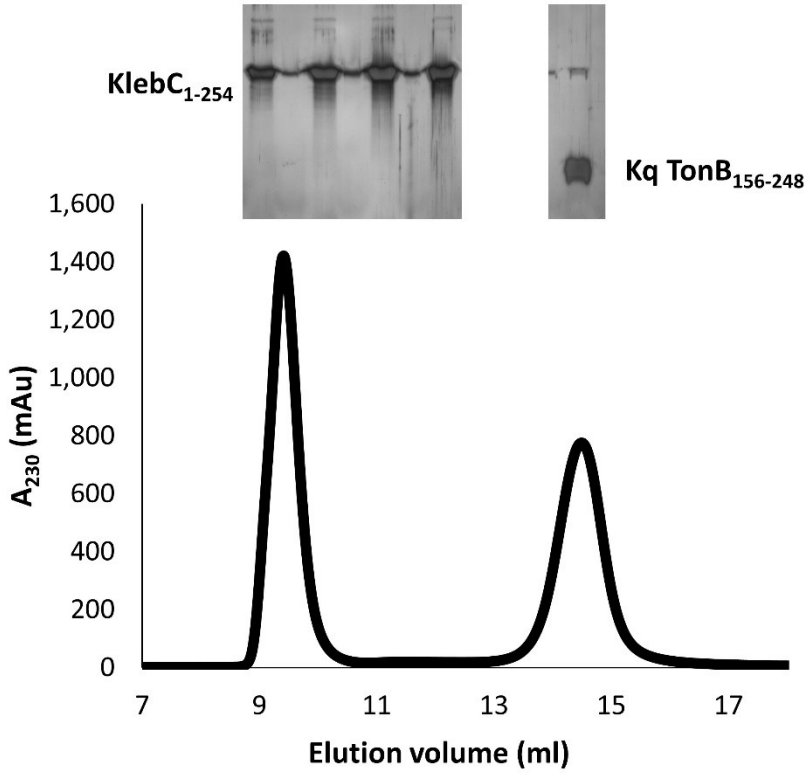


Figure 3.8 Kq TonB$_{156-248}$ does not form a complex with KlebC$_{1-254}$ as determined by analytical SEC
Kq TonB$_{156-248}$ (28 µM) was incubated overnight at 4°C with KlebC$_{1-254}$ (28 µM). The mixture (0.5 ml, blue trace) was run (0.5 ml/min) on a Superdex 75 Increase 10/300 GL column, equilibrated in 25 mM Tris-HCl, pH 7.50, 150 mM NaCl. Fractions from both peaks were run on a 15% SDS-PAGE gel. The gel was stained with Coomassie blue first and then silver. Only the gel after silver staining is shown here. Fractions from each peak only contained one protein, shown as one protein band detected by SDS-PAGE. No complex formed between Kq TonB$_{156-248}$ and KlebC$_{1-254}$.

3.5 Thermodynamic characterisation of the KlebC-TonB complex by ITC

If the interaction between Kq $TonB_{156-248}$ and $KlebC_{1-254}$ was weak, it is feasible that the complex dissociates over the SEC column. Therefore, to rationalise analytical SEC data, binding affinity between Kq $TonB_{156-248}$ and $KlebC_{1-254}$ was measured by ITC. Proteins were buffer matched. $KlebC_{1-254}$ (160 µM) was injected into Kq $TonB_{156-248}$ (16 µM) and an exothermic reaction, as indicated by heats of dilution, was observed (figure 3.9 A). No heat change was observed when 160 µM $KlebC_{1-254}$ was injected into buffer (figure 3.9 A). Data were fitted to a single site 1:1 binding model giving a K_D of 8.7 µM. An averaged K_D of 6.02 µM (standard deviation = 3.08 µM) was observed over three independent runs. The maximum heat change measured from these reactions were 0.10 µcal/sec, providing noisy data and increasing errors on K_D calculations.

To overcome this, higher protein concentrations were used to increase the signal-to-noise ratio. Titration of 800 µM $KlebC_{1-254}$ into 40 µM Kq $TonB_{156-248}$ resulted in a calculated K_D of 66.2 µM (figure 3.9 B, C). This is a relatively weak K_D that explains why no complex formation was observed by analytical SEC (figure 3.8). Higher concentrations of both proteins and chemical crosslinking would stabilise more complex, to be assessed by analytical SEC.

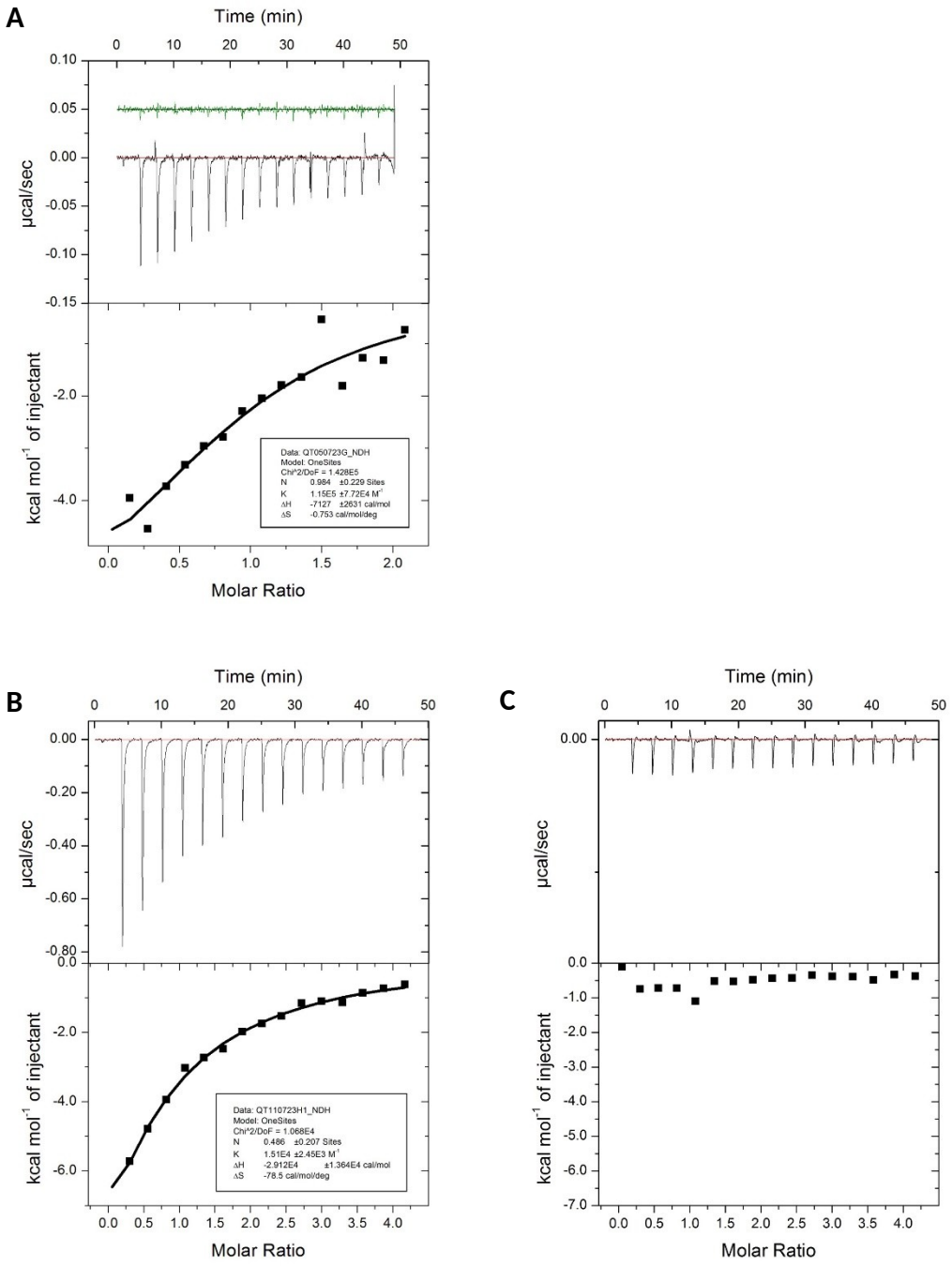


Figure 3.9 ITC confirms a weak complex formation between Kq TonB$_{156-248}$ and KlebC$_{1-254}$ at pH 7.5

(A) Representative ITC results (n = 3) of injection of 160 µM KlebC$_{1-254}$ into 16 µM Kq TonB$_{156-248}$ and the associated heat change. Both proteins were in 25 mM Tris-HCl, pH 7.5, 150 mM NaCl buffer. Baseline data were subtracted following the injection of 160 µM KlebC$_{1-254}$ into buffer only (green line). Data were fitted to a single site binding model. (B) ITC results increasing concentrations to inject 800 µM KlebC$_{1-254}$ into 40 µM Kq TonB$_{156-248}$. Data were fitted to a one to one binding model. (C) The corresponding control injecting of 800 µM KlebC$_{1-254}$ into buffer was also performed.

To independently validate analytical SEC results, the binding affinity beween KlebC$_{1-254}$ and Ec TonB$_{33-240}$ was measured by ITC. Proteins were buffer matched. KlebC$_{1-254}$ (300 µM) was injected into Ec TonB$_{33-240}$ (20 µM) (Figure 3.10 A). At pH 7.5, no heat change indicative of binding, was detected. Increasing protein concentrations to 400 µM KlebC$_{1-254}$ and 40 µM Ec TonB$_{33-240}$ (Figure 3.10 B) did not result in binding. The pH of buffer can cause different protonation states of residues therefore to test the effect of pH on KlebC – TonB interactions, a buffer with a low pH (6.0) was used to evaluate the binding (figure 3.11). At pH 6.0, an endothermic reaction was observed when 140 µM KlebC$_{1-254}$ was titrated into 14 µM Ec TonB$_{33-240}$ (figure 3.11 A) or 160 µM Ec TonB$_{33-240}$ was titrated into 16 µM KlebC$_{1-254}$ (figure 3.11 C). However, endothermic reactions were also observed when single protein control samples were injected into buffer (figure 3.11 B, D). These results need further experiments to replace the Tris-based buffer, which is unable to maintain an accurate pH 6.0.

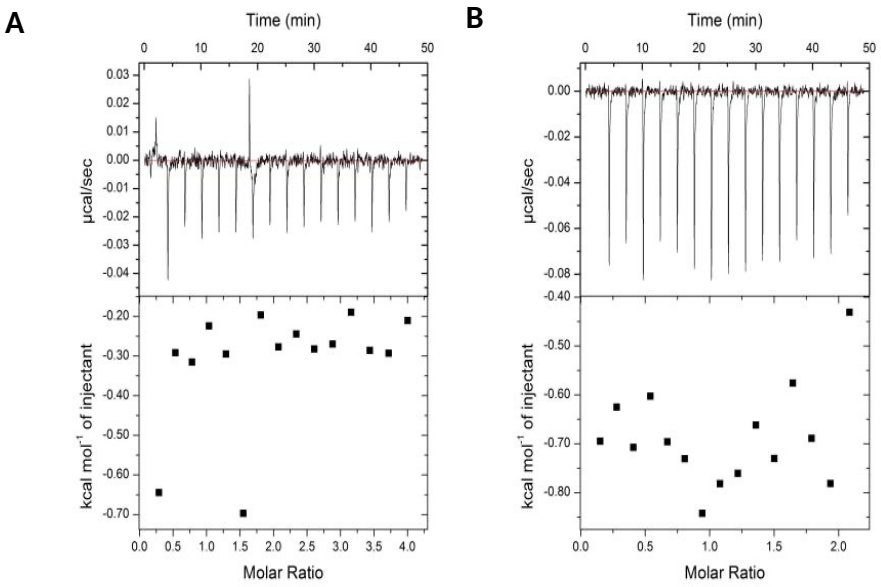


Figure 3.10 ITC detects no binding between Ec TonB$_{33-240}$ and KlebC$_{1-254}$ at pH 7.5
Two concentration combinations were performed on ITC to measure heat change during titration between Ec TonB$_{33-240}$ and KlebC$_{1-254}$. (A) 300 µM KlebC$_{1-254}$ injected into 20 µM Ec TonB$_{33-240}$. (B) 400 µM KlebC$_{1-254}$ injected into 40 µM Ec TonB$_{33-240}$. Both proteins were in 25 mM Tris-HCl, pH 7.5, 150 mM NaCl buffer.

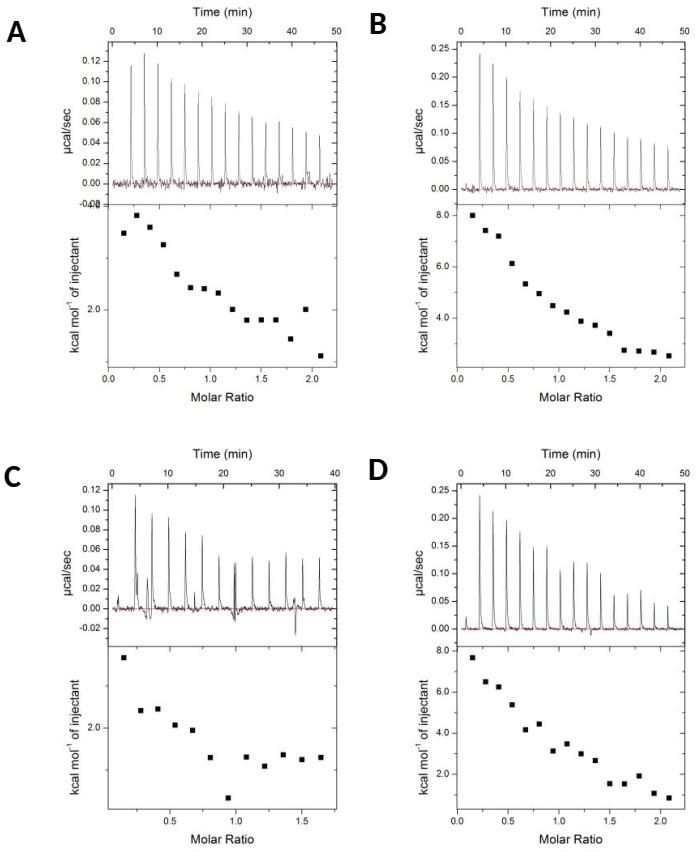


Figure 3.11 ITC detects no binding between Ec TonB$_{33-240}$ and KlebC$_{1-254}$ at pH 6.0 Different concentration combinations were performed on ITC to measure heat change during titration between Ec TonB$_{33-240}$ and KlebC$_{1-254}$. (A)140 µM KlebC$_{1-254}$ injected into 14 µM Ec TonB$_{33-240}$. (B) 140 µM KlebC$_{1-254}$ injected into buffer. (C) 160 µM Ec TonB$_{33-240}$ injected into 16 µM KlebC$_{1-254}$. (D) 160 µM Ec TonB$_{33-240}$ injected into buffer. Both proteins were in 25 mM Tris-HCl, pH 6.0, 150 mM NaCl buffer.

3.6 Predicted binding site between KlebC$_{1-254}$ and *K. quasipneumoniae* TonB

Three residues at the N-terminus of KlebC (Met16, Val17 and Leu19) have previously been shown to be essential for the cytotoxic activity of KlebC (Housden et al., 2021). To further confirm if this is due to mutation of these residues resulting in impaired TonB binding, Alphafold 2.0 was used to model the TonB-KlebC complex. AlphaFold 2.0 successfully predicted a complex structure between *K. quasipneumoniae* TonB and KlebC$_{1-254}$ (figure 3.12 A). Domain I and II of TonB (figure 1.4.2.4) were correctly

predicted as an amphipathic single α-helix, and a polyproline helix, respectively (figure 3.12 A). The predicted domain III of *K. quasipneumoniae* TonB showed a similar structure to the *E. coli* TonB in the BtuB-TonB structure (figure 1.4.2.1 and 3.12 A) (Shultis et al., 2006). Two β strands followed by disordered region are correctly predicted at the N-terminus of KlebC and the receptor-binding domain of KlebC is predicted to be a helical hairpin which is highly similar to the crystal structure solved experimentally (figure 1.4.2.4) (Housden et al., 2021). Two proteins interacted through the C-terminal domain III of TonB and the N-terminal disordered domain of KlebC (figure 3.12).

Relatively high plDDT scores (> 80) at the binding interface (C-terminus of TonB and the N-terminus KlebC) indicate that the prediction model is confident in the accuracy of the structure (figure 3.12 B, C). The predicted aligned error (PAE) scores of the binding site are both low, which indicated low positional errors at this interface (figure 3.13, inset). In total, ten hydrogen bonds are predicted to form between the C-terminus of TonB and the N-terminus of KlebC (figure 3.13). Of these H-bonds, six are amide backbone interactions and four are hydrogen bonds between side chains and side chains. Side chain interactions are more likely to form specific TonB binding sites rather than generic backbone interactions. Interestingly no side chain interactions were observed at Met16, Val17 and Leu19, previously identified to be important for KlebC activity (Housden et al., 2021).

The predicted structure suggests that residues Glu26, Glu27 and Met29 of KlebC are involved in the interaction with TonB. These new residues may indicate an extended

TonB box. If the prediction is accurate, mutation of these side chain interactions should affect the interaction with TonB, which would be reflected in the cytotoxic ability of KlebC.

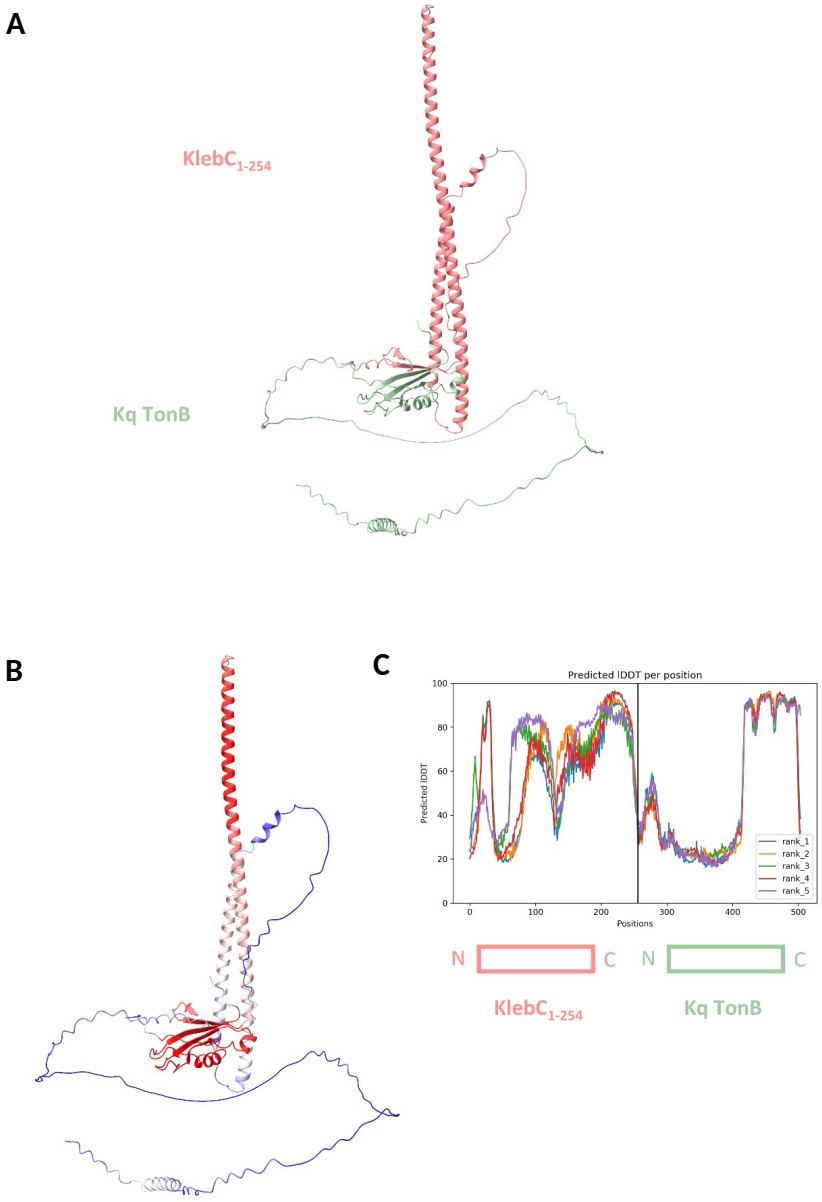


Figure 3.12 Structural prediction of KlebC$_{1-254}$-Kq TonB complex by Alphafold 2.0 (A) Alphafold 2.0 was used to model the complex between KlebC$_{1-254}$ (pink) and full-length *K. quasipneumoniae* TonB (green). (B) The predicted structure was coloured by plDDT scores (red – high, white – median, blue - low), which is an estimate of confidence. Structural domains with high scores have similar structures to those experimental results. (C) plDDT scores across proteins are shown. The N-terminus of KlebC$_{1-254}$ and the C-terminus of Kq TonB have high plDDT scores.

To investigate the importance of these AlphaFold 2.0 structures, predictions were repeated when side chains were mutated to Ala or Ser, E26A/E27A/M29S. These mutations abolished the predicted complex. To validate this experimentally, mutagenesis studies were performed.

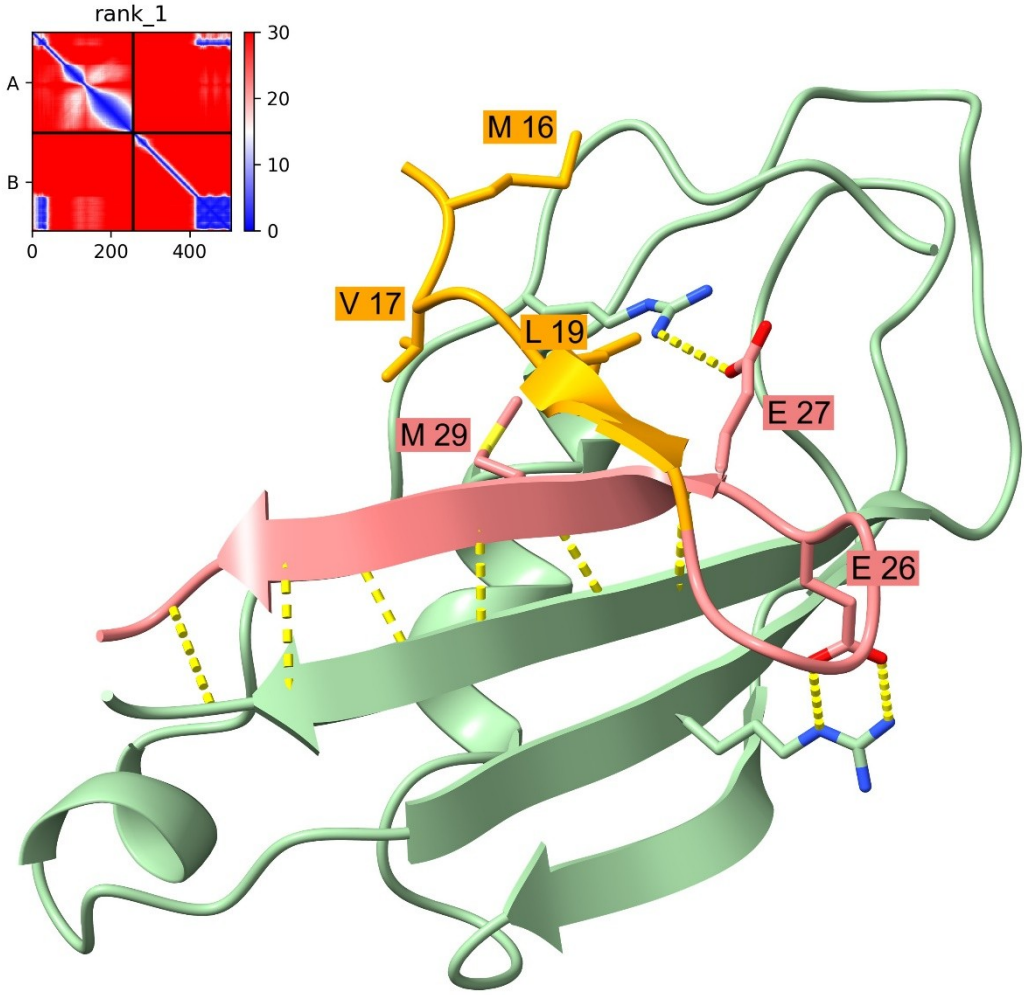


Figure 3.13 AlphaFold 2.0 predicts *K. quasipneumoniae* TonB binds to KlebC$_{1-254}$ through beta-strand augmentation
The binding interface between KlebC$_{1-254}$ (pink and orange) and *K. quasipneumoniae* TonB (green) is shown. Sequence (Met16-Leu19) previously predicted to be involved in TonB binding (Housden et al., 2021) is shown in orange. Residues with side chains involved in interface interactions are shown as sticks. The PAE score plot of the highest rank is shown as inset. Position number is as the same as shown in figure 3.12 C.

Full-length KlebC constructs containing three mutated residues, E26A/E27A/M29S were created. The protein was successfully purified (figure 3.14) and via SEC resembled that of WT KlebC suggesting the protein was folded (figure 3.1 A). The cytotoxic activity of this new mutant was tested relative to WT KlebC and the M16S/ V17V/L19G triple mutant by killing assays. KlebC M16S/V17V/L19G completely abolished activity against *K. quasipneumoniae* QMP M1-977 (figure 3.15 A), indicating that these mutations are deleterious to KlebC function. KlebC E26A/E27A/ M29S activity reduced relatively to wild-type KlebC, killing *K. quasipneumoniae* QMP M1-977 down to concentrations of 1 µM (figure 3.15 C), with wild-type killing to 0.98 nM (figure 3.2 A). Neither mutant was active against *E. coli* MG1655 (figure 3.15 B, D). Since the killing activity of KlebC is dependent on the association of the N-terminal disordered domain with TonB, the loss of function in the M16S/V17V/L19G mutant suggests that these residues are likely involved in TonB binding. The impact of the E26A/E27A/M29S mutation was less pronounced

suggesting that this region is more likely involved in periphery interactions or have an alternative function such as receptor recognition and threading.

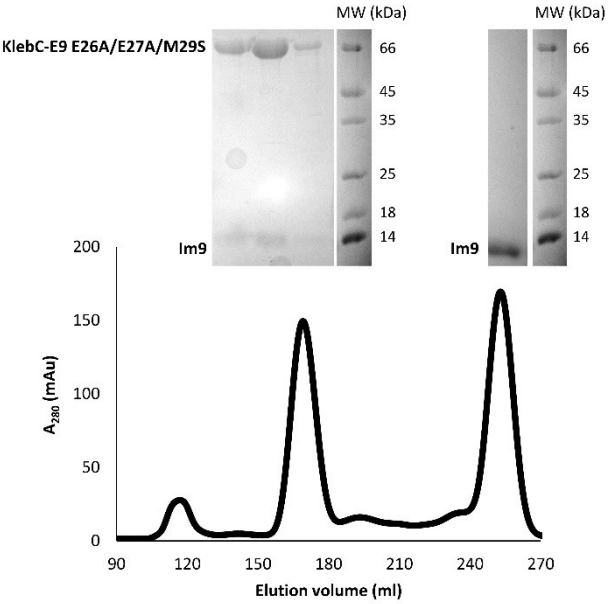
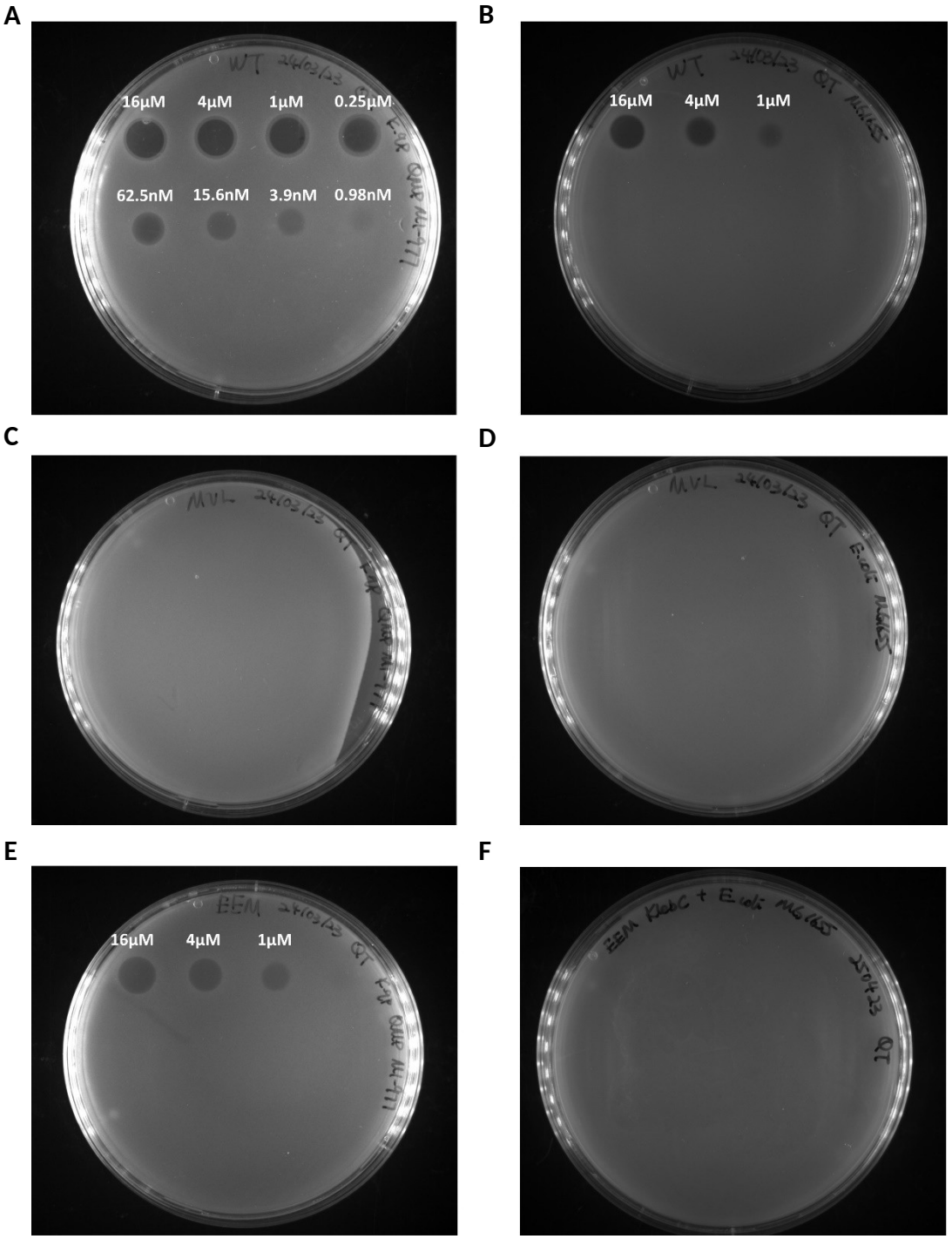


Figure 3.14 Purification of KlebC, E26A/E27A/M29S and KlebC, M168S/V171W/L196G

Proteins were purified by affinity chromatography and further purified through SEC. Samples were loaded onto a HiLoad 26/600 Superdex 200 pg column, equilibrated in 25 mM Tris-HCl, pH 7.5, 150 mM NaCl and run at 2 mL/min. Fractions containing KlebC, E26A/E27A/M29S (A, B) or KlebC, M168S/V171W/L196G (C, D) were collected during elution. Boiled fractions were run on a 12% SDS-PAGE gel, stained with Coomassie blue, and destained overnight. (KlebC, E26A/E27A/M29S: 10.3 kDa; KlebC, M168S/V171W/L196G: 10.6 kDa). The peak eluted at 69 mL contained the purified protein.

Figure 3.15 Plate killing assay of KlebC, E26A/E27A/M29S and KlebC, M168S/V171W/L196G

5 µL of KlebC, WT (A, B), KlebC, E26A/E27A/M29S (C, D), or KlebC, E26A/E27A/M29S/M168S/V171W/L196G (E, F) were spotted onto agar plates containing *K. quasipneumoniae* QMP M1-977 (A, C, E) or *E. coli* MG1655 (B, D, F) lawns. Plates were incubated at 37 °C overnight. Zones of clearance indicate killing activity. KlebC, M168S/V171W/L196G was not active against either stain. Whilst KlebC, E26A/E27A/M29S was able to kill *K. quasipneumoniae* QMP M1-977 at concentrations from 1 to 16 µM.



Like other group B bacteriocins, KlebC needs to interact with TonB to enter cells and elicit cytotoxic effects. Here, the interaction between these two proteins was characterised to further understand import of these Group B bacteriocins. This interaction was validated by detecting complex formation between KlebC$_{1-254}$ and Ec TonB$_{33-240}$ by analytical SEC. Further evidence of this interaction was sought through ITC to determine a binding constant for the interaction. In these experiments no binding event was detected which may be because the addition of Im9 significantly affected the pI and charge of Ec TonB$_{33-240}$. In contrast, although no complex was detected for the Kq TonB$_{156-248}$ and KlebC$_{1-254}$ by analytical SEC, complex formation was detected and measured by ITC. High concentrations of both proteins (800 µM KlebC$_{1-254}$ and 40 µM Kq TonB$_{156-248}$) was required to generate data with a low noise-to-background ratio and a reliable fit of one site model to the experimental data. This gave a K_D of 66.2 µM for the KlebC-Kq TonB$_{156-248}$ interaction. This is a relatively low binding affinity for a complex through which PMF is transduced, however it is consistent with previous data such as the interaction between the FhuA TonB box peptide and *E. coli* TonB (K_D= 36±7 µM) measured also by ITC (Peacock et al., 2005). These indicated that the binding affinity between a bacteriocin TonB box and TonB is similar to that between TBDT TonB box and TonB.

The location of the TonB box within KlebC was investigated through structural modelling and mutagenesis. Alphafold 2.0 was used to generate a model of the KlebC$_{1-254}$-Kq TonB complex. This model predicted that a single β-strand from residues Glu26 to Gly33 of Kq TonB was required for binding to KlebC. The location of this β-strand was different to the TonB box previously predicted by Housden et al. (2021).

Mutagenesis of residues Glu26, Glu27, and Met29 do not completely abolish the cytotoxic activity of KlebC. However, the previously discovered TonB box plays more significant role in the uptake of KlebC (Housden et al., 2021). The role of each residue in the binding should be investigated with future structural data. A high resolution KlebC-TonB structure would allow unambiguous confirmation of the binding site. The flexibility of the disordered N-terminus of KlebC may pose challenges to achieve high-resolution at the binding site by Cryo-EM. Other structural methods, such as X-ray crystallography, can also be applied in future study to further characterise this interaction between KlebC and Kq $TonB_{156-248}$.

Chapter 4. Assembly of the KlebC translocon

To further understand how KlebC gains entry into cells via TolC and TonB, methods were optimised to generate a ternary complex amenable for single-particle Cryo-EM. Cryo-EM has been previously used to solve the complex of TolC-$KlebC_{1-254}$ and TolC-ColE1 (Budiardjo et al., 2022; Housden et al., 2021). In the TolC-$KlebC_{1-254}$ structure, only residues 77-151 of KlebC were resolved, which lacks sequences involved in binding TonB. It was proposed that the lack of density for the N-terminus of KlebC was due to the inherent flexibility in this domain. To overcome this, we proposed to

add TonB, which can bind to the N-terminus of KlebC thus reducing flexibility, similar to that reported for the ColE9 translocon (Francis et al., 2021).

4.1 Purification optimisation of TolC

Attempts to purify TolC according to previously published data (Housden et al., 2021) resulted in low protein yields. Tracking the protein throughout the purification procedure using SDS-PAGE, suggested that despite a high expression level for TolC, the protein was largely localised to inclusion bodies and was not soluble. To increase the amount of TolC in the soluble fraction, changes to induction temperatures and growth media were compared. To prevent TolC from aggregating in inclusion bodies, the growth media, containing lower concentration of salt, was used to grow cells. By comparing two growth media, low salt caused a relatively lower amount of inclusion body in the cell pellet (figure 4.1). Since proteins were still lost in the inner membrane fraction and the washing step, only outer membrane solubilisation was decided to avoid protein loss. After all these optimisations, a single symmetrical peak of TolC was observed on chromatogram. But the protein yield is lower than expected. To further increase the yield, all available growth media from different companies were compared (figure 4.2). Comparing the amount of TolC in the cell pellet, cell lysate and soluble membrane extract, media 8 generated the highest amount of TolC in both the cell lysate and soluble membrane extract, although inclusion bodies still exist (figure 4.2). The removal of IM solubilization and washing

Figure 4.1 Growth media comparison for TolC purification
Growth media, containing different concentrations of salt, were compared to assess optimal levels for the expression of soluble TolC. Boiled fractions from each purification step were run on a 12% SDS-PAGE gel, stained with Coomassie blue.

steps avoided protein loss during membrane solubilization, as the band intensity between total membrane extract and soluble membrane extract are similar, and loss of TolC was not significant in the final insoluble pellet (figure 4.3). After this optimisation, TolC was successfully purified and reached a reasonable yield (1.2 mg/l) as a membrane protein (figure 4.4 A, B). A single and symmetrical peak was detected on SEC chromatogram (figure 4.4 B).

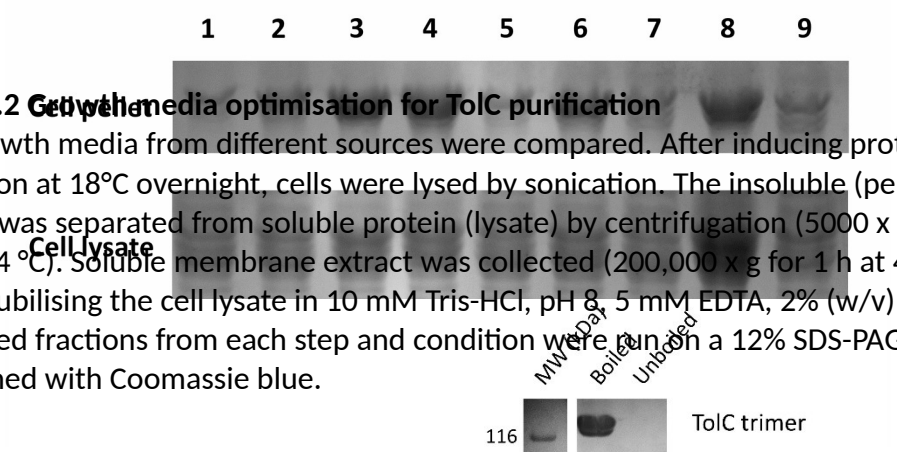


Figure 4.2 Growth media optimisation for TolC purification
Nine growth media from different sources were compared. After inducing protein expression at 18°C overnight, cells were lysed by sonication. The insoluble (pellet) fraction was separated from soluble protein (lysate) by centrifugation (5000 x g, 15 min, 4 °C). Soluble membrane extract was collected (200,000 x g for 1 h at 4°C) after solubilising the cell lysate in 10 mM Tris-HCl, pH 8, 5 mM EDTA, 2% (w/v) β-OG. Boiled fractions from each step and condition were run on a 12% SDS-PAGE gel, stained with Coomassie blue.

4.2

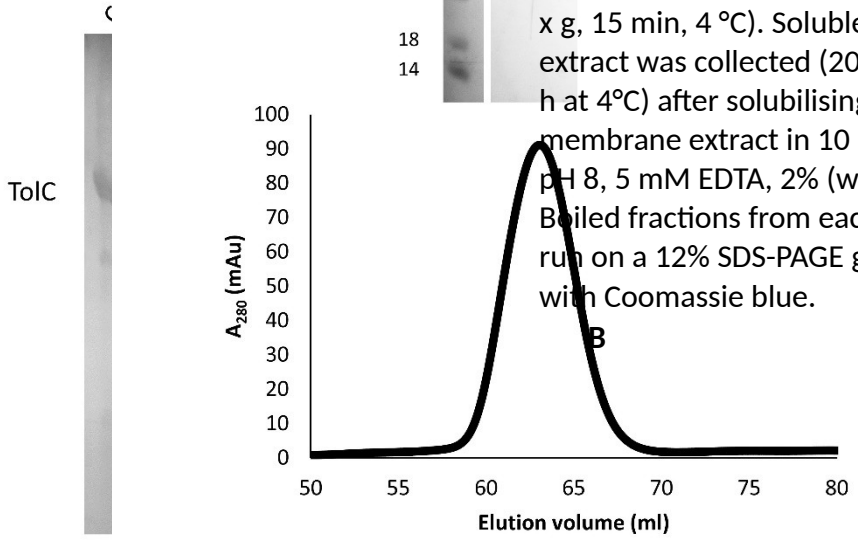


Figure 4.3 Optimal TolC solubilisation from OM
Cells, carrying the TolC construct, were grown in media 8 and induced at 18°C overnight. Cells were lysed by sonication. The insoluble (pellet) fraction was separated from soluble protein (lysate) by centrifugation (5000 x g, 15 min, 4 °C). Soluble membrane extract was collected (200,000 x g for 1 h at 4°C) after solubilising the cell total membrane extract in 10 mM Tris-HCl, pH 8, 5 mM EDTA, 2% (w/v) β-OG. Boiled fractions from each step were run on a 12% SDS-PAGE gel, stained with Coomassie blue.

Figure 4.4 Kq TolC purification
(A) After OM solubilisation, TolC was bound to a HisTrap column and eluted through a gradient (0-100%) from 5 mM to 500 mM imidazole over 12 column volumes. Samples from the peak, detected (280 nm absorbance) during elution, were evaluated on a 12% SDS-PAGE gel confirming that TolC was in the main elution peak. (B) TolC was further purified by SEC following application to a HiLoad 16/600 Superdex 200 pg column, equilibrated in 25 mM Tris-HCl, pH 7.50, 150 mM NaCl, 1% β-OG. Proteins sizes were checked on a 12% SDS-PAGE gel to validate the presence of TolC. Unboiled and boiled fractions were run on the gel to check the trimeric state of TolC.

To test if the purified TolC was assembled and interacted with KlebC, complex formation was tested using analytical SEC. Complex formation between $KlebC_{1-254}$, $KlebC_{51-254}$ and TolC have been validated previously using this method (Housden et al., 2021). An equimolar ratio of two components at 5 µM were mixed and incubated overnight at 4 °C (chapter 2.9). Applying mixtures of either $KlebC_{1-254}$ or $KlebC_{51-254}$ with TolC to a Superdex 200 increase 10/300 GL column resulted in the appearance of a new peak at a lower elution volume, compared to individual protein controls (figure 4.5). This is consistent with the formation of a higher-mass complex for KlebC-TolC, which was confirmed by SDS-PAGE. To form the KlebC translocon, TonB needs to form a stable complex with KlebC and TolC. Both Ec $TonB_{33-240}$ and Kq $TonB_{156-248}$ aggregate in buffer, containing 1% β-OG. Protein aggregation would prevent the formation of the ternary complex and damage the SEC columns. Thus, detergent needs to be removed from the buffer for the complex assembly. The high resolution of the TolC-ColE1 complex structure solved by Cryo-EM was achieved through the use of lipid nanodiscs, therefore, nanodisc was selected over amphipol for stabilising TolC in the absence of detergent.

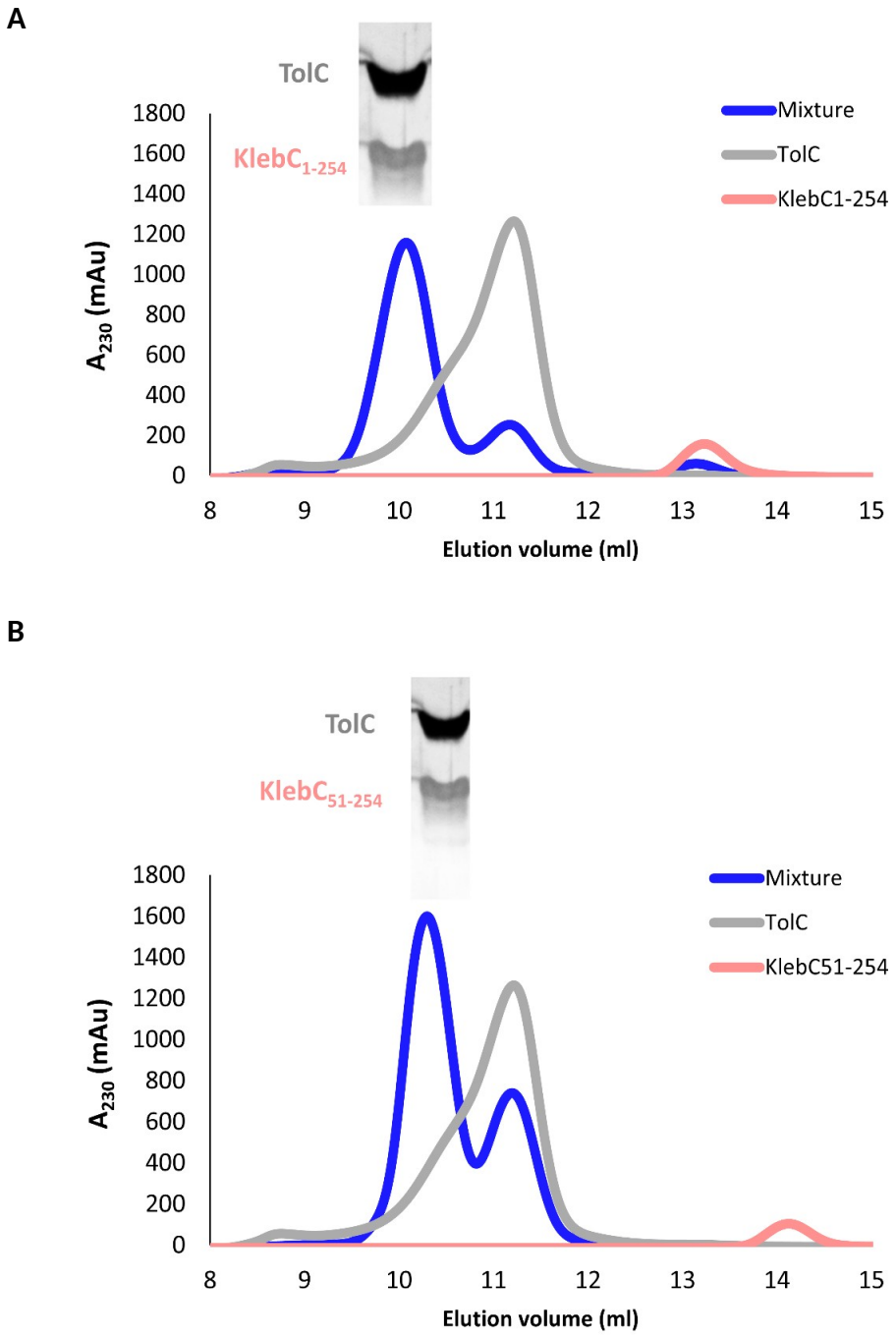


Figure 4.5 Analytical SEC of *in vitro* complex formation between TolC and KlebC
TolC (5 µM) was incubated overnight at 4°C with either $KlebC_{1-254}$ (5 µM, A) or $KlebC_{51-254}$ (5 µM, B). The mixture (0.5 ml) was run (0.5 ml/min) on Superdex S200 Increase 10/300 GL column, equilibrated in 25 mM Tris-HCl, pH 7.50, 150 mM NaCl, 1% β-OG (blue trace). Individual protein controls (TolC – grey absorbance trace, KlebC – pink absorbance trace) were also run onto the same column separately. Traces from different runs were overlaid. Fractions from different sections of the mixture trace were run on 12% SDS-PAGE gels, stained with Coomassie blue to confirm the identity of proteins present in each peak. Both variants of KlebC formed complexes with TolC as indicated by a peak shift (blue trace) towards lower elution volume and confirmed by SDS-PAGE.

4.3 TolC-Nanodisc formation optimisation

As a membrane protein, the hydrophobic β-barrel domain of TolC needs to be protected by detergent or lipids. Nanodiscs can overcome the use of detergent by stabilising membrane proteins through lipids constrained by a belt formed by a scaffold protein. Formation of nanodiscs allows for the transfer of membrane proteins into detergent-free buffer for translocon assembly.

The TolC-ColE1 structure was solved in nanodisc, made with POPC lipid and MSP1D1 scaffold protein (Budiardjo et al., 2022). This protocol was adopted here to generate TolC-nanodiscs, substituting MSPD1 for MSP1D1G1, which contains an extra glycine residue but is otherwise identical. Reconstituting membrane proteins into nanodiscs requires mixing of components (lipid, protein, and scaffold) at a certain stoichiometric ratio that generates a homogenous disc size, followed by detergent removal to initial disc formation.

To generate a nanodisc sample of homogenous size, several lipid:scaffold protein ratios were tested. To achieve this, samples were mixed, incubated with Bio-beads SM2 to remove detergent and loaded onto a Superose 6 increase 10/300 GL column. Monitoring absorbance at 230 and 280 nm revealed that a ratio of 50:1 gave an elution profile with readily resolved symmetric peaks (Figure 4.6). This shows that specific populations of nanodiscs are formed that can be readily separated, a property that is essential for generating a sample for single particle Cryo-EM.

Detergent can be removed by dialysis, detergent binding columns and detergent binding beads. In line with the previously published protocol, dialysis and Bio-beads SM2, a polystyrene-based detergent binding bead, were tested to form empty nanodiscs (Figure 4.7). A substantial loss of material was observed by SDS-PAGE after the overnight dialysis step. To achieve higher yield of empty nanodisc, the number of Bio-beads SM2 was increased and the dialysis step was removed. Detergent in the buffer was removed through running the sample through a desalting column.

Following initial optimisation steps, TolC was reconstituted into a nanodisc at a POPC:MSP1D1G1:TolC ratio of 50:1:0.2 (figure 4.8). The reconstitution of TolC into nanodisc was validated by a peak shift to a lower elution volume relative to the empty nanodisc control. An empty nanodisc formed with the same ratio of components resulted in a single peak that eluted at 16.2 ml (figure 4.8 A). Addition of TolC results in appearance of a unique peak at 15.2 ml (figure 4.9 B). These indicate the successful reconstitution of TolC into nanodisc.

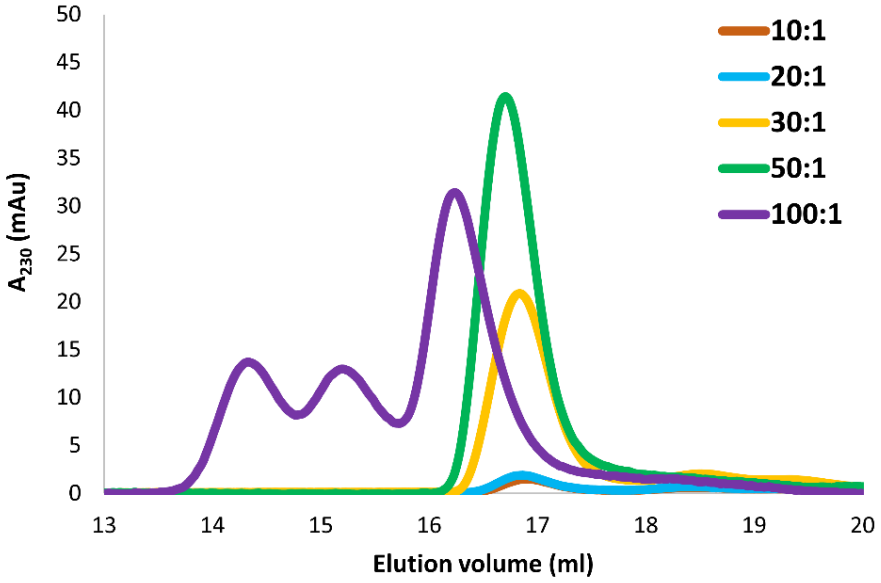
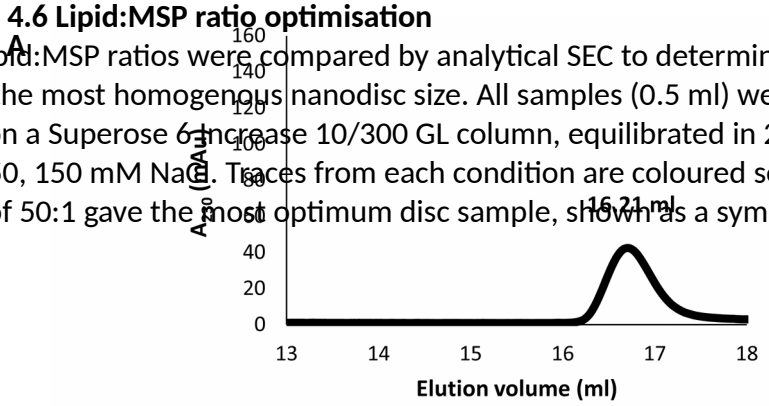


Figure 4.6 Lipid:MSP ratio optimisation
Five lipid:MSP ratios were compared by analytical SEC to determine what ratio gives the most homogenous nanodisc size. All samples (0.5 ml) were run (0.5 ml/min) on a Superose 6 increase 10/300 GL column, equilibrated in 25 mM Tris-HCl, pH 7.50, 150 mM NaCl. Traces from each condition are coloured separately. A ratio of 50:1 gave the most optimum disc sample, shown as a symmetrical peak.



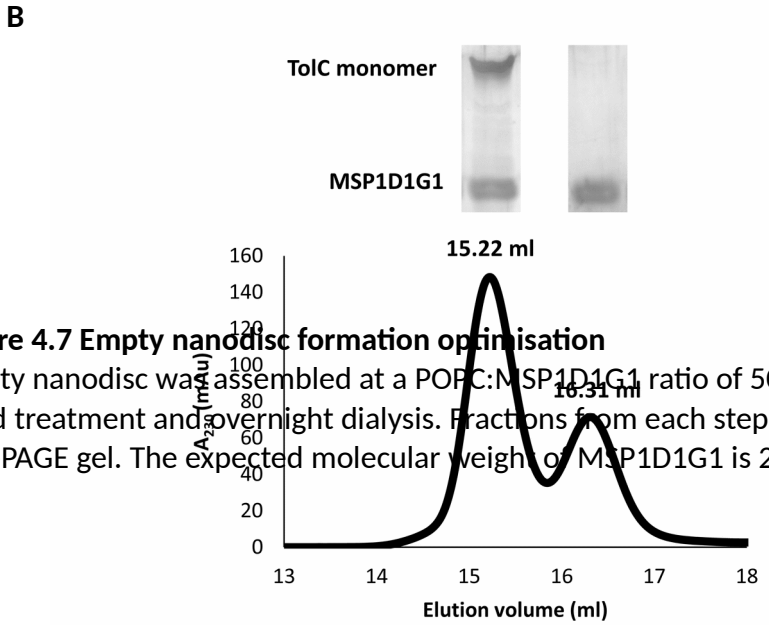


Figure 4.7 Empty nanodisc formation optimisation
Empty nanodisc was assembled at a POPC:MSP1D1G1 ratio of 50:1 following Bio-bead treatment and overnight dialysis. Fractions from each step were run a 12% SDS-PAGE gel. The expected molecular weight of MSP1D1G1 is 22.10 kDa.

Figure 4.8 Reconstitution of TolC into nanodisc
(A) Empty nanodisc was assembled at a POPC : MSP1D1G1 ratio of 50:1. (B) TolC-nanodisc was assembled at a POPC : MSP1D1G1 : TolC ratio of 50 (5 mM) : 1 (100 µM) : 0.2 (20 µM). Both samples were run (0.5 ml/min) on Superose 6 Increase 10/300 GL column, equilibrated in 25 mM Tris-HCl, pH 7.50, 150 mM NaCl. (B) Boiled fractions were assessed by SDS-PAGE. Silver stained gel (shown as insets above peaks) showed two protein bands from the first peak at 15.22 ml, thus TolC was successfully reconstituted into nanodisc.

4.4 Ternary complex formation in nanodisc

To test for complex formation between the TolC-nanodisc and KlebC$_{1-254}$, fluorescently labelled KlebC$_{1-254}$ with Alexa fluor 647 (a gift from Dr Nicholas Housden) was used. Monitoring dual wavelengths at 230 nm and 647 nm, during analytical SEC, allowed for tracking of both the protein signal and the AF647 fluorescent signal that was associated with KlebC$_{1-254}$. Individual KlebC$_{1-254}$-AF647 and TolC-nanodisc resulted in peaks at 16.3 ml and 15.2 ml, respectively (figure 4.9 A and 4.8 B). The addition of KlebC$_{1-254}$-AF647 to the TolC-nanodisc at a 2x molar ratio gave rise to two elution peaks from the SEC column (figure 4.9 B). The first peak eluting at 14.1 ml corresponded to a complex between KlebC and TolC as indicated as an increase in absorbance at both wavelengths and a smaller elution volume compared to the individual protein control.

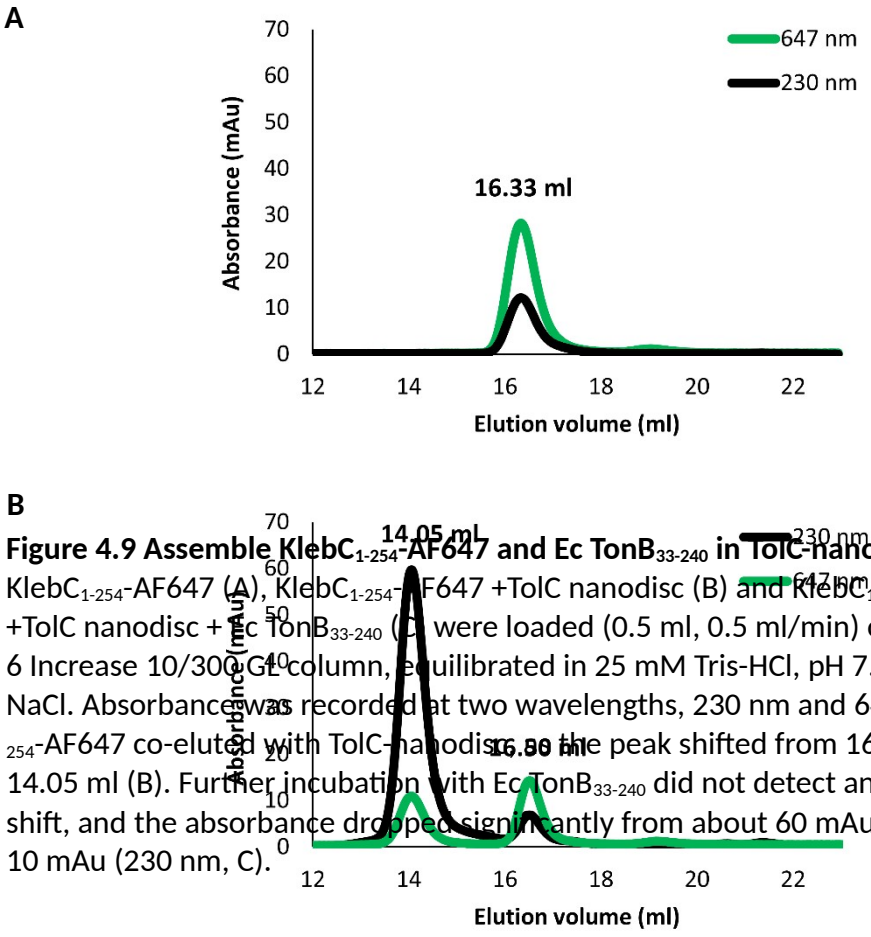
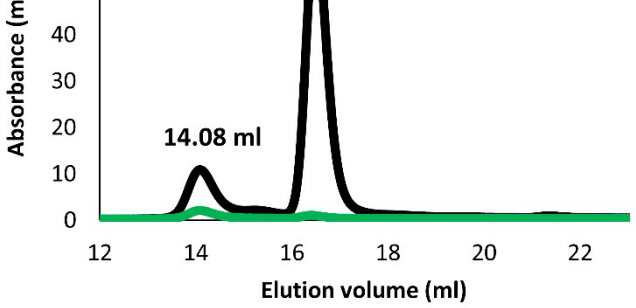


Figure 4.9 Assemble KlebC$_{1-254}$-AF647 and Ec TonB$_{33-240}$ in TolC-nanodisc
KlebC$_{1-254}$-AF647 (A), KlebC$_{1-254}$-AF647 +TolC nanodisc (B) and KlebC$_{1-254}$-AF647 +TolC nanodisc + Ec TonB$_{33-240}$ (C) were loaded (0.5 ml, 0.5 ml/min) on a Superose 6 Increase 10/300 GL column, equilibrated in 25 mM Tris-HCl, pH 7.5, 150 mM NaCl. Absorbance was recorded at two wavelengths, 230 nm and 647 nm. KlebC$_{1-254}$-AF647 co-eluted with TolC-nanodisc, so the peak shifted from 16.33 ml (A) to 14.05 ml (B). Further incubation with Ec TonB$_{33-240}$ did not detect another peak shift, and the absorbance dropped significantly from about 60 mAu (230 nm, B) to 10 mAu (230 nm, C).





The fr l. To attem $B_{156-248}$, Ec $TonB_{33-240}$ was used as binary complex formation was only detected between Ec $TonB_{33-240}$ and $KlebC_{1-254}$ by analytical SEC (figure 3.7, 3.8). The mixture was once again run over the analytical SEC column to look for complex formation (figure 4.9 C). The maximal absorbance signal detected for the sample was significantly less following concentrating the complex and reapplication to the column. To avoid protein loss during ternary complex formation, $KlebC_{1-254}$ and Ec $TonB_{33-240}$ were sequentially incubated with the TolC-nanodisc, before analysis by SEC (figure 4.10). To achieve this, Ec $TonB_{33-240}$ was initially added in a 10-fold excess. Proteins were incubated together overnight at 4°C before running over a Superose 6 increase 10/300 column. Analysis of concentrated fractions from the first peak by SDS-PAGE showed four protein bands, which confirmed that a ternary complex has formed. $KlebC_{1-254}$ and Ec $TonB_{33-240}$ should bind to each other in a 1:1 stoichiometry ratio, but the band of Ec $TonB_{33-240}$ did not appear as strong as that of $KlebC_{1-254}$. This revealed that the binding site of $KlebC_{1-254}$ was not saturated and the majority of the sample is $KlebC_{1-254}$-TolC-nanodisc.

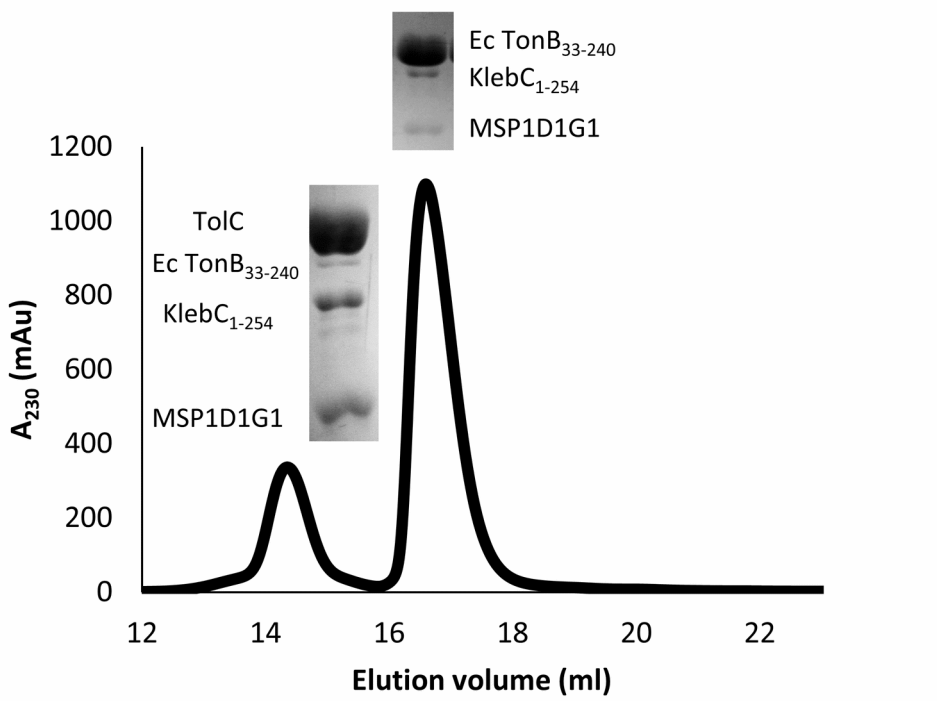


Figure 4.10 The formation of KlebC$_{1-254}$-TolC-Ec TonB$_{33-240}$ complex in nanodisc
The ternary complex among KlebC$_{1-254}$, TolC-nanodisc and Ec TonB$_{33-240}$ was assembled and separated (0.5 ml/min) on Superose 6 Increase 10/300 GL column, equilibrated in 25 mM Tris-HCl, pH 7.50, 150 mM NaCl. Boiled fractions from each peak were run on a 15% gel, stained with Coomassie blue.

To overcome this, Kq TonB$_{156-248}$ was used for ternary complex formation. Because previous data had shown that the binding affinity of KlebC and Kq TonB$_{156-248}$ was low such that the complex did not persist during analytical SEC (figure 3.8), chemical crosslinking was employed to stabilise the ternary complex prior to SEC. The KlebC$_{1-254}$-TolC-nanodisc complex was assembled as described above for Ec TonB$_{33-240}$. Kq TonB$_{156-248}$ was added to KlebC$_{1-254}$-TolC-nanodisc at a molar ratio of 8:1 and formaldehyde (1%) was used to crosslink amine moieties within 0.2 nm. Both crosslinked and un-crosslinked samples were compared by analytical SEC, which revealed near identical absorbance profiles for both suggesting that no ternary complex was present (figure 4.11 and 4.12). This was confirmed by SDS-PAGE where

bands corresponding to TolC, KlebC$_{1-254}$ and MSP1D1G1 were resolved but no band consistent with Kq TonB$_{156-248}$ was detected using Coomassie stain. Silver staining of the gel did resolve a faint band running at a molecular weight consistent with Kq TonB$_{156-248}$ in the formaldehyde crosslinked sample (Figure 4.12).

As no Kq TonB$_{156-248}$ band can be seen after Coomassie blue staining, there was still not enough intact ternary complex to determine a structure using Cryo-EM. To further increase the proportion of ternary complex in the final sample, a larger excess of Kq TonB$_{156-248}$ was added to the KlebC$_{1-254}$-TolC-nanodisc sample (25:1, TonB:KlebC). To achieve this Kq TonB$_{156-248}$ was lyophilised and re-constituted in a high concentration (800 µM), to avoid protein loss often observed through centrifugation concentrating. Following mixing, the complex was crosslinked with formaldehyde and run on analytical SEC. A similar peak distribution was observed as above (figure 4.13). The first elution peak previously shown to contain ternary complex was pooled and concentrated. Concentrated protein was analysed by SDS-PAGE, followed by Coomassie blue staining. This time, four protein bands for TolC, KlebC$_{1-254}$, Kq TonB$_{156-248}$, and MSPD1G1 were visualised. The complex was plunge frozen in liquid ethane onto Quantifoil 1.2/1.3 grids for grid optimisation and sample screening.

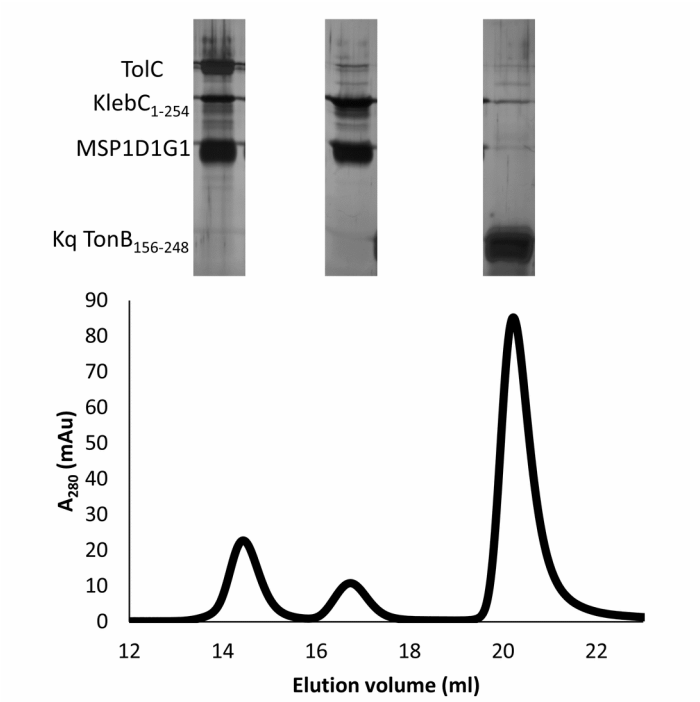


Figure 4.11 The formation of KlebC$_{1-254}$-TolC-Kq TonB$_{156-248}$ complex in nanodisc
KlebC$_{1-254}$ (20 µM) and Kq TonB$_{156-248}$ (80 µM) were incubated overnight at 4°C with TolC-nanodisc (11 µM) and the mixture (0.5 ml) was separated (0.5 ml/min) on a Superose 6 Increase 10/300 GL column, equilibrated in 25 mM Tris-HCl, pH 7.50, 150 mM NaCl. Boiled fractions from each peak were run on a 12% gel, stained with silver stain (insets shown above peaks). SDS-PAGE confirms that no Kq TonB$_{156-248}$ co-eluted with the KlebC$_{1-254}$-TolC-nanodisc, in the first (14.44 ml) and second (16.73 ml) peaks. All TonB eluted in a later peak at 20.22 ml.

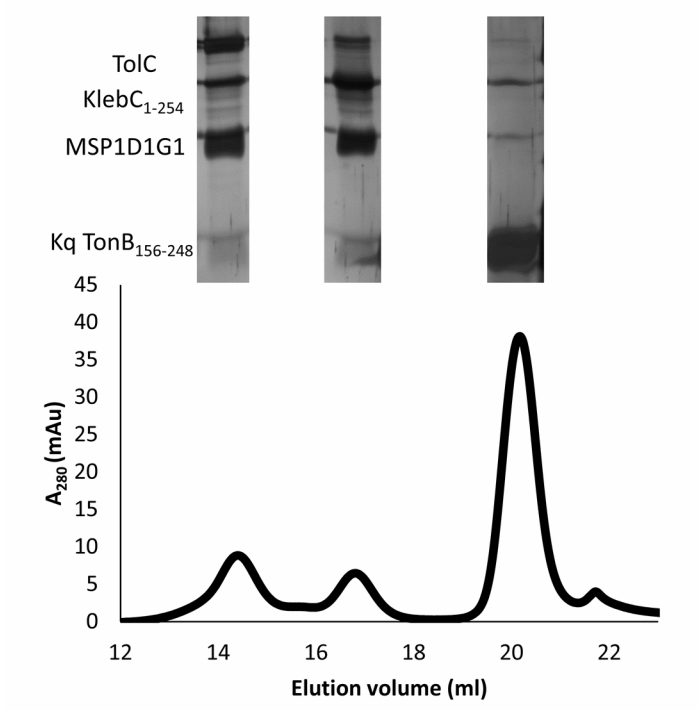


Figure 4.12 The formation of crosslinked KlebC$_{1-254}$-TolC- Kq TonB$_{156-248}$ complex in nanodisc

KlebC$_{1-254}$ (20 µM) and Kq TonB$_{156-248}$ (80 µM) were incubated overnight at 4°C with TolC-nanodisc (11 µM) and the mixture (0.5 ml) was crosslinked with 1% formaldehyde prior to application (0.5 ml/min) on a Superose 6 Increase 10/300 GL column, equilibrated in 25 mM Tris-HCl, pH 7.50, 150 mM NaCl. Boiled fractions from each peak were run on a 12% gel, stained with silver (insets shown above peaks). A small amount of Kq TonB$_{156-248}$ co-eluted with KlebC$_{1-254}$-TolC-nanodisc (peak at 14.40 ml), indicating that crosslinking successfully stabilised the ternary complex.

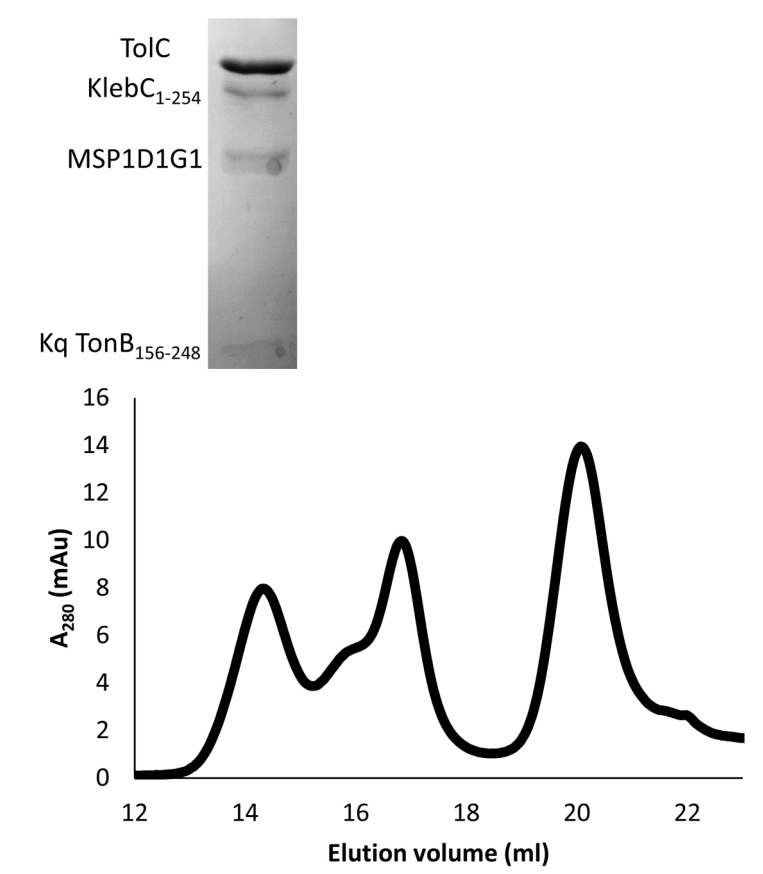


Figure 4.13 The formation of high-yield crosslinked KlebC$_{1-254}$-TolC-Kq TonB$_{156-248}$ complex in nanodisc

KlebC$_{1-254}$ (17.2 µM) and Kq TonB$_{156-248}$ (220 µM) were incubated with TolC-nanodisc (8.6 µM) sequentially, and the mixture was crosslinked with 1% formaldehyde and separated (0.5 ml/min) on a Superose 6 Increase 10/300 GL column, equilibrated in 25 mM Tris-HCl, pH 7.50, 150 mM NaCl. Boiled and concentrated fractions from the first peak (14.33 ml) were run on a 12% gel, stained with Coomassie blue (insets shown above peaks). Kq TonB$_{156-248}$ co-eluted with KlebC$_{1-254}$-TolC-nanodisc consistent with an increase in yield the protein is now visualised with coomassie staining. Remaining two elution peaks contain KlebC TolC nanodisc (16.83 ml) and Kq TonB$_{156-248}$ (20.07 ml), respectively. .

4.5 Visualisation of ternary complex on grid

Ternary complexes of TolC-KlebC$_{1-254}$-Ec TonB$_{33-240}$ and TolC-KlebC$_{1-254}$-Kq TonB$_{156-248}$ in nanodisc were applied to Cryo-EM grids at 1.9 mg/ml and 0.8 mg/ml, respectively. Higher concentrations of complex showed significant aggregation of particles (figure 4.14). Dilution of the sample to 0.8 mg/ml resolved aggregation, suggesting that the sample was likely to be aggregating prior to or upon application to grids (Figure 4.15).

The crosslinked KlebC$_{1-254}$-TolC-Kq TonB$_{156-248}$ complex in nanodisc was subsequently applied to grids at 0.7 mg/ml to prevent aggregation. Again individual complexes were observed on the grid (figure 4.16). Furthermore, the contrast in this sample was much better with thinner ice allowing for imaging at a low defocus value (-1 µm) whereas the previous sample required high defocus (-2 µm) to achieve similar contrast. Because TonB is a small protein, high resolution 2D classes and 3D reconstruction will be required to validate the formation of the ternary complex.

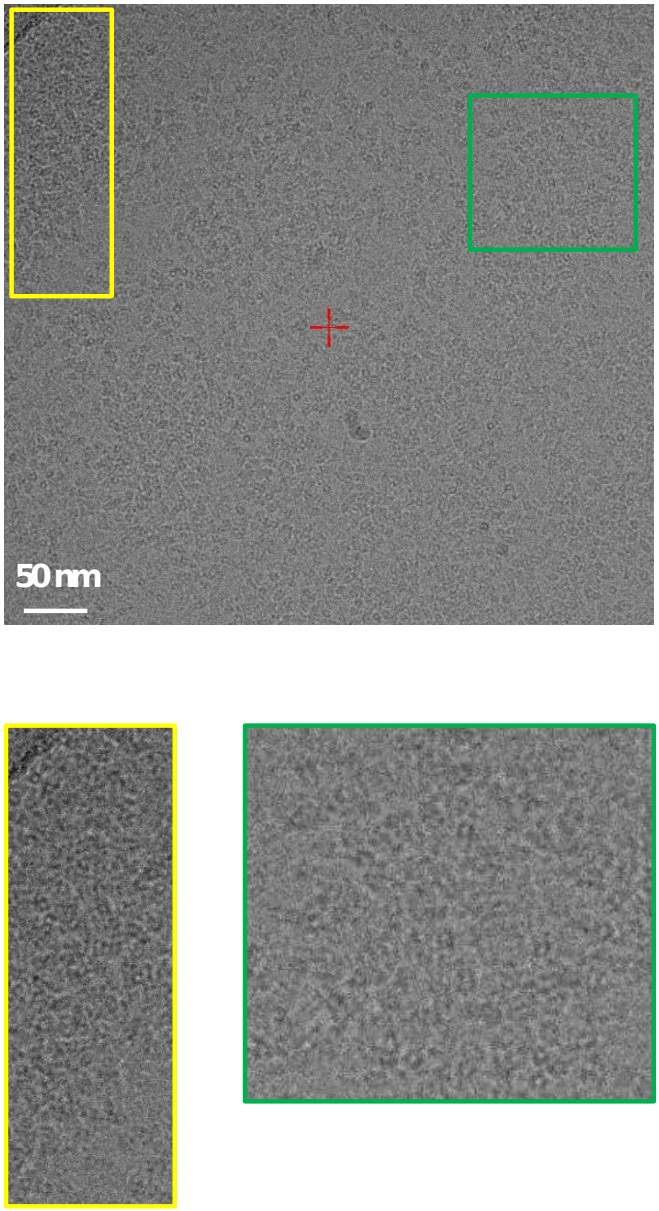


Figure 4.14 Representative grid images of KlebC$_{1-254}$-TolC-Ec TonB$_{33-240}$ complex in nanodisc

Ternary complex of KlebC$_{1-254}$-TolC-Ec TonB$_{33-240}$ complex in nanodisc (1.9 mg/ml) was imaged using a Arctica (Thermofisher) 200 kV microscope. Significant aggregation of protein was apparent on grids making individual particles hard to resolve (yellow and green boxes). Defocus: -2 µm

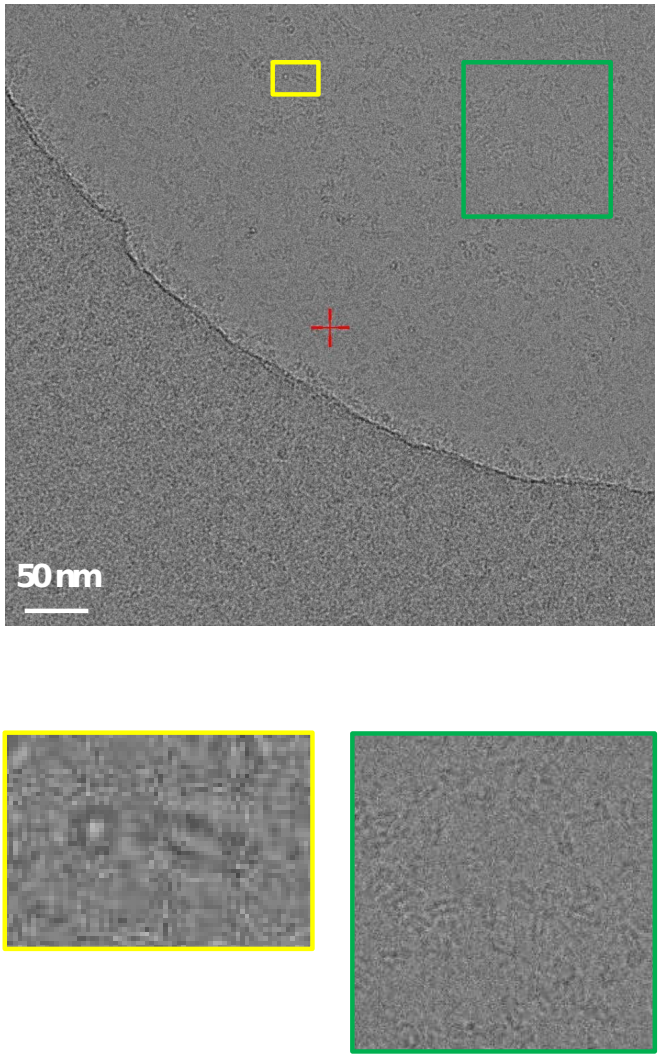


Figure 4.15 Representative grid images of KlebC$_{1-254}$-TolC-Ec TonB$_{33-240}$ complex in nanodisc

Reducing the concentration of ternary complex, KlebC$_{1-254}$-TolC-Ec TonB$_{33-240}$ complex in nanodisc (0.8 mg/ml), and imaging with Talos Arctica 200 kV microscope was successful for reducing the aggregation in some areas of the grid (1.2/1.3 quantifoil). Top and side views of TolC are observed (yellow box). Particles distribute on the grid evenly with an ideal density for data collection (green box). Defocus: -2 µm

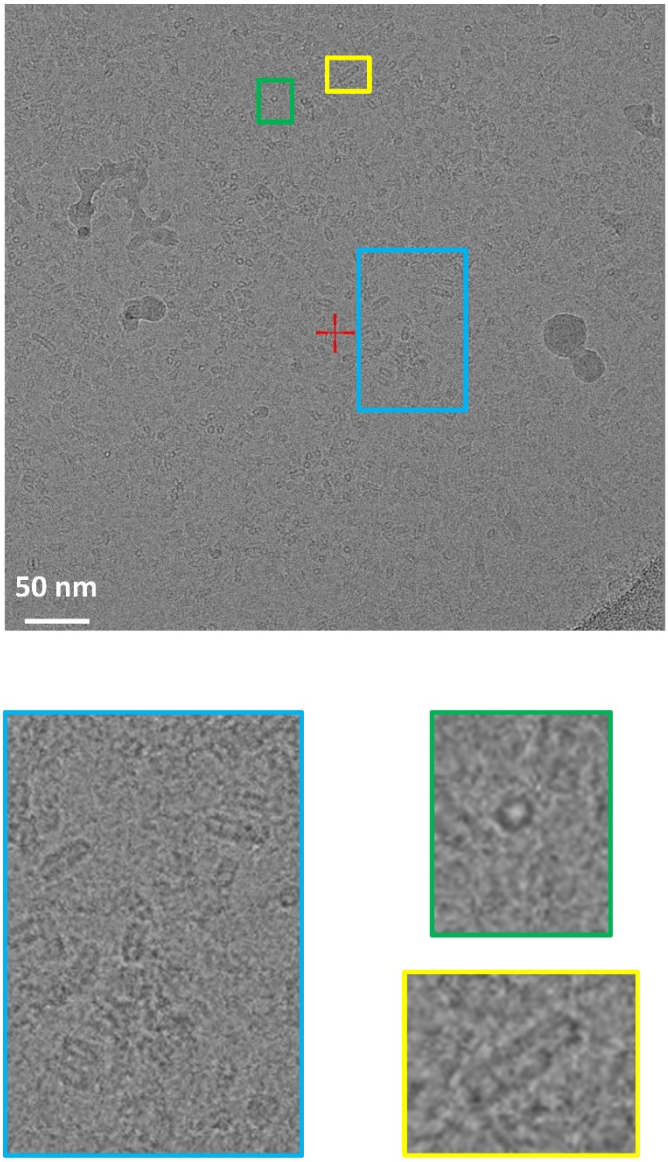


Figure 4.16 Representative grid images of crosslinked KlebC$_{1-254}$-TolC-Kq TonB$_{156-248}$ complex in nanodisc

Crosslinked KlebC$_{1-254}$-TolC-Kq TonB$_{156-248}$ complex in nanodisc was applied to Quantifoil 1.2/1.3 grids (0.7 mg/ml) and imaged using a Talos Arctica 200 kV microscope (Thermofisher). Top view (green box) and side view (yellow box) of the complex are observed from the grid. Particles distribute on the grid evenly with an ideal density for data collection (green box). This grid also has a thin ice amenable to high resolution data collection with individual particles resolved at a defocus of -1 µm.

4.6 Discussion

To study the intact KlebC translocon, individual component parts were expressed and purified. This required optimisation of the TolC purification in order to increase yield. Changes in induction temperatures and growth media were successful for generating more soluble TolC. Future work would look to further increase the yield through reducing the amount of protein in inclusion bodies. In future studies, a low concentration of IPTG can be used to induce protein expression. Moreover, different competent cell lines, such as the BL21(DE3) ΔABCF cell, can be used to decrease the amount of major OMPs in the membrane, which would allow more insertion of TolC (Meuskens et al., 2017).

Following successful purification of TolC, the assembly of KlebC translocon was achieved in nanodisc. The optimum stoichiometry ratio of POPC:MSP1D1G1:TolC discovered in this study is 50:1:0.2. A stoichiometry ratio of 36:1:0.4 (POPC:MSP1D1:TolC) was previously used in the assembly of ColE1 and *E. coli* TolC in nanodisc (Budiardjo et al., 2022). The same ratio was not tested in this study due to a low yield of TolC. Stabilisation of TolC in a nanodisc allowed for the removal of detergent from the buffer system allowing the the ternary complex of TolC, KlebC and TonB to be assembled. In the presence of detergent, TonB aggregated. This is the first study to successfully assemble a group B bacteriocin uptake complex.

The weak binding (K_D = 66.2 μM) of $KlebC_{1-254}$ to Kq $TonB_{156-248}$ likely led to its dissociation upon application to cryo-EM grids. To circumvent this problem, Kq $TonB_{156-248}$ was added in a 25-fold molar excess to KlebC and crosslinked using

formaldehyde to saturate all binding sites and stabilise the intact complex, respectively. This was successful however the yield of intact ternary complex as judged by SDS-PAGE staining was still likely <30%. To overcome this, future work should investigate different methods for trapping the intact complex, such as that used previously for trapping the ColE9 translocon (Housden et al 2013, Francis et al 2021). Here a disulphide bond was used to stabilise and trap the intact translocon complex in the lipid bilayer before detergent extraction. It is plausible that a disulphide in the TonB box of KlebC could be designed through guided binding studies.

Grids, containing crosslinked $KlebC_{1-254}$-TolC-Kq $TonB_{156-248}$ complex in nanodisc have been optimised and prepared. Collection of movies and processing to generate 3D maps of the complex can provide valuable molecular details of how group B bacteriocins interact with TonB, to transport through OM. A high-resolution 3D reconstitution can provide valuable insights on the interactions between the TonB box on KlebC and TonB, which can be also used to assess the accuracy of Alphafold 2.0. The ability of AlphaFold 2.0 to predict the complex structure was shown to be limited with mutagenesis studies guided by the predicted complex structure, failing to obliterate KlebC-TonB complex formation. This shows that despite the recent advances in structure prediction algorithms there is still a need for experimental data and structures to validate predictions.

Chapter 5. Conclusion

This study continues elucidating the uptake mechanism of KlebC. The complex formation between KlebC$_{1-254}$ and Ec TonB$_{33-240}$ was observed by analytical SEC. However, this interaction was not measured by ITC. Cleavage of the Im9 after the purification of Ec TonB$_{33-240}$ may resolve this issue in the future. A weak complex between KlebC$_{1-254}$ and Kq TonB$_{156-248}$ was detected by ITC. This explains that no complex formation was observed between these two proteins when only small amounts of them were evaluated by analytical SEC. High concentration of Kq TonB$_{156-248}$ and chemical crosslinking significantly improve the formation of the ternary KlebC translocon (KlebC$_{1-254}$-TolC-Kq TonB$_{156-248}$) in nanodisc. Nanodisc was used in this study to assemble the KlebC translocon, for structural study by single-particle Cryo-EM. A high-resolution of complex structure can help us understand molecular details of protein interactions within the complex, especially the location of the TonB box. The TonB box, predicted by Alphafold 2.0, was proved to be inaccurate by mutagenesis study. After optimisation, TolC was successfully assembled into nanodisc. The addition of KlebC and TonB components to TolC-nanodisc was also achieved. However, the proportion of ternary complex in the final sample is low, which will require a large amount of particle collection during Cryo-EM. After optimisation, particles are not aggregating on the grids and a high contrast of particles (crosslinked KlebC$_{1-254}$-TolC-Kq TonB$_{156-248}$ ternary complex in nanodisc) is achieved. This grid is ready for subsequent single-particle Cryo-EM to solve the structure of ternary KlebC translocon.

References:

Aires, J.R. and Nikaido, H. (2005). Aminoglycosides Are Captured from both Periplasm and Cytoplasm by the AcrD Multidrug Efflux Transporter of Escherichia coli. *Journal of Bacteriology*, 187(6), pp.1923–1929. doi:https://doi.org/10.1128/jb.187.6.1923-1929.2005.

Andersen, C., Koronakis, E., Bokma, E., Eswaran, J., Humphreys, D., Hughes, C. and Koronakis, V. (2002). Transition to the open state of the TolC periplasmic tunnel entrance. *Proceedings of the National Academy of Sciences*, 99(17), pp.11103–11108. doi:https://doi.org/10.1073/pnas.162039399.

Arunmanee, W., Pathania, M., Solovyova, A.S., Brun, L., Ridley, H., Baslé, A., Van Den Berg, B. and Lakey, J.H. (2016). Gram-negative trimeric porins have specific LPS binding sites that are essential for porin biogenesis. *PNAS*, 113(34). doi:https://doi.org/10.1073/pnas.1602382113.

Atanasković, I., Khédidja Mosbahi, Sharp, C., Housden, N.G., Kaminska, R., Walker, D. and Kleanthous, C. (2020). Targeted Killing of Pseudomonas aeruginosa by Pyocin G Occurs via the Hemin Transporter Hur. *Journal of Molecular Biology*, 432(13), pp.3869–3880. doi:https://doi.org/10.1016/j.jmb.2020.04.020.

Benn, G., Mikheyeva, I.V., Inns, P.G., Forster, J.C., Ojkic, N., Bortolini, C., Ryadnov, M.G., Kleanthous, C., Silhavy, T.J. and Hoogenboom, B.W. (2021). Phase separation in the outer membrane of Escherichia coli. *Proceedings of the National Academy of Sciences*, 118(44), p.e2112237118. doi:https://doi.org/10.1073/pnas.2112237118.

Benz, R., Maier, E. and Gentschev, I. (1993). TolC of Escherichia coli Functions as an Outer Membrane Channel. *Zentralblatt für Bakteriologie*, 278(2-3), pp.187–196. doi:https://doi.org/10.1016/s0934-8840(11)80836-4.

Bhattacharyya, P., Wendt, L., Whitney, E. and Silver, S. (1970). Colicin-Tolerant Mutants of Escherichia coli: Resistance of Membranes to Colicin El. *Science*, 168(3934), pp.998–1000. doi:https://doi.org/10.1126/science.168.3934.998.

Bohnert, J.A., Karamian, B. and Nikaido, H. (2010). Optimized Nile Red Efflux Assay of AcrAB-TolC Multidrug Efflux System Shows Competition between Substrates. *Antimicrobial Agents and Chemotherapy*, 54(9), pp.3770–3775. doi:https://doi.org/10.1128/aac.00620-10.

Budiardjo, S.J., Stevens, J.J., Calkins, A.L., Ikujuni, A.P., Wimalasena, V.K., Firlar, E., Case, D.A., Biteen, J.S., Kaelber, J.T. and Slusky, J.S. (2022). Colicin E1 opens its hinge to plug TolC. *eLife*, 11. doi:https://doi.org/10.7554/elife.73297.

Cadieux, N., Phan, P.G., Cafiso, D.S. and Kadner, R.J. (2003). Differential substrate-induced signaling through the TonB-dependent transporter BtuB. *Proceedings of the National Academy of Sciences*, 100(19), pp.10688–10693. doi:https://doi.org/10.1073/pnas.1932538100.

Cascales, E., Buchanan, S.K., Duche, D., Kleanthous, C., Lloubes, R., Postle, K., Riley, M., Slatin, S. and Cavard, D. (2007). Colicin Biology. *Microbiology and Molecular Biology Reviews*, 71(1), pp.158–229. doi:https://doi.org/10.1128/mmbr.00036-06.

Celia, H., Botos, I., Ni, X., Fox, T., De Val, N., Lloubes, R., Jiang, J. and Buchanan, S.K. (2019). Cryo-EM structure of the bacterial Ton motor subcomplex ExbB–ExbD provides information on structure and stoichiometry. *Communications Biology*, 2(1). doi:https://doi.org/10.1038/s42003-019-0604-2.

Chauleau, M., Mora, L., Serba, J. and de Zamaroczy, M. (2011). FtsH-dependent Processing of RNase Colicins D and E3 Means That Only the Cytotoxic Domains Are Imported into the Cytoplasm. *Journal of Biological Chemistry*, 286(33), pp.29397–29407. doi:https://doi.org/10.1074/jbc.m111.242354.

Chyan Leong Ng, Lang, K., Meenan, N.A.G., Sharma, A., Kelley, A.C., Kleanthous, C. and Ramakrishnan, V. (2010). Structural basis for 16S ribosomal RNA cleavage by the cytotoxic domain of colicin E3. *Nature Structural & Molecular Biology*, 17(10), pp.1241–1246. doi:https://doi.org/10.1038/nsmb.1896.

de Zwaig, R.N. and Luria, S.E. (1967). Genetics and Physiology of Colicin-tolerant Mutants of Escherichia coli. *Journal of Bacteriology*, 94(4), pp.1112–1123. doi:https://doi.org/10.1128/jb.94.4.1112-1123.1967.

Deme, J.C., Johnson, S., Vickery, O., Aron, A., Monkhouse, H., Griffiths, T., James, R.H., Berks, B.C., Coulton, J.W., Stansfeld, P.J. and Lea, S.M. (2020). Structures of the stator complex that drives rotation of the bacterial flagellum. *Nature Microbiology*, 5(12), pp.1553–1564. doi:https://doi.org/10.1038/s41564-020-0788-8.

Denkovskiene, E., Misiunas, A. and Ražanskienė, A. (2020). *Klebicins for the control of Klebsiella*.

Denkovskienė, E., Šarūnas Paškevičius, Audrius Misiūnas, Stočkūnaitė, B., Urtė Starkevič, Astra Vitkauskienė, Hahn-Löbmann, S., Schulz, S., Anatoli Giritch, Gleba, Y. and Aušra Ražanskienė (2019). Broad and Efficient Control of Klebsiella Pathogens by Peptidoglycan-Degrading and Pore-Forming Bacteriocins Klebicins. *Scientific Reports*, 9(1). doi:https://doi.org/10.1038/s41598-019-51969-1.

Dowhan, W. (1997). Molecular basis for membrane phospholipid diversity: why are there so many lipids? *Annual Review of Biochemistry*, 66, pp.199–232. doi:https://doi.org/10.1146/annurev.biochem.66.1.199.

Du, D., Wang, Z., James, N.R., Voss, J.E., Klimont, E., Ohene-Agyei, T., Venter, H., Chiu, W. and Luisi, B.F. (2014). Structure of the AcrAB–TolC multidrug efflux pump. *Nature*, 509(7501), pp.512–515. doi:https://doi.org/10.1038/nature13205.

El Ghachi, M., Bouhss, A., Barreteau, H., Touzé, T., Auger, G., Blanot, D. and Mengin-Lecreulx, D. (2006). Colicin M Exerts Its Bacteriolytic Effect via Enzymatic Degradation of Undecaprenyl Phosphate-linked Peptidoglycan Precursors. *Journal of Biological Chemistry*, 281(32), pp.22761–22772. doi:https://doi.org/10.1074/jbc.m602834200.

Field, D., Fernandez, M., R. Paul Ross and Field, D. (2023). After a century of nisin research, where are we now and where are we going? *Fems Microbiology Reviews*. doi:https://doi.org/10.1093/femsre/fuad023.

Fitzpatrick, A.W.P., Llabrés, S., Neuberger, A., Blaza, J.N., Bai, X.-C., Okada, U., Murakami, S., van Veen, H.W., Zachariae, U., Scheres, S.H.W., Luisi, B.F. and Du, D. (2017). Structure of the MacAB–TolC ABC-type tripartite multidrug efflux pump. *Nature Microbiology*, 2(7). doi:https://doi.org/10.1038/nmicrobiol.2017.70.

Fleming, A. (1929). On the Antibacterial Action of Cultures of a Penicillium, with Special Reference to Their Use in the Isolation of B. influenzae. *Clinical Infectious Diseases*, 2(1), pp.129–139. doi:https://doi.org/10.1093/clinids/2.1.129.

Francis, M.R., Webby, M.N., Housden, N.G., Kaminska, R., Elliston, E., Chinthammit, B., Lukoyanova, N. and Kleanthous, C. (2021). Porin threading drives receptor disengagement and establishes active colicin transport through Escherichia coli OmpF. *The EMBO Journal*, 40(21). doi:https://doi.org/10.15252/embj.2021108610.

Freed, D.S., Lukasik, S.J., Sikora, A., Mokdad, A. and Cafiso, D.S. (2013). Monomeric TonB and the Ton Box Are Required for the Formation of a High-Affinity Transporter–TonB Complex. *Biochemistry*, 52(15), pp.2638–2648. doi:https://doi.org/10.1021/bi3016108.

Graille, M., Mora, L., Buckingham, R.H., van Tilbeurgh, H. and de Zamaroczy, M. (2004). Structural inhibition of the colicin D tRNase by the tRNA-mimicking immunity protein. *The EMBO Journal*, 23(7), pp.1474–1482. doi:https://doi.org/10.1038/sj.emboj.7600162.

Gratia, A. (1925). Sur un remarquable exemple d'antagonisme entre deux souches de colibacille. *C. R. Soc. Biol.*, 93, pp.1040–1042.

Grinter, R., Milner, J. and Walker, D. (2012). Bacteriocins active against plant pathogenic bacteria. *Biochemical Society Transactions*, 40(6), pp.1498–1502. doi:https://doi.org/10.1042/bst20120206.

Gumbart, J., Wiener, M.C. and Tajkhorshid, E. (2007). Mechanics of Force Propagation in TonB-Dependent Outer Membrane Transport. *Biophysical Journal*, 93(2), pp.496–504. doi:https://doi.org/10.1529/biophysj.107.104158.

Henderson, J.C., Zimmerman, S.M., Crofts, A.A., Boll, J.M., Kuhns, L.G., Herrera, C.M. and Trent, M.S. (2016). The Power of Asymmetry: Architecture and Assembly of the Gram-Negative Outer Membrane Lipid Bilayer. *Annual Review of Microbiology*, 70(1), pp.255–278. doi:https://doi.org/10.1146/annurev-micro-102215-095308.

Hickman, S.J., Cooper, R.E.M., Bellucci, L., Paci, E. and Brockwell, D.J. (2017). Gating of TonB-dependent transporters by substrate-specific forced remodelling. *Nature Communications*, 8(1). doi:https://doi.org/10.1038/ncomms14804.

Hiraoka, S., Matsuzaki, H. and Shibuya, I. (1993). Active increase in cardiolipin synthesis in the stationary growth phase and its physiological significance in Escherichia coli. *FEBS Letters*, 336(2), pp.221–224. doi:https://doi.org/10.1016/0014-5793(93)80807-7.

Housden, N.G., Hopper, J.T.S., Lukoyanova, N., Rodriguez-Larrea, D., Wojdyla, J.A., Klein, A., Kaminska, R., Bayley, H., Saibil, H.R., Robinson, C.V. and Kleanthous, C. (2013). Intrinsically Disordered Protein Threads Through the Bacterial Outer-Membrane Porin OmpF. *Science*, 340(6140), pp.1570–1574. doi:https://doi.org/10.1126/science.1237864.

Housden, N.G., Webby, M.N., Lowe, E.D., El-Baba, T.J., Kaminska, R., Redfield, C., Robinson, C.V. and Kleanthous, C. (2021). Toxin import through the antibiotic efflux channel TolC. *Nature Communications*, 12(1). doi:https://doi.org/10.1038/s41467-021-24930-y.

Jarosławski, S., Duquesne, K., Sturgis, J.N. and Scheuring, S. (2009). High-resolution architecture of the outer membrane of the Gram-negative bacteria Roseobacter denitrificans. *Molecular Microbiology*, 74(5), pp.1211–1222. doi:https://doi.org/10.1111/j.1365-2958.2009.06926.x.

Jiri Koedding, Howard, P., Kaufmann, L., Polzer, P., Lustig, A. and Welte, W. (2004). Dimerization of TonB Is Not Essential for Its Binding to the Outer Membrane Siderophore Receptor FhuA of Escherichia coli. *Journal of Biological Chemistry*, 279(11), pp.9978–9986. doi:https://doi.org/10.1074/jbc.m311720200.

Jumper, J., Evans, R., Pritzel, A., Green, T., Figurnov, M., Ronneberger, O., Tunyasuvunakool, K., Bates, R., Žídek, A., Potapenko, A., Bridgland, A., Meyer, C., Kohl, S.A.A., Ballard, A.J., Cowie, A., Romera-Paredes, B., Nikolov, S., Jain, R., Adler, J. and Back, T. (2021). Highly accurate protein structure prediction with AlphaFold. *Nature*, 596(7873), pp.583–589.

Khursigara, C.M., De Crescenzo, G., Pawelek, P.D. and Coulton, J.W. (2003). Enhanced Binding of TonB to a Ligand-loaded Outer Membrane Receptor. *Journal of Biological Chemistry*, 279(9), pp.7405–7412. doi:https://doi.org/10.1074/jbc.m311784200.

Kim, Y.C., Tarr, A.W. and Penfold, C.N. (2014). Colicin import into E. coli cells: A model system for insights into the import mechanisms of bacteriocins. *Biochimica et Biophysica Acta (BBA) - Molecular Cell Research*, 1843(8), pp.1717–1731. doi:https://doi.org/10.1016/j.bbamcr.2014.04.010.

Kleanthous, C. (2010). Swimming against the tide: progress and challenges in our understanding of colicin translocation. *Nature Reviews Microbiology*, 8(12), pp.843–848. doi:https://doi.org/10.1038/nrmicro2454.

Kleanthous, C., Rassam, P. and Baumann, C.G. (2015). Protein–protein interactions and the spatiotemporal dynamics of bacterial outer membrane proteins. *Current Opinion in Structural Biology*, 35, pp.109–115. doi:https://doi.org/10.1016/j.sbi.2015.10.007.

Kobylka, J., Kuth, M.S., Müller, R.T., Geertsma, E.R. and Pos, K.M. (2019). AcrB: a mean, keen, drug efflux machine. *Annals of the New York Academy of Sciences*, 1459(1), pp.38–68. doi:https://doi.org/10.1111/nyas.14239.

Koronakis, V., Eswaran, J. and Hughes, C. (2004). Structure and Function of TolC: The Bacterial Exit Duct for Proteins and Drugs. *Annual Review of Biochemistry*, 73(1), pp.467–489. doi:https://doi.org/10.1146/annurev.biochem.73.011303.074104.

Koronakis, V., Li, J., Koronakis, E. and Stauffer, K. (1997). Structure of TolC, the outer membrane component of the bacterial type I efflux system, derived from two-

dimensional crystals. *Molecular Microbiology*, 23(3), pp.617–626. doi:https://doi.org/10.1046/j.1365-2958.1997.d01-1880.x.

Koronakis, V., Sharff, A., Koronakis, E., Luisi, B. and Hughes, C. (2000). Crystal structure of the bacterial membrane protein TolC central to multidrug efflux and protein export. *Nature*, 405(6789), pp.914–919. doi:https://doi.org/10.1038/35016007.

Maté, M.J. and Kleanthous, C. (2004). Structure-based Analysis of the Metal-dependent Mechanism of H-N-H Endonucleases. *Journal of Biological Chemistry*, 279(33), pp.34763–34769. doi:https://doi.org/10.1074/jbc.m403719200.

Mathers, A.J., Crook, D.W., Vaughan, A.S., Barry, K.E., Vegesana, K., Stoesser, N., Parikh, H.I., Sebra, R., Shireen Meher Kotay, A. Sarah Walker and Sheppard, A.E. (2019). Klebsiella quasipneumoniae Provides a Window into Carbapenemase Gene Transfer, Plasmid Rearrangements, and Patient Interactions with the Hospital Environment. *Antimicrobial Agents and Chemotherapy*, 63(6). doi:https://doi.org/10.1128/aac.02513-18.

Meddens, M.B.M., de Keijzer, S. and Cambi, A. (2014). High Spatiotemporal Bioimaging Techniques to Study the Plasma Membrane Nanoscale Organization. *Fluorescence Microscopy*, pp.49–63. doi:https://doi.org/10.1016/b978-0-12-409513-7.00004-x.

Merianos, H.J., Cadieux, N., Cindy S.-Y. Lin, Kadner, R.J. and Cafiso, D.S. (2000). Substrate-induced exposure of an energy-coupling motif of a membrane transporter. *Nature Structural Molecular Biology*, 7(3), pp.205–209. doi:https://doi.org/10.1038/73309.

Meuskens, I., Michalik, M., Chauhan, N., Linke, D. and Leo, J.C. (2017). A New Strain Collection for Improved Expression of Outer Membrane Proteins. *Frontiers in Cellular and Infection Microbiology*, 7, p.464. doi:https://doi.org/10.3389/fcimb.2017.00464.

Mirdita, M., Schütze, K., Moriwaki, Y., Heo, L., Ovchinnikov, S. and Steinegger, M. (2022). ColabFold: making protein folding accessible to all. *Nature Methods*, 19, pp.679–682. doi:https://doi.org/10.1038/s41592-022-01488-1.

Morona, R., Manning, P.A. and Reeves, P. (1983). Identification and characterization of the TolC protein, an outer membrane protein from Escherichia coli. *Journal of Bacteriology*, 153(2), pp.693–699. doi:https://doi.org/10.1128/jb.153.2.693-699.1983.

Murray, C.J. (2022). Global Burden of Bacterial Antimicrobial Resistance in 2019: A Systematic Analysis. *The Lancet*, 399(10325), pp.629–655. doi:https://doi.org/10.1016/S0140-6736(21)02724-0.

Nikaido, H. (2003). Molecular Basis of Bacterial Outer Membrane Permeability Revisited. *Microbiology and Molecular Biology Reviews*, 67(4), pp.593–656. doi:https://doi.org/10.1128/mmbr.67.4.593-656.2003.

Nikaido, H. and Vaara, M. (1985). Molecular basis of bacterial outer membrane permeability. *Microbiological Reviews*, 49(1), pp.1–32. doi:https://doi.org/10.1128/mr.49.1.1-32.1985.

Noinaj, N., Guillier, M., Barnard, T.J. and Buchanan, S.K. (2010). TonB-Dependent Transporters: Regulation, Structure, and Function. *Annual Review of Microbiology*, 64(1), pp.43–60. doi:https://doi.org/10.1146/annurev.micro.112408.134247.

O'Neill, J. (2016). Tackling Drug-resistant Infections Globally: Final Report and Recommendations. *London: Review on Antimicrobial Resistance*. doi:https://doi.org/10.4103/2045-080x.186181.

Ogawa, T., Tomita, K., Ueda, T., Watanabe, K., Tohru Uozumi and Hara, M. (1999). A Cytotoxic Ribonuclease Targeting Specific Transfer RNA Anticodons. *Science*, 283(5410), pp.2097–2100. doi:https://doi.org/10.1126/science.283.5410.2097.

Papadakos, G., Wojdyla, J.A. and Kleanthous, C. (2012). Nuclease colicins and their immunity proteins. *Quarterly reviews of biophysics*, 45(1), pp.57–103. doi:https://doi.org/10.1017/S0033583511000114.

Parker, M.W., Pattus, F., Tucker, A.D. and Tsernoglou, D. (1989). Structure of the membrane-pore-forming fragment of colicin A. *Nature*, 337(6202), pp.93–96. doi:https://doi.org/10.1038/337093a0.

Pawelek, P.D., Croteau, N., Ng-Thow-Hing, C., Khursigara, C.M., Moiseeva, N., Allaire, M. and Coulton, J.W. (2006). Structure of TonB in Complex with FhuA, E. coli Outer Membrane Receptor. *Science*, 312(5778), pp.1399–1402. doi:https://doi.org/10.1126/science.1128057.

Peacock, R.S., Weljie, A.M., Howard, S.P., Price, F.D. and Vogel, H.J. (2005). The Solution Structure of the C-terminal Domain of TonB and Interaction Studies with TonB Box Peptides. *Journal of Molecular Biology*, 345(5), pp.1185–1197. doi:https://doi.org/10.1016/j.jmb.2004.11.026.

Pei, X.-Y., Hinchliffe, P., Symmons, M.F., Koronakis, E., Benz, R., Hughes, C. and Koronakis, V. (2011). Structures of sequential open states in a symmetrical opening transition of the TolC exit duct. *Proceedings of the National Academy of Sciences*, 108(5), pp.2112–2117. doi:https://doi.org/10.1073/pnas.1012588108.

Plésiat, P., Julio Ramos Aires, Godard, C. and Thilo Köhler (1997). Use of steroids to monitor alterations in the outer membrane of Pseudomonas aeruginosa. *Journal of Bacteriology*, 179(22), pp.7004–7010. doi:https://doi.org/10.1128/jb.179.22.7004-7010.1997.

Plésiat, P. and Nikaido, H. (1992). Outer membranes of Gram-negative bacteria are permeable to steroid probes. *Molecular Microbiology*, 6(10), pp.1323–1333. doi:https://doi.org/10.1111/j.1365-2958.1992.tb00853.x.

Raetz, C.R.H. and Whitfield, C. (2002). Lipopolysaccharide Endotoxins. *Annual Review of Biochemistry*, 71(1), pp.635–700. doi:https://doi.org/10.1146/annurev.biochem.71.110601.135414.

Rajapaksha, P., Ojo, I., Yang, L., Pandeya, A., Abeywansha, T. and Wei, Y. (2021). Insight into the AcrAB-TolC Complex Assembly Process Learned from Competition Studies. *Antibiotics*, 10(7), p.830. doi:https://doi.org/10.3390/antibiotics10070830.

Rassam, P., Copeland, N.A., Birkholz, O., Tóth, C., Chavent, M., Duncan, A.L., Cross, S.J., Housden, N.G., Kaminska, R., Seger, U., Quinn, D.M., Garrod, T.J., Sansom, M.S.P., Piehler, J., Baumann, C.G. and Kleanthous, C. (2015). Supramolecular assemblies underpin turnover of outer membrane proteins in bacteria. *Nature*, 523(7560), pp.333–336. doi:https://doi.org/10.1038/nature14461.

Ratliff, A.C., Buchanan, S.K. and Celia, H. (2022). The Ton Motor. *Frontiers in Microbiology*, 13. doi:https://doi.org/10.3389/fmicb.2022.852955.

Saier, M.H., Paulsen, I.T., Sliwinski, M.K., Pao, S.S., Skurray, R.A. and Nikaido, H. (1998). Evolutionary origins of multidrug and drug-specific efflux pumps in bacteria. *The FASEB Journal*, 12(3), pp.265–274. doi:https://doi.org/10.1096/fasebj.12.3.265.

Schauer, K., Rodionov, D.A. and de Reuse, H. (2008). New substrates for TonB-dependent transport: do we only see the 'tip of the iceberg'?. *Trends in Biochemical Sciences*, 33(7), pp.330–338. doi:https://doi.org/10.1016/j.tibs.2008.04.012.

Shultis, D.D., Purdy, M.D., Banchs, C.N. and Wiener, M.C. (2006). Outer Membrane Active Transport: Structure of the BtuB:TonB Complex. *Science*, 312(5778), pp.1396–1399. doi:https://doi.org/10.1126/science.1127694.

Soelaiman, S., Jakes, K., Wu, N., Li, C. and Shoham, M. (2001). Crystal Structure of Colicin E3. *Molecular Cell*, 8(5), pp.1053–1062. doi:https://doi.org/10.1016/s1097-2765(01)00396-3.

Sulavik, M.C., Houseweart, C., Cramer, C., Jiwani, N., Murgolo, N., Greene, J., DiDomenico, B., Shaw, K.J., Miller, G.H., Hare, R. and Shimer, G. (2001). Antibiotic Susceptibility Profiles ofEscherichia coli Strains Lacking Multidrug Efflux Pump Genes. *Antimicrobial Agents and Chemotherapy*, 45(4), pp.1126–1136. doi:https://doi.org/10.1128/aac.45.4.1126-1136.2001.

Szczepaniak, J., Press, C. and Kleanthous, C. (2020). The multifarious roles of Tol-Pal in Gram-negative bacteria. *FEMS Microbiology Reviews*. doi:https://doi.org/10.1093/femsre/fuaa018.

Taylor, A.L. and Trotter, C.D. (1967). Revised linkage map of Escherichia coli. *Bacteriological Reviews*, 31(4), pp.332–353. doi:https://doi.org/10.1128/br.31.4.332-353.1967.

Thomas, S., Holland, I.B. and Schmitt, L. (2014). The Type 1 secretion pathway — The hemolysin system and beyond. *Biochimica et Biophysica Acta (BBA) - Molecular Cell Research*, 1843(8), pp.1629–1641. doi:https://doi.org/10.1016/j.bbamcr.2013.09.017.

Tomita, K., Ogawa, T., Tohru Uozumi, Watanabe, K. and Hara, M. (2000). A cytotoxic ribonuclease which specifically cleaves four isoaccepting arginine tRNAs at their anticodon loops. *Proceedings of the National Academy of Sciences of the United States of America*, 97(15), pp.8278–8283. doi:https://doi.org/10.1073/pnas.140213797.

Van den Berg, B. (2010). Going Forward Laterally: Transmembrane Passage of Hydrophobic Molecules through Protein Channel Walls. *ChemBioChem*, 11(10), pp.1339–1343. doi:https://doi.org/10.1002/cbic.201000105.

Verhoeven, G.S., Dogterom, M. and den Blaauwen, T. (2013). Absence of long-range diffusion of OmpA in E. coliis not caused by its peptidoglycan binding domain. *BMC Microbiology*, 13(1). doi:https://doi.org/10.1186/1471-2180-13-66.

Walker, D., Mosbahi, K., Vankemmelbeke, M., James, R. and Kleanthous, C. (2007). The Role of Electrostatics in Colicin Nuclease Domain Translocation into Bacterial Cells. *Journal of Biological Chemistry*, 282(43), pp.31389–31397. doi:https://doi.org/10.1074/jbc.m705883200.

Wallis, R., Moore, G.R., James, R. and Kleanthous, C. (1995). Protein-Protein Interactions in Colicin E9 DNase-Immunity Protein Complexes. 1. Diffusion-

Controlled Association and Femtomolar Binding for the Cognate Complex. *Biochemistry*, 34(42), pp.13743–13750. doi:https://doi.org/10.1021/bi00042a004.

Wandersman, C. and Delepelaire, P. (1990). TolC, an Escherichia coli outer membrane protein required for hemolysin secretion. *Proceedings of the National Academy of Sciences*, 87(12), pp.4776–4780. doi:https://doi.org/10.1073/pnas.87.12.4776.

Wang, Z., Fan, G., Hryc, C.F., Blaza, J.N., Serysheva, I.I., Schmid, M.F., Chiu, W., Luisi, B.F. and Du, D. (2017). An allosteric transport mechanism for the AcrAB-TolC multidrug efflux pump. *eLife*, 6, p.e24905. doi:https://doi.org/10.7554/eLife.24905.

Webby, M.N., Oluwole, A.O., Pedebos, C., Inns, P.G., Olerinyova, A., Prakaash, D., Housden, N.G., Benn, G., Sun, D., Hoogenboom, B.W., Kukura, P., Mohammed, S., Robinson, C.V., Khalid, S. and Kleanthous, C. (2022). Lipids mediate supramolecular outer membrane protein assembly in bacteria. *Science Advances*, 8(44). doi:https://doi.org/10.1126/sciadv.adc9566.

Welch, R.A., Dellinger, E.P., Minshew, B. and Falkow, S. (1981). Haemolysin contributes to virulence of extra-intestinal E. coli infections. *Nature*, 294(5842), pp.665–667. doi:https://doi.org/10.1038/294665a0.

White, P., Joshi, A., Rassam, P., Housden, N.G., Kaminska, R., Goult, J.D., Redfield, C., McCaughey, L.C., Walker, D., Mohammed, S. and Kleanthous, C. (2017). Exploitation of an iron transporter for bacterial protein antibiotic import. *Proceedings of the National Academy of Sciences*, 114(45), pp.12051–12056. doi:https://doi.org/10.1073/pnas.1713741114.

Wyres, K.L. and Holt, K.E. (2018). Klebsiella pneumoniae as a key trafficker of drug resistance genes from environmental to clinically important bacteria. *Current Opinion in Microbiology*, 45, pp.131–139. doi:https://doi.org/10.1016/j.mib.2018.04.004.

Zakharov, S.D., Eroukova, V.Y., Rokitskaya, T.I., Zhalnina, M.V., Sharma, O., Loll, P.J., Zgurskaya, H.I., Antonenko, Y.N. and Cramer, W.A. (2004). Colicin Occlusion of OmpF

and TolC Channels: Outer Membrane Translocons for Colicin Import. *Biophysical Journal*, 87(6), pp.3901–3911. doi:https://doi.org/10.1529/biophysj.104.046151.